HEAT TRANSFER IN TURBULENT NANOFLUIDS: SEPARATION FLOW STUDIES AND DEVELOPMENT OF NOVEL CORRELATIONS

ELHAM MONTAZER

FACULTY OF ENGINEERING
UNIVERSITY OF MALAYA
KUALA LUMPUR

2019

HEAT TRANSFER IN TURBULENT NANOFLUIDS: SEPARATION FLOW STUDIES AND DEVELOPMENT OF NOVEL CORRELATIONS

ELHAM MONTAZER

THESIS SUBMITTED IN FULFILMENT OF THE REQUIREMENTS FOR THE DEGREE OF DOCTOR OF PHILOSOPHY

FACULTY OF ENGINEERING
UNIVERSITY OF MALAYA
KUALA LUMPUR

2019

UNIVERSITY OF MALAYA

ORIGINAL LITERARY WORK DECLARATION

Name of Candidate: Elham Montazer

Matric No: KHA130146

Name of Degree: **DOCTOR OF PHILOSOPHY**

Title of Project Paper/Research Report/Dissertation/Thesis ("this Work"):

HEAT TRANSFER IN TURBULENT NANOFLUIDS: SEPARATION FLOW STUDIES AND DEVELPMENT OF NOVEL CORRELATIONS

Field of Study: Heat Transfer

I do solemnly and sincerely declare that:

(1) I am the sole author/writer of this Work;
(2) This Work is original;
(3) Any use of any work in which copyright exists was done by way of fair dealing and for permitted purposes and any excerpt or extract from, or reference to or reproduction of any copyright work has been disclosed expressly and sufficiently and the title of the Work and its authorship have been acknowledged in this Work;
(4) I do not have any actual knowledge nor do I ought reasonably to know that the making of this work constitutes an infringement of any copyright work;
(5) I hereby assign all and every rights in the copyright to this Work to the University of Malaya ("UM"), who henceforth shall be owner of the copyright in this Work and that any reproduction or use in any form or by any means whatsoever is prohibited without the written consent of UM having been first had and obtained;
(6) I am fully aware that if in the course of making this Work I have infringed any copyright whether intentionally or otherwise, I may be subject to legal action or any other action as may be determined by UM.

Candidate's Signature Date:

Subscribed and solemnly declared before,

Witness's Signature Date:

Name:

Designation:

HEAT TRANSFER IN TURBULENT NANOFLUIDS: SEPARATION FLOW STUDIES AND DEVELOPMENT OF NOVEL CORRELATIONS

ABSTRACT

Convective heat transfer plays a significant role in many industrial heating and cooling applications. This mode of heat transfer can be passively enhanced by reconfiguring flow passage, boundary conditions, or fluid thermophysical properties. The broader scope of nanotechnology initiated many studies of heat transfer and thermal engineering. Nano-fluids are one of such technology which can be thought of engineered colloidal fluids with nano-sized particles. Experimental investigation on turbulent forced convection heat transfer to nanofluids in an axisymmetric abrupt expansion has conducted in this research work. A number of studies on the effect of nanofluids on heat transfer augmentation have taken care in addition to the investigation of rearrangement on flow passage configurations. In heat transfer investigation, this study has focused on functionalized multiwalled carbon nanotubes (MWCNT-COOH), polycarboxylate functionalized graphene nanoplatelets (F-GNP), SiO_2 and ZnO water based nanofluids. In this investigation the convective heat transfer coefficient and friction factor at fully developed turbulent flow of nanofluids flowing through the sudden expansion with the expansion ratio (ER) of 2 was experimentally determined at constant wall heat flux of 12,128.56 W/m^2. The experiments were conducted at the Reynolds number range of 4,000–16,000. The observed Nusselt numbers are greater than data obtained in the fully developed pipe flow which indicates that the level of the turbulent transport is high even though the recirculating velocities are a few percentages of the bulk mean velocity. This feature supports the existence of the turbulent transport processes in the recirculating flows. The influence of the volume fraction of nanofluids and Reynolds number on heat transfer and

friction losses were examined. All the results reveal that the enhancement of weight concentration and Reynolds number, augments the local Nusselt number with the increment of axial ratios in all the cases which is representing higher heat transfer rates than that of base fluid. Results show that the maximum Nu were occurred at the distance of almost ten times step height in the downstream zone. Comparison between the examined four types of nanofluids, show that the carbon-based nanofluids have a greater effect on enhancing heat transfer (33.7% and 16.7% heat transfer performance improvement for F-GNP and MWCNT nanofluids respectively at 0.1 wt% concentration) at the downstream of the sudden expansion pipe. In general, none of the existing correlations appear entirely satisfactory for the general use in the sudden expansion of pipe. Last part of the present study was undertaken for developing more generally applicable correlations, based on the research concepts. In conclusion, three applicable correlations for the average Nu, f and local Nu have proposed whereas the first two correlations predict the average Nu and friction factor relating Re, Pr and volume fraction with reasonably good accuracy. There is no available work dealing with the prediction of the local Nu with the distance of the axial ratio of flow through sudden expansion. So, the third correlation which is proposed for the first time, expresses the local Nu versus axial ratio, Re, Pr and volume fraction of nanoparticles acceptable for the base fluid and the nanofluids. This correlation has satisfied the data from all the considered sources rather than from just one or two of the sources.

Keywords: Separation flow, Heat transfer, Nanofluid, Multiple regression, Response surface methodology (RSM).

PEMINDAHAN HABA DALAM NANOFLUIDS TURBULEN: KAJIAN ALIRAN PEMISAHAN DAN PEMBANGUNAN KORELASI NOVELNYA

ABSTRAK

Pemindahan haba konvensional memainkan peranan penting dalam banyak pemanasan industri dan aplikasi penyejukan. Cara pemindahan haba ini boleh dipertingkat secara pasif dengan menyusun semula laluan laluan, keadaan sempadan, atau sifat termofisis cecair. Skop bidang nanoteknologi yang lebih luas telah memulakan banyak kajian pemindahan haba dan kejuruteraan terma. Cecair Nano adalah salah satu daripada teknologi sedemikian yang boleh difikirkan cecair koloid terperinci dengan zarah berukuran nano.Penyiasatan eksperimen mengenai perpindahan panas perpindahan terpaksa bergelora kepada nanofluid dalam pengembangan axisymmetric mendadak telah dijalankan dalam kerja penyelidikan ini. Sejumlah kajian mengenai kesan nanofluid pada pembesaran pemindahan haba telah dijaga sebagai tambahan kepada penyiasatan penyusunan semula pada konfigurasi saluran aliran. Dalam penyelidikan pemindahan haba, kajian ini memberi tumpuan kepada nanotiub karbon multiwalled yang berfungsi (MWCNT-COOH), nanofluid berdasarkan kandungan graphene nanoplatelets (F-GNP), SiO2 dan ZnO berasaskan air. Dalam penyiasatan ini, pekali pemindahan haba konveksi dan faktor geseran di aliran nanofluid turbulen yang dikembangkan sepenuhnya melalui pengembangan mendadak dengan nisbah pengembangan (ER) 2 adalah ditentukan secara eksperimen pada fluks haba dinding tetap 12,128.56 W / m2. Eksperimen-eksperimen itu dijalankan di rangkaian nombor Reynolds sebanyak 4,000-16,000. Bilangan Nusselt yang diperhatikan adalah lebih besar daripada data yang diperolehi dalam aliran paip yang dibangunkan sepenuhnya yang menunjukkan bahawa tahap pengangkutan yang bergelora tinggi walaupun halaju peredaran adalah beberapa peratus dari halaju purata pukal. Ciri

ini menyokong kewujudan proses pengangkutan bergelora dalam aliran mengitar semula. Pengaruh pecahan jumlah nanofluid dan nombor Reynolds pada pemindahan haba dan kehilangan geseran telah diperiksa. Semua keputusan menunjukkan bahawa peningkatan kepekatan berat dan nombor Reynolds, menambah bilangan Nusselt tempatan dengan kenaikan nisbah paksi dalam semua kes yang mewakili kadar pemindahan haba yang lebih tinggi daripada bendalir asas. Keputusan menunjukkan bahawa maksimum Nu berlaku pada jarak hampir sepuluh kali ketinggian langkah di zon hiliran. Perbandingan antara empat jenis nanofluid yang diperiksa, menunjukkan bahawa nanofluid berasaskan karbon mempunyai kesan yang lebih besar untuk meningkatkan pemindahan haba (33.7% dan 16.7% peningkatan prestasi pemindahan haba untuk F-GNP dan MWCNT nanofluids pada 0.1% berat) di hiliran paip pengembangan tiba-tiba. Secara umumnya, tiada korelasi yang ada kelihatan sepenuhnya memuaskan untuk penggunaan umum dalam pengembangan paip secara mendadak. Bahagian terakhir kajian ini dijalankan untuk membangunkan korelasi yang lebih umum, berdasarkan konsep penyelidikan. Kesimpulannya, tiga korelasi yang berkaitan untuk purata Nu, f dan Nu tempatan telah dicadangkan manakala dua korelasi pertama meramalkan purata Nu dan faktor geseran yang berkaitan Re, Pr dan pecahan pecahan dengan ketepatan yang cukup baik. Tidak ada kerja yang tersedia dengan ramalan Nu yang tempatan dengan jarak nisbah paksi aliran melalui pengembangan mendadak. Oleh itu, korelasi ketiga yang dicadangkan buat kali pertama, menyatakan nisbah Nu versus paksi tempatan, Re, Pr dan pecahan isipadu nanopartikel boleh diterima untuk cecair asas dan nanofluid. Hubungan ini telah memuaskan data daripada semua sumber yang dipertimbangkan dan bukan hanya dari satu atau dua sumber.

Keywords: Separation flow, Heat transfer, Nanofluid, Multiple regression, Response surface methodology (RSM).

ACKNOWLEDGMENTS

This thesis is dedicated to my parents, who have been there for me since the day I was born.

First and foremost, I would like to express my heartfelt thanks and gratitude to God for his blessings throughout my life and for giving me the opportunity to successfully complete my Ph.D degree.

A work like this involves so many amazing people. I would like to thank my advisor Assoc. Prof. Dr. Kazi Md. Salim Newaz for inviting me on this journey and having confidence in me and helping me navigate all the bumps in the road. Thanks to Dr. Ahmad Badarudin bin Mohamad Badry my co-advisor for being there constantly to provide vision and help guide my work.

Research requires resources and I am grateful to the University of Malaya for sponsoring me with the University Malaya Research Grant (UMRG). I would like to thank the staff of the Department of Mechanical Engineering. Sincere thanks are extended to the Department of Chemical Engineering and relevant personnel from different discipline of the University of Malaya. My gratitude is also extended to Dr. Mohd Ridha Bin Muhamad and Dr. Zaira Zaman Chowdhury for their support and encouragement.

A special thanks to my family. Words cannot express how grateful I am to my mother and father for all of the sacrifices that you've made on my behalf. Your prayer for me was what sustained me thus far. I would also like to thank all of my friends who supported me in writing and encouraged me to strive towards my goal.

TABLE OF CONTENTS

LIST OF FIGURES

LIST OF TABLES

LIST OF SYMBOLS AND ABBREVIATIONS

A_c	:	Surface Area of Cross Section
C_p	:	Specific Heat Capacity, J/kg K
CCD	:	Central Composite Design
CFD	:	Computational Fluid Dynamics
CNT	:	Carbon Nanotube
CTAB	:	Cetyl Trimethylammonium Bromide
CVD	:	Chemical vapor deposition method
D	:	Pipe Diameter after Expansion
d	:	Pipe Diameter before Expansion
d_{bf}	:	Equivalent Diameter of a Base Fluid Molecule
d_{np}	:	Nanoparticle diameter
DoE	:	Design of Experiments
Di Water	:	Distillate Water
ER	:	Expansion Ratio
f	:	Friction Factor
FEM	:	Finite Element Method
F-GNP	:	Polycarboxylate Functionalized Graphene Nanoplatelets
FSA	:	Fence Subtended Angle
FVM	:	Finite Volume Method

GO	:	Graphene Oxide
GNP	:	Graphene nanoplatelets
H	:	Step Height
h	:	Convective heat transfer coefficient
I	:	Electrical current, A
IEP	:	Isoelectric Point
k	:	Thermal conductivity, W/m.K
K_b	:	Boltzmann Constant
k_{eff}	:	Effective Thermal Conductivity
L	:	Tube length, m
L_f	:	Fence Position
LDA	:	Laser Doppler Anemometry
Max	:	Maximum
MHD	:	Magnetohydrodynamics Drive
MHFS	:	Multiple Hot-film Sensor
MWCNT	:	Multi-wall carbon nanotube
MWCNT-COOH	:	Functionalized Multiwalled Carbon Nanotubes
$\dot{m}$	:	Mass Flow Rate
NS	:	Navier Stokes
Nu	:	Nusselt Number

$Nu_{(x/H)}$	:	Local Nusselt Number
$\overline{Nu}$	:	Average Nusselt Number
PEC	:	Performance evaluation criterion
PI	:	Performance Index
PIV	:	Particle Image Velocimetry
PLC	:	Programmable logic controller
Pr	:	Prandtl number
Q	:	Heater power
q	:	Wall Heat Flux
R_{bd}	:	Interfacial Thermal Resistance
Re	:	Reynolds Number
Re_{cr}	:	Critical Reynolds Number
R^2	:	Coefficient of Determination
RTD	:	Resistance temperature detector
RSM	:	Response Surface Methodology
SDBS	:	Sodium dodecyl benzene sulfonate
SDS	:	Sodium dodecyl sulfonate
SHMP	:	Sodium Hexametaphosphate
SiO_2	:	Silicon Dioxide
SS_{tot}	:	Total sum of squares

SS_{res}	:	Residual sum of squares
SSE	:	Sum of Squared Errors
SWCNT	:	Single-wall carbon nanotube
T	:	Temperature
T_{fr}	:	Freezing Point of the base fluid
$T_{b(x/H)}$	:	Bulk temperature of fluid at the axial ratio x/H
$T_{s(x/H)}$	:	Wall temperature of fluid at the axial ratio x/H
TEM	:	Transmission Electron Microscopy
u	:	Velocity
U_{avg}	:	Mean Velocity
u_{cr}	:	Critical Velocity
u_B	:	Brownian Velocity
U_t	:	Setting Velocity
VFBN	:	Viscoelastic Fluid-based Nanofluid
VIF	:	Variance Inflation Factor
VOF	:	Volume of Fluid
VONOS	:	Variable-Order Non-Oscillatory Scheme
W	:	Watt
W_p	:	Weight Coefficient
ZnO	:	Zinc Oxide

X/H	:	Axial Ratio
ΔP	:	Pressure Drop
Wt.%	:	Weight Percentage
$\emptyset$	:	Nanoparticles Volume Concentration
ρ	:	Density
ρ_{bfo}	:	Mass Density of the Base Fluid
μ	:	Viscosity
μ_{eff}	:	Effective Viscosity
ε	:	Performance Index
δ_t	:	Thickness of Thermal Boundary Layer

Subscripts

avg	:	Average
b	:	Bulk
bf	:	Base Fluid
in	:	inlet
nf	:	Nanofluid
np	:	Nanoparticle
out	:	Outlet
x/H	:	Axial Ratio
s	:	Surface

LIST OF APPENDICES

CHAPTER 1: INTRODUCTION

1.1 Background

Advances in thermal science and technology are continually focusing on heat exchangers optimization to enhance the heat transfer rate and minimize the surface of heat transfer simultaneously. The flows of fluid via sudden expansions are among the basic topics within the discipline of fluid mechanics. The comprehension of these types of flows has attracted a great volume of research, attributable to their wide usage in numerous fluid applications such as heat exchangers, dump combustors, nuclear reactors and diffusers; as well as pipe-flow systems within the chemical and petroleum industries, pharmaceutical, medical science, air-conditioning ducts, and fluidic devices. The separation of fluid flow occurred due to the change in pressure gradient that caused by the increase or decrease of the cross-sectional area of the circular flow channels. Numerous researchers have experienced enhancement of heat transfer at the flow separation region and up to the reattachment point. Thus, heat transfer enhancement was obtained at the cost of pressure loss.

In addition, improvement of thermal transport properties of heating fluids enhances the efficiency of heat exchangers, shrinks the size of the systems and reduces the operational cost. Recently, suspension of the solid particles among the fluid has shown enhanced thermal conductivity of the fluid. At first, the suspension of the mini and micro solid particles in fluids were offered. Although these particles improved the heat transfer characteristics of conventional fluids, where some of the problems, such as high pressure drop and instability of the particles, appeared due to the large size of the particles. The particles of the size of nano-meter have solved the problem of stability and sedimentation

on one hand and increase of the heat transfer efficiency on the other hand. Nanofluids contain particles with dimensions smaller than 100 nm and are suspended in a base fluid, such as water, ethylene glycol, etc. The term nanofluid was first time used by Chol (1995) for these suspensions. It has been reported in a number of studies (Abu-Nada, 2008; Roy et al., 2004; Xuan & Roetzel, 2000) that the dispersion of the solid nanoparticles in a base fluid significantly changes the thermo-physical properties of the base fluids. Because the nanoparticles are so fine, gravity becomes less important and thus chances of sedimentation are also less which makings the nanofluids more stable. However, nanofluids may not remain stable of its own so it needs either sonication, surfactant or functionalization to keep the stability which is essential for application as a heat exchanging liquid. Nanofluids have been considered in many engineering applications, e.g., solar collectors (Allahyari et al., 2011), engine cooling systems (Kakaç & Pramuanjaroenkij, 2009), micromechanics and instrumentation systems (Murshed et al., 2008b). Since such suspension of nanoparticles in liquids has shown an improvement of the liquids thermo-physical properties, it is important to further improve the understanding of heat transfer and fluid flow behaviour of nanofluids. However, the study of nanofluids flow in abrupt expansion is very limited. This study will provide a new idea to meet the request of heat transfer enhancements for turbulent forced convection flow in sudden expansion devices. The effect of Reynolds number was examined for four types of water based nanofluids (F-GNP, MWCNT-COOH, SiO_2 and ZnO) at various weight fractions ranging from 0 to 0.2 on the forced convection heat transfer to turbulent flow through an abrupt expansion of diameters ratio 2.

1.2 Problem Statement

In thermal energy transportation, huge energy is lost due to lack of efficient heat exchanging equipment and use of inefficient materials. Many methods have applied by the manufacturers, researchers and users to improve the situation, among them, use of

efficient materials, adjusting process parameters, modifications of design etc. are notable. Now researchers are more involved in exploration of better heat exchanging liquid. Nanostructured materials are holding a great effect on the liquids employed for the transport of heat in heat exchangers. The effective thermal conductivity increases substantially, when non-metallic or metallic particles of higher thermal conductivity and lower dimensions (less than 100 nm) are dispersed in conventional heat transfer liquids. Step flow in the form of backward facing, play a vital role in the design of many equipment and engineering applications where heat transfer is concerned.

It is expected that in addition to the substantial augmentation of thermal conductivity and the heat capacity of the nanofluid, the main reasons of heat transfer enhancement of them are from enhanced turbulence or eddies, suppression or interruption of the boundary layer as well as dispersion or mixing of the suspended nanoparticles by Brownian motion. Therefore, the convective heat transfer coefficient of the nanofluids is a function of the properties, dimension and volume fractions of the suspended nanoparticles as well as the flow velocities. The conventional convective heat transfer correlations of the Newtonian fluids are not applicable to the nanofluids. To understand the mechanism of heat transfer enhancement of nanofluids and to accelerate practical applications of the nanofluids, more investigations are therefore needed to clarify fundamental features of convective heat transfer and flow performance of the nanofluids. Accordingly, this research is aimed for studying the heat transfer performance of the nanofluids in a sudden expansion passage for the turbulent flow and also developing heat transfer correlation from the experimental data.

1.3 Organization of the Thesis

This thesis is sub-divided into five chapters. Chapter one contains the basic concepts, importance, objectives, and motivations for this study. A brief introduction to

the separation flow in different configurations and effects on heat transfer to fluids and nanofluids are also incorporated in this section. Chapter two is related to the experimental and numerical studies covering turbulent and laminar flow through sudden expansion, over backward facing steps, and no step in pipe with constant wall heat flux. In addition, study of previous works and the relevant correlations of heat transfer performance and the variable parameters have presented. Chapter three is representing the experimental setup, materials and stability analysis and regression process. The flowchart of the research methodology is presented as well. Chapter four is consisted of the preparation of nanofluids, measuring their thermo-physical properties, measuring heat transfer properties and developing new correlations to represent the heat transfer performance of the nanofluids and analysis of the results of the concerned data. Chapter five is consisted of the conclusions and recommendations for future works linked to the separation of nanofluid flow through this configuration.

1.4 Research Objectives

The main objectives of this research can be summarized as follows:

- To investigate the effect of flow separation on the heat transfer characteristics of a turbulent flow in sudden expansion pipe flow configuration.
- To determine the effects of nanofluids type, nanoparticle concentrations and Reynolds number on the heat transfer enhancement.
- To develop multiple linear and non-linear regressions models of heat transfer performance and improve the correlated equations over the previous equations by considering the influence of nanoparticles and axial ratio of passage dimensions on flow through sudden expansion passage configuration.

1.5 Account of Research Progress Linking the Research Papers

The first published article entitled "A Brief Review Study of Flow Phenomena Over a Backward-Facing Step and its Optimization", has focused on the studies of flow specifications of fluid moving via plain abrupt enlargement and with, varying configurations, for both Newtonian and non-Newtonian fluids, in order to search for the best possible comprehension of this area.

The second published article entitled "Development of a New Density Correlation for Carbon Based Nanofluids Using Response Surface Methodology" presented the model which determines the effective density of the nanofluids as a function of nanoparticle mass fraction, temperature, nanoparticle and the base fluid densities. The aim of the study is to minimize the total mean squared error between desired output and net output through optimization.

In third submitted manuscript entitled "Heat Transfer to Turbulent Nanofluids Separation Flow – Studies in Evaluation of its Novel Correlations" on turbulent forced convection heat transfer to nanofluids in an axisymmetric abrupt expansion heat exchanger is investigated experimentally. The main objective of this study is to develop the local Nusselt number and the average Nusselt number correlations which are validated for different kinds of nanofluids in various concentrations and Reynolds numbers.

CHAPTER 2: LITERATURE REVIEW

2.1 Introduction

Liquid flow via expansion geometries is additionally related to some practical engineering applications such as extrusion processes, processing of food stuff, mold filling, ceramics, pharmaceutical matters and other relevant fields. For an extensive period, research on the flow of channels with reversals that face the transformation from symmetry to asymmetry has been met with great enthusiasm. To aid in further numerical and experimental researches of such flows, the flow through a sudden expansion has been regarded as a benchmark because it comprises of a layout among the most primary geometries. However, the simplicity of its geometry need not necessarily indicate that the flow concept is simple as well. Furthermore, reattachment, flow separation and multiple re-circulating zones of fluid flow are those rich areas in which the majority of the researchers are interested. Application of sudden expansion configurations are quite large. The volume of existing literature that focuses on the area of plain sudden expansion is extensive.

There are many experimental and numerical studies adopted the effect of separation flow on the performance of heat transfer with different configurations and boundary conditions. Most of those investigations were carried out for separation air flow and few of them for separation liquid flow in sudden expansion. In the last decade the researchers used nanofluid in their studies for further augmentation of heat transfer.

Study of heat transfer to nanofluid flow in sudden expansion or over backward and forward-facing steps is very limited for the laminar range and most of those studies were numerical as well as turbulent range of nanofluid flow has not been investigated in-depth. The literature review presents that the main efforts for studying the separation flow were

done in the late 1950's. All of these efforts were performed experimentally using many flow visualization techniques and deal exclusively with turbulent or laminar flows. This chapter covered most of the investigations that studied heat transfer and pressure drop of separation flow with conventional fluid and nanofluid in sudden expansion and backward facing step, including the previous correlations which were developed on Nusselt number and friction factor.

2.2 Sudden Expansion

Various engineering systems such as heat exchangers, oil and natural gas pipeline, air conditioning and refrigeration, and electronic systems, need the flow of fluid in channels. Such as systems do not always use straight channels; it comes to the point where an area change is required in order to meet the design specifications. Sudden expansion occurs, when an area of a channel abruptly changes from small to large; whereas for sudden contraction, the area abruptly changes from larger to smaller.

At the point where the fluid flow experiences a sudden area change, there not only occurs velocity fluctuation but also develops static pressure at the downstream. This is a requirement in some engineering systems which requires such flow, because greater heat transfer is required at the cost of higher pumping power required by the fluid in sudden expansion or contraction. It is therefore necessary to study the mechanism of the flow through systems with sudden area change in order to optimize the efficiency heat transfer gain and subsequent friction loss.

2.2.1 Turbulence Flow

A notable numerical work within this area of plain abrupt enlargement was conducted by Abbott and Kline (1962), who experimentally studied the subsonic turbulent flow over both single and double backward-facing steps. Figure 2.1 presents a diagram of the double-step expansion being investigated by them. An investigation was

performed on separated regions of subsonic and turbulent fluid flow at the downstream of 2D systems of backward-facing steps for the Re ranges from a value of 2×10^4 to 5×10^4.

It was concluded that three zones of flow exist within the turbulent separation flow regions: (1) A 3D zone exists directly downstream of step face, and possesses possibly multiple vortexes that rotate around an axis normal to the direction of through flow; (2) a 2D zone downstream of the previous zone, which comprises classic stall patterns of flow moving upstream across the wall, and downstream adjacent to the through flow; and (3) a time-dependent tail zone that momentarily varies in size.

They also mentioned that the three zones have varying lengths for ratios of area over 1.5 for double-step configuration that shows the existence of flow asymmetry. However, for expansion ratios lower than 1.5, the double step approach is used for single step configurations with symmetrical stall areas. According to Figure 2.2, the Reynolds number and the turbulence intensity values ($\sqrt{u}/u_{cr}$) hold a significant impact on flow patterns or reattachment lengths.

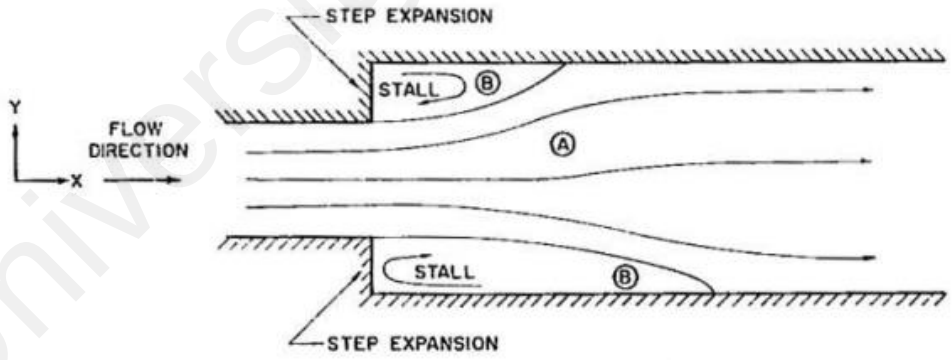

Figure 2. 1: Typical double-step expansion (Abbott & Kline, 1962)

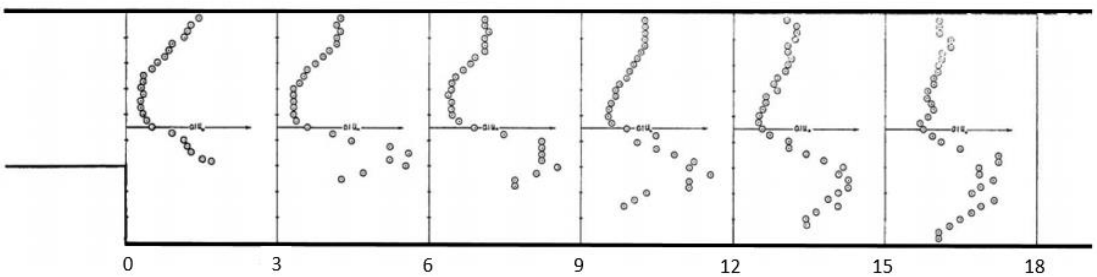

Figure 2. 2: Turbulence intensity for single step (Abbott & Kline, 1962)

Khezzar et al. (1999) experimentally carried out quantitative analyses of combusting and isothermal flows at the downstream of plain abrupt enlargement. They considered an expansion ratio of 2.86, and a Re of 20000 and obtained the equivalent ratios for the rough and smooth combustion as 0.92 and 0.72 respectively. The final result demonstrated that the degree of asymmetry position of the isothermal flows was decreased by coupling the pressure among the two areas of recirculation.

Mizushima and Shiotani (2000) in their work on structural instabilities of bifurcation graph discovered that flows in a symmetrical channel with a sudden expansion have a transition from a symmetrical flow, to an asymmetrical flow, because of a symmetry-breaking pitchfork bifurcation with raising of the Re values in the case of precisely symmetrical system. An inconsiderable imperfection in the model can cause the pitchfork bifurcation to become imperfect. The research developed non-linear stability analyses on a weekly basis to study the structural instability in the bifurcation of these flows. The researchers came up with an amplitude equation for a disturbance by considering the impact of the imperfection of the models. They stressed that this considered weekly non-linear stability theory demonstrated the important and skeleton dynamics of the bifurcation concept, which made the examination of the associated physics of these instabilities possible. In this work, the amplitude equation was used to evaluate the equilibrium amplitude value of the disturbance and then it was compared with the two experimental outcomes of the earlier cases, as well as with the computational solution of the entire non-linear flow equations in mildly asymmetric channels. Comparing the result of the weekly non-linear stability analyses process, to the numerical and experimental results, made it possible to suggest that the parameter range by which the weekly non-linear stability theory provides an accurate approximation limited to the vicinity of the critical point.

Pressure drop and heat transfer for turbulent airflow within an abrupt enlargement pipe equipped with spiral spring item or a propeller swirl generator with multiple pitch ratios were studied by Zohir and Gomaa (2013). They conducted the tests at the Re ranges of 7500 to 18500, and at uniform heat flux conditions. The experimental tests were carried out in three independent pitch ratios for the spiral spring (P/D = 10, 15, 20) and in three zones for a propeller fan (n = 15 blades; blade angle = 650). The effect of the utilization of the freely rotating propeller was discussed, as the input spiral spring on heat transfer improvement and pressure drop. In these trials, the spiral spring and swirl generator were utilized to produce a swirl within the tube flow. They considered both mean Nusselt numbers and relative mean pressure drop and compared them with those acquired from various analogous scenarios. The outcomes from experimentation suggest that the tubes with the propeller at the entrance have shown a great development of heat transfer ratio compared to the plain tube, about 1.69 times for X/H = 5. Regarding the tubes with spiral springs, the heat transfer rate compared to the plain tubes was about 1.37 times higher for the case of P/d = 20. The higher in pressure with utilization of the propeller was shown to be 3 times, and for the case of the spiral spring it was 1.5 times compared to the plain tube. The researchers had developed correlations for the average Nusselt number, spiral spring pitch and the fan location.

Zohir et al. (2011) considered heat transfer and pressure drop properties for turbulent air-flow within an abrupt expanded channel (d/D = 0.72) along with a propeller swirl generator with varying blade angles. The diagram of the considered test section is presented in Figure 2.3. The researchers had examined the effect of Re, in the range of 10000 to 40000 at uniform heat flux conditions. In these tests three different propeller fans with five blades and swirl angles of $\theta = 15^{\circ}, 30^{\circ}, 45^{\circ}$ for the upstream flow; and one propeller fan with swirl angle of 45° for the downstream flow were added separately to the test section. The swirl propeller fan was positioned at various locations inside the test

pipe, S = 10H, 20H and 40H for the upstream values of the tube were maintained for the higher rate of heat transfer (up to 190%) for all of the swirl angles with the highest values at $\theta = 45^{\circ}$.

They concluded that addition of the propeller at the downstream of the tube allows further enhancement in the rate of heat transfer, and putting the propeller at the upstream of the tube also allows further improvement. Moreover, in the case of the propeller at the upstream of the tube at a swirl angle of $\theta = 45^{\circ}$, the rate of heat transfer was increased to 225%. The optimal value of the enhancement factor for the downstream swirl was approximately 326%, while this value was around 213% for its upstream counterpart. Figure 2.4 displays correlations for the relative mean Nusselt number and the enhancement factors for the various fan positions, swirl angles and the Re.

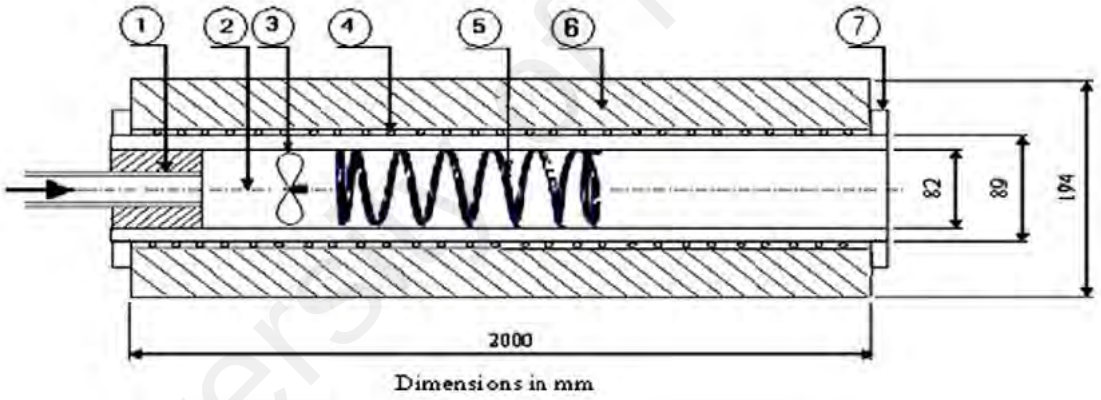

Figure 2. 3: The test section detail (Zohir et al., 2011),

1- Teflon Piston, 2- Test Sections, 3- Propeller Fan, 4- Electric Heater, 5- Spring, 6- Insulation, 7- Flange

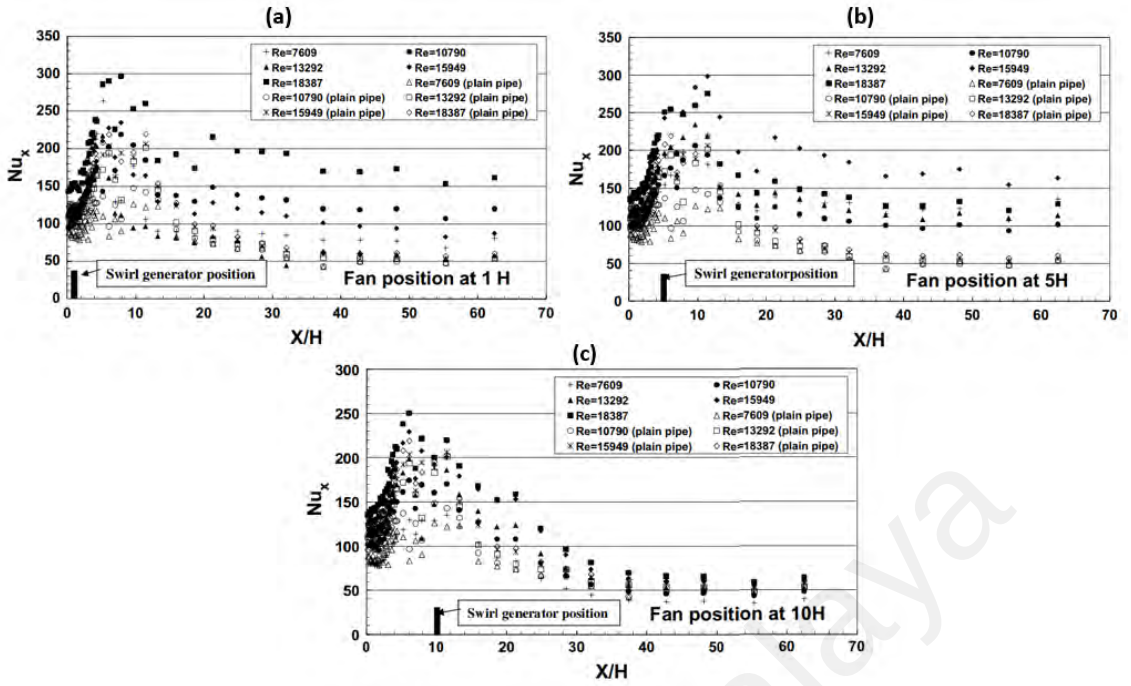

Figure 2. 4: Local Nusselt number variation with dimensionless tube length values for a propeller type swirl generator located at (a) X/H=1, (b) X/H=5, (c) X/H=10 in the plane pipe at various Reynolds numbers (Zohir et al., 2011).

2.2.2 Laminar Flow

Macagno and Hung (1967) examined flow embodiment within a sudden expansion experimental setup for the axisymmetric flows at the Re ranges of 36 to 4500, by computational simulation. The aspect ratio was considered 2; where Re reached a peak of 200. For laminar flow determined the primary task of the eddy is to shape the flow with a quite low energy exchange.

Durst et al. (1974) studied the Newtonian fluid flow within a 1:3 planar symmetrical enlargement by using laser Doppler anemometry (LDA). After several trials, two symmetrical vortices across the walls of enlargement were recorded at Re = 56. In the case of Re = 114, the flow bifurcation was directly seen with vortices of disparate sizes in both of the prominent corners.

The empirical estimations of Cherdron et al. (1978) depended on LDA as well, but they were far more generalized, and they also recorded flow patterns and irregularities in channels with the symmetrical enlargements. The impact of the aspect ratio of the tested

geometry was also studied. Their investigation for conduits with moderate enlargement values showed that, in the case of lower Re values, the channel flow remained steady, 2D and symmetric with two separation locations in close proximity of the enlargement corners, in which the overall size was improved with the increase in Re. On the other hand, for greater estimation of Re, the overall flow generally remains steady, and 2D, nevertheless it also turns into asymmetric, with two different separation areas of varying lengths that can be linked to the lower or upper walls of the corresponding conduit. At a greater Re, further recirculation areas are seen across the walls of the channel.

Armaly et al. (1983) used LDA to search the reattachment lengths and the velocity distribution at the downstream of a single backward-facing step within a 2D conduit. In their work laminar, the transitional and the turbulent air flow at the Re range of 70 to 8000 were considered. They recorded that the several flow phenomena were controlled by common variations of the separation lengths with Re. The results suggest that regardless of the manner in which the inlet flow was 2D and fully developed, the flows at the downstream of the step remained in 2D at both the value of high and low Re. They realized that a secondary vortex was created on both sides of the conduit, with high Re along with the primary recirculating flow area at the downstream of the step.

Oliveira and Pinho (1997) also investigated the Laminar flow of a Newtonian fluid within an axisymmetric channel enlargement area. They studied a limited-volume method for the numerical phase. The result after the computational phase for the flow specifications, e.g. recirculation strength, length, and location centre, were co-ordinated with the existing empirical correlations and data. The primary reason for this work is to quantify the coefficient of pressure loss for several Reynolds numbers, and then compare the results obtained from the simplified theory. This was based on an lD balance of energy and momentum. The researchers discovered great differences in this evaluation, and thus created modified theoretical equations for the estimation of 1D. Moreover, they also

concluded with a correlation value for computing the local loss coefficient as a primary function of Re for the expansion ratio of 1 to 2.6 and the entirely developed conditions. Drikakis (1997) discovered that the critical Re for the symmetry-breaking bifurcation was decreased in the case there was a raise in the expansion ratio. The empirical investigation by Fearn et al. (1990) in a 1:3 planar enlargement suggested a similar flow bifurcation at Re equals to 40.5.

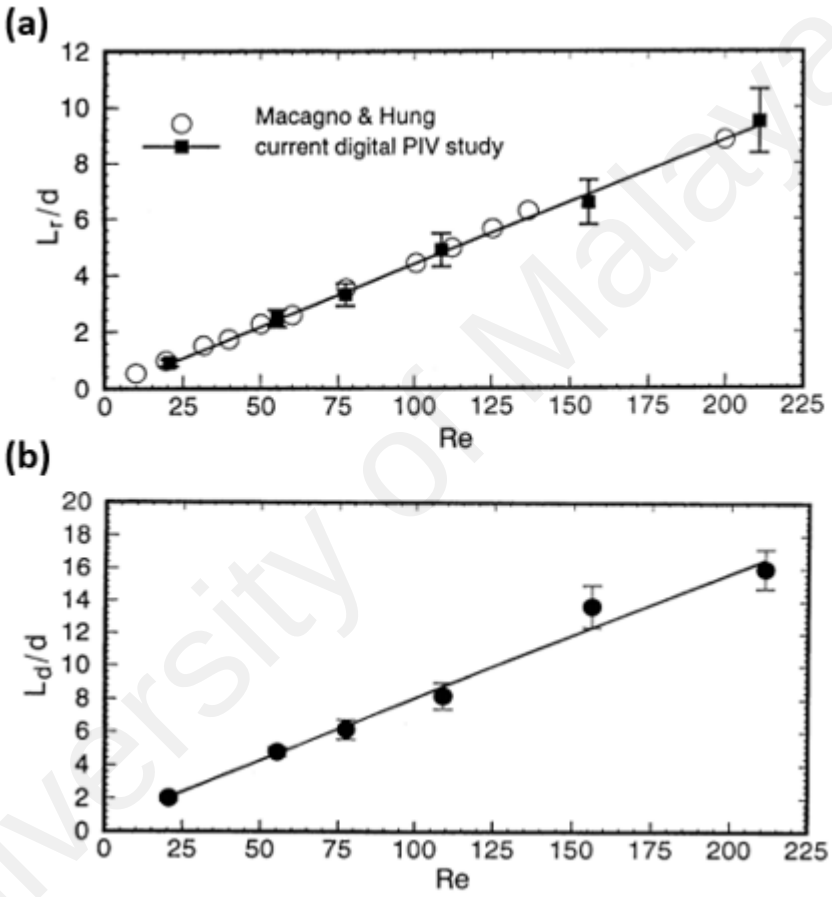

Figure 2. 5: Dependence of (a) reattachment length and (b) of redevelopment length on Reynolds number (Hammad et al., 1999).

Hammad et al. (1999) applied real-time particle image velocimetry (PIV) in a study on laminar flow via an axisymmetric abrupt enlargement that has an area ratio of 2. In this practical experiment, the estimations enclosed the separation areas, reattachment as well as re-development. Velocity maps of two dimensions were acquired on the vertical plane for a total of six different Reynolds numbers, in the bounds of 20 and 211. They investigated the reliance of reattachment and re-development lengths, and the

recirculating flow strength on the Reynolds number. Figure 2.5 illustrates that, not only the reattachment length alone, but also the redevelopment length at the downstream of the reattachment, was generally a linear function of Re. The recirculation eddy strength, however, was nonlinear, and dependent on Re. In addition, they mentioned that the recirculation eddy strength becomes weak with the increase in the Reynolds number value.

Hawa and Rusak (2001) conducted bifurcation analyses, linear stability examination and direct numerical simulations with the dynamics of a 2D, incompressible laminar flow in the symmetric long conduit with abrupt enlargement configuration. The bifurcation analyses of solutions of a set of steady Navier Stokes equations focused on the equilibrium conditions around the critical Re, in which the asymmetric states were simultaneously prevailing. The stability analyses performed were based on the underlying liberalized motion equations for the development of irrelevant 2D disorders enacted on both the steady asymmetric and symmetric conditions. The simulations suggested the relation among the linear stability result and the asymptotic behaviour time of the flow, as mentioned by the asymptotic steady-state solutions. Figure 2.6 shows that the symmetric flows with $Re < Re_c$ are linearly stable in 2D disturbances, while the symmetric conditions with $Re > Re_c$ remain unstable. The dynamics of large and small domain disturbances within the flow are defined, as well as the transformation from symmetric to asymmetric flow is clearly presented. Therefore, the researcher mentions that the critical state is an exchange point of stability for the asymmetric and the symmetric conditions. The overall image of the present research is; in the case of sufficiently lower Re value, the flow is unable to successfully sustain the disturbance or any primary disturbance which diminishes via viscous dissipation. With an increase in the Re value, the viscous dissipation was decreased, and the symmetric flow was altered to stability.

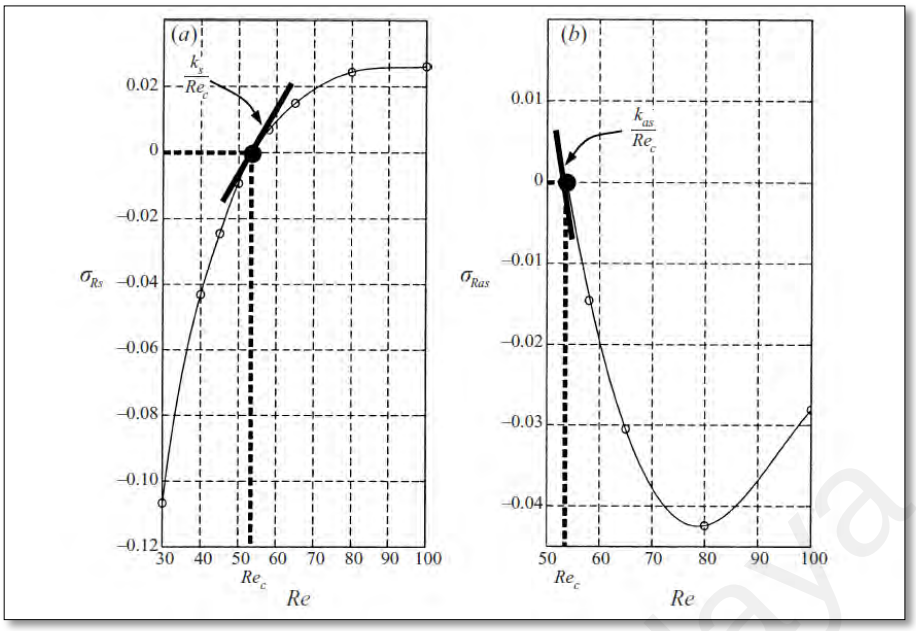

Figure 2. 6: A growth rate of (a) the symmetric and (b) asymmetric states as a function of Re for a channel with D/d=3 (Hawa & Rusak, 2001).

In numerous real-world scenarios, the fluid flowing through flow devices are non-Newtonian, and thus it displayed behaviour as per the complex rheological character. More precisely, they show shear-thinning viscosity, based on the kind of fluid, and it was thus related to examine the non-Newtonian fluid flow in planar enlargements, starting with simplified rheological systems, to individually examine the effect of particular rheological particularities on the flow properties. The non-Newtonian solutions are not very concentrated, and the flows seem to possess a high Re, which leads to turbulent flow. The backward-facing step is a well-defined configuration for work on laminar flow instabilities at high Re. In the past few years, this has attracted scientists in the area of non-Newtonian fluid mechanics who desire to investigate the complicated interaction among these bifurcations and fluid rheology, more specifically, viscoelasticity. The non-Newtonian power – law model is the most simplified one for an entirely viscous fluid that is able to reflect the behaviour of Newtonian fluids and shear-thickening by changing the model parameter, n, which is the power law index.

2.2.2.1 Flow through Planner Sudden Expansion

Kadja and Bergeles (2002) numerically carried out an examination of bifurcation phenomena that occurs in flows via planar abrupt enlargements. A novel convection arrangement; the Variable-Order Non-Oscillatory Scheme (or VONOS), with a multiple grid algorithm, was employed for a detailed examination of bifurcation phenomena occurring in flows via planar abrupt expansion. This new arrangement attributes to a great rise of convergence rate and accuracy. These outlooks allow for a suitable qualitative behaviour of the parameters of flow bifurcation. Figure 2.7 presents the Reynolds numbers under Re_{cr} (Re_{cr}=200); where the flow generally remains symmetric in the entire development period. During this time, the recirculation lengths steadily increases in the direction of their stationary values. However, at the Reynolds numbers over Re_{cr}. The flow was transformed from a symmetric layout to an asymmetric layout in the steady state. One of the primary recirculation areas grow into longer compared to the other, and a third area was seen as the short primary recirculation area on the same side.

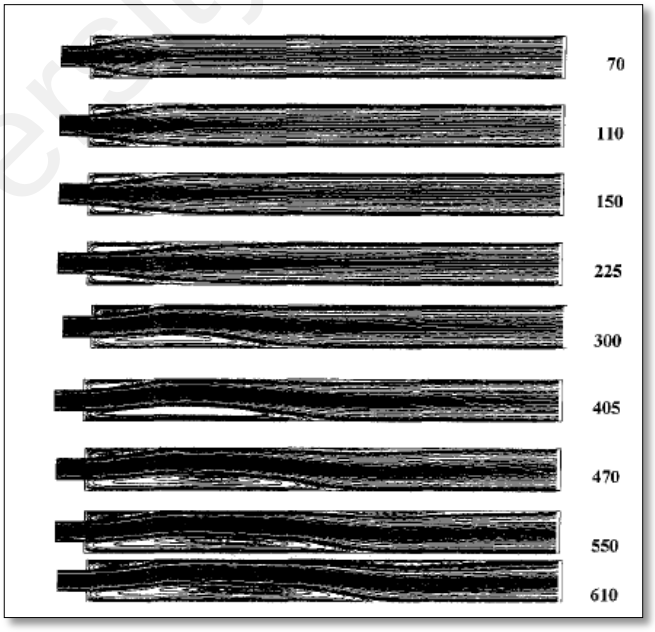

Figure 2. 7: Structure of the internal flow as a function of the Reynolds number (Kadja & Bergeles, 2002).

Mishra and Jayaraman (2002) experimentally studied the asymmetric steady flow pattern of the shear thinning fluid via planar abrupt expansion with a large area ratio (namely, ER = 16). Manica and De Bortoli (2004) also investigated the power-law fluids flow within a 1:3 planar abrupt enlargement, with the different values of: n = 0.5, 1 and 1.5. They listed the observed vortex properties for the values of Re and n which was maintained in the bounds of 30 and 125. They concluded that the bifurcation flow for the shear thinning fluids takes place at the critical Re greater than the values for the Newtonian fluids, whereas the shear-thickening fluid shows the least critical Re.

Neofytou (2006) considered the Casson and power law models and assessed the transformation of symmetric to an asymmetric flow of power-law fluids such as pure viscous fluids by using power-law indices within the bounds of 0.3 and 3 in 1:2 planar abrupt enlargement. Moreover, the impact of the Re on flow patterns was investigated.

Ternik (2009) investigated the flow via 1:3 planar symmetric expansions of non-Newtonian fluid with a shear-thickening function with the use of power-law and quadratic viscosity models. They provided a comparison of the outcomes of the two models, with the models of Newtonian fluids, and mentioned that the flow asymmetry was significantly affected by the shear thickening behaviour. Afterwards, Ternik calculated the shear-thinning fluids flow with power-law indices (n) of 0.6 and 0.8 within a 1:3 planar abrupt enlargement. With the further increase of the general Reynolds number there appears a subsequent flow bifurcation following the initial bifurcation of an asymmetric flow where the shear-thinning causes a delay of the onset of the subsequent bifurcation.

Ternik (2010) also recently once again considered the general Newtonian flow within a 2D, 1:3 abrupt enlargement, configuration by using the FOAM CFD open source software application. The fluid was demonstrated once again by the popular power-law model with a power law index kept within the bounds of 0.6 and 1.4. A set of simulations were carried out for general Reynolds numbers within the bounds of 10^{-4} and 10, and with

emphasizing the analyses of low Reynolds number flow, under the critical condition for the pitchfork bifurcation onset. A low recirculation, common of creeping flow was seen for all of the fluids with shear-thinning behaviour where decreasing the overall strength and size of the secondary flow. Several simulations of power-law fluids flow in a planar 1:3 sudden expansion with the use of open source programs were also investigated by several works. It was discovered that the convergence was frequently a great restriction during the utilization of these codes, especially in the case of non-Newtonian behaviour.

2.2.2.2 Flow through Sudden Expansion in Diffuser

Chakrabarti et al. (2003) extensively investigated the efficiency of sudden expansion from the diffuser perspective. They considered the general momentum and mass conservation formulas in the bounds of 20 and 100, and an aspect ratio of 1.5 to 4, and solved the 2D steady differential equations for the uniform velocity profile and the entirely developed velocity profile at the inlet, as well as for the varying inlet lengths. Moreover, they also investigated in detail the impact of every considered variable on the efficiency of the diffuser, as well as the stagnation pressure drop gradient.

2.2.3 Effect of Geometrical Parameters

So and Ahmed (1989) studied the impact of geometrical parameters and turbulent flow on the efficiency of dump combustors. They investigated two varying expansion ratios and the impact on the flow behaviour of rotation where they discovered that when all of the inlet geometrical and flow parameters with the exception of the step height, remain as it is then the net impact of the expansion ratio on the flow inside the combustor is generally too low.

2.2.4 Effect of Viscous Flow

Shapira et al. (1990) investigated the existence and stability of several solutions for the viscous flow within a sudden expansion channel. They have also investigated the linear stability of a 2D flow via a symmetric conduit. They carried out numerical calculations of the flow field, as well as linear disturbances with the use of the time-dependent finite element technique. The considered conduit's semi-angle was within the bounds of 100 and 900. Their work suggested steady non-symmetrical solutions for high Re compared to a particular critical value. The primary trait of their study lies in how the stability in the lowest stable mode was specified, with the use of an energy-based approach. In their study, there was neither prior proof of the plurality of stable and non-symmetric solutions nor any other limitation points on the non-symmetric divisions.

Foumeny et al. (1996) carried out a numerical investigation on the bifurcations of incompressible Newtonian flow via planar symmetric conduit enlargements. Their investigation placed focus on the specification of the Reynold's critical value, over which the flow was asymmetric based on the conduit configuration. They investigated two models. Firstly, they involved a conduit model where the conduit walls downstream to the enlargement were constructed with no-slip conditions. The second was in the form of a cascade model, where the cyclic boundary conditions were determined. They evaluated the acquired outcome with the numerical and experimental data collected by prior investigations.

The transformation of flow patterns for the simultaneous flow of water and high viscous oil was investigated by Balakhrisna et al. (2010) in a sudden expansion and contraction horizontal channel. From the investigation results, they concluded that these abrupt variations within the cross-sectional area greatly impacted the lube oil and water flow at the downstream phase distribution. The observation indicated a rather simplified technique to produce a core flow, and a technique to prohibit pipe wall, and the witness

of several key differences in flow of water and low viscous oil in similar experimental setup. Numerous kinds of core-annular flows were witnessed for the previous scenario, where a greater interfacial distribution variety characterizes systems of kerosene water. They also investigated the pressure profiles in the simultaneous flow of water and lube oil in the abrupt expansion and contraction, and compared the results with the data of flow of water and low viscous oil. The pressure profiles were considered independent of liquid viscosity, as well as the loss coefficients were witnessed as to be autonomous of flow patterns in both of the two cases.

2.2.5 Different Numerical Methods

Mandal et al. (2011) carried out numerical analyses and efficiency simulation of an abrupt enlargement configuration with a fence observed as a diffuser. The computational domain is shown in Figure 2.8. A simple algorithm was applied to address 2D steady differential equations for the momentum and mass conservation. The Reynolds number was in the bounds of 20 and 100, as well as a fence subtended angle (FSA) within the range of 10° to 30°. The fence's position from the throat varied from 0.2 to 2.6. An aspect ratio of 2 was considered for all the calculations.

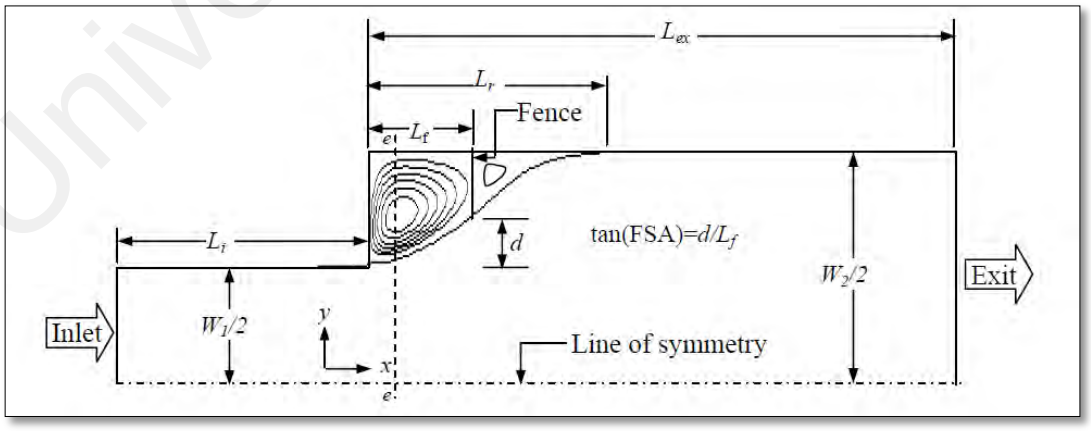

Figure 2. 8: Computational domain (Mandal et al., 2011).

They investigated the impact of every factor on mean static pressure, overall distance of maximum static pressure gain, overall diffuser effectiveness and the average

stagnation pressure. Moreover, they provided a comparison between these with the simple sudden expansion in absence of the fence. Figures 2.9 and 2.10 show the effect of non-dimensional L_f and FSA on mean static pressure. Computation reveals that for smaller Reynolds values the accuracy of possessing a fence was worthy, based on the location and subtended angle of the fence. At any position, the fence consistently presented the advantage at relatively higher Re for any subtended angle of the fence. They revealed that the position of the fence and the subtended angle had no considerable effect on the distance of the optimal static pressure gain from the throat, and average stagnation pressure drop at a certain Re.

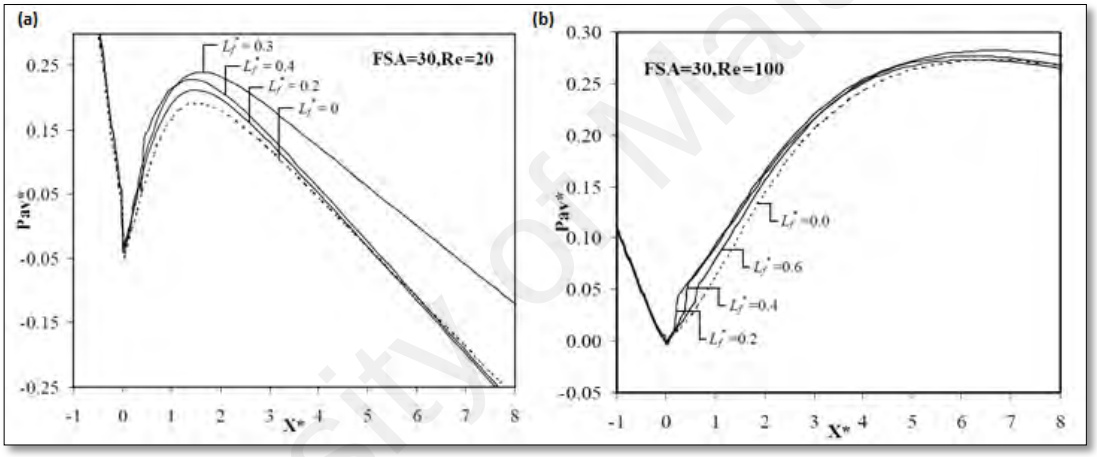

Figure 2. 9: Impact of Non-dimensional L_f on mean static pressure at FSA=30, (a) Re=20 and (b) Re=100. (Mandal et al., 2011)

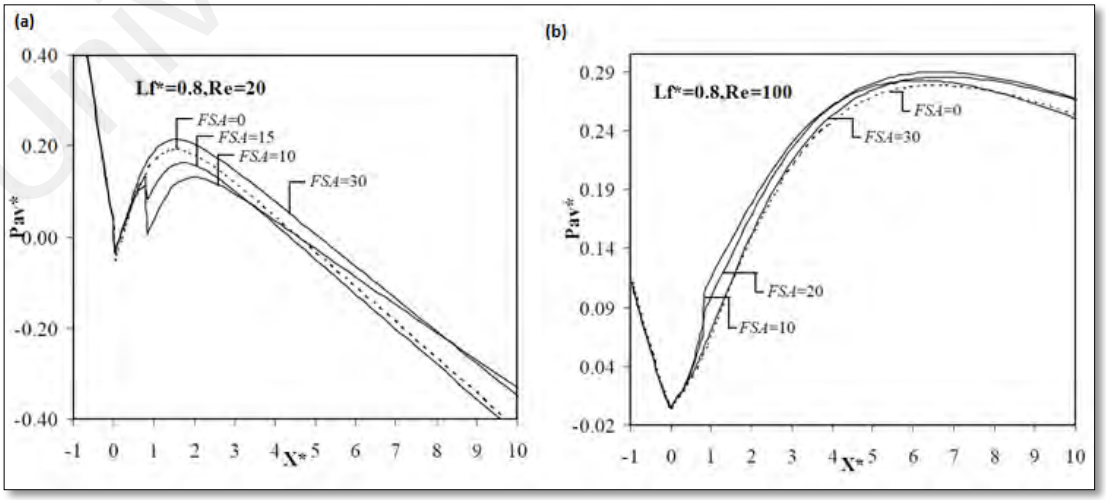

Figure 2. 10: Impact of FSA on mean static pressure at non-dimensional L_f = 0.8, (a) Re=20 and (b) Re=100. (Mandal et al., 2011)

Alleborn et al. (1997) studied the 2D laminar flow of a generally viscous and incompressible fluid in a conduit with abrupt enlargement. They employed a continuance approach to investigate the bifurcation layout of the discretized governing formulas. An Arnoldi-based iterative approach was applied to determine the stability of various solution branches via computing the most unstable Eigen modes of liberalized equations for all the disturbance values. During this observation process more solution branches and bifurcation points were calculated. They investigated the functions of key eigenvalues within the neighbourhood of all these bifurcation points. In the present investigation the numerical outcomes for the limiting cases, for all the flow and geometrical factors, were evaluated with the existing analytical solutions. The investigation showed the existence of weak viscous eddies, referred to as "Moffat eddies", at the expansion corners within the creeping flow limit. The numerically calculated stream procedure was compared for the corner vortices regions with an approximation equation obtained by Moffat, where a suitable agreement with previous results, was established.

Experimental and numerical investigation of a 2D backward-facing step flow was conducted by T. Lee and Mateescu (1998). They applied multiple element hot-film sensor arrays in order to determine the separation and reattachment lengths on the lower and upper walls at Re below 3000, as well as the expansion values of 1.17 and 2.0 respectively. The outcomes achieved from their tests demonstrate that, with the application of multiple hot-film sensors (MHFS), arrays functioned with a set of constant temperature anemometers, the positions of flow separation and reattachment points on the lower and upper walls of the 2D conduit may be computed, simultaneously and non-intrusively. They concluded that the outcomes yielded in using this approach were sufficiently precise within the outcomes estimated by the numerical analyses.

Poole and Ridley (2007) applied the Fluent software in order to numerically compute the development-length needed to obtain fully developed laminar pipe flow for

inelastic power-law fluids. The authors were not able to obtain a converging solution for n values less than 0.4. Ternik et al. (2006) mentioned that the iterative convergence became more time-intensive with a decrease in the power-law indicator and for n values less than 0.6. There were no converged solutions yielded with the use of Foam software. Lima et al. (2008) carried out several simulations of the 2D laminar flow for a backward-facing step channel by the use of two commercial computational fluid dynamics (CFD) codes. The authors assessed the three recirculation flow regions in a unilateral abrupt enlargement. The result for laminar air flow for the Re value was less than 2500. The numerical model equations (of momentum and mass conservation) were addressed with finite element (FEM), and finite volume (FVM) approaches as well as a segregated method to evaluate the separation flow phenomena. To enable the grid to become independent, numerous refinement works were conducted. The final result was compared with the experimental data, and obtained relatively good agreement.

Zdanski and Vaz (2009) yielded results for incompressible, laminar, as well as non-isothermal polymer melt flow within abrupt enlargements. The energy, momentum, and mass conservation laws in the framework of a general Newtonian formulation were incorporated in the model. Two fundamental relationships were used to explain the non-Newtonian flow behaviour, more specifically the Modified Arrhenius Power-law and Cross models. The primary formulas were discretized by the finite difference approach based on central, second-order accurate equations for both the diffusive and convective terms. Velocity and pressure coupling were addressed by considering a pressure Poisson formula. They offered outcomes for two commercially available polymers, and showed the key flow parameters, including viscosity distribution and pressure drop, which were greatly impacted by heat transfer specifications. They finally determined that for the two polymers having similar boundary conditions and regardless of the flow topology resemblance, the variation in pressure calculated was changed because of the viscosity

impact. In this range of issues, the viscosity was much depended on temperature. Consequently, this introduced a strongly coupled property to the issue. The parametric analyses exhibited the pressure distribution with the channel to greatly relate to the expansion ratio as well as the inlet polymer temperature. For a particular expansion ratio, the pressure coefficient was reduced in a linear fashion with the rise in inlet temperature. Regarding the considered conditions, the pressure drop along the channel was decreased by 40% with a decrease in the expansion ratio from 4.0 to 2.0.

Zhang et al. (2010) showed a numerical study of the laminar forced convection of supercritical CO_2 flow within a horizontal channel, along with planar symmetrical abrupt enlargement, as well as its bifurcation phenomenon. The calculations were carried out using differing Reynolds values for cases of various wall heat fluxes. They presented a factor referred to as recirculation disturbance intensity, with the aim to draw conclusions on the decrease of flow stability in the case of an increase in the Re or wall heat flux. The Nusselt number's distribution within the symmetrical flow pattern was shown; the varying peak for the Nusselt number and its relative location were investigated. The pressure coefficient distribution values and wall friction coefficient value are discussed. It was seen that, in contrast to the gas flow, the overall size of the recirculation area had enlarged with the wall heat flux increase, which is attributable to the thermally supported improvement of the reverse pressure difference. The optimal Nusselt value improved as the wall heat flux or Re was raised. With a raise in the Reynolds value, the place of the maximum Nusselt value was not consistently within the area of recirculation, and the location was shifted to the region of recirculation from downstream, and the shifts were moved upstream in the direction of the inlet. Increase in the wall heat flux, the overall movement of the location became irregular. With an increase in the temperature gradient at the wall for greater heating intensity, this irregular value can result from the steep transformation of thermo-physical characteristics close to the wall. The critical Re was

reduced with an increase in the wall heat flux. The increase in the recirculation disturbance intensity makes the flow disturbance stronger, and therefore the flow become less stable; and the critical Re is then reduced.

Nassar et al. (2011) applied a constitutive model that solves the problem with the elastic behaviour of any viscoelastic liquids. They applied the formula in the case of an expansion-contraction axisymmetric flow. Subsequently, a comparison of the result using experimental data from the related literature was presented. For steady, inertia less mathematical solutions were acquired for finding a solution to the balance formulas of momentum and mass through the finite element technique. Thus, for various combinations of the governing parameters they acquired the velocity and stress fields. It was seen that elasticity causes great variations in the position and shape of the yield surface, the deformation fields' rate in the cavity and impacting the extra stress. The trends seen were in line qualitatively with the graphical outcomes existing in the related works.

Kaushik et al. (2012) worked on a computational fluid dynamic simulation to study the core annular flow via abrupt expansion and contraction. They modelled a core annular flow of water and lubricating oils with a VOF approach, and a good match among the numerical data and the outcomes from the experimental setup was yielded. A deep investigation was carried out to produce the profiles of velocity, pressure, and volume fraction through an extensive variety of water and oil velocities, for sudden contraction and expansion. Additionally, an asymmetric nature of velocity along the radial plane in the two cases was reported by them.

2.2.6 Sudden Expansion in Rectangular Duct

Durst et al. (1993) investigated the planar symmetrical abrupt enlargement flow for several low Re. They conducted several numerical predictions and measurements for the flow via a planar 2D channel with an asymmetric abrupt enlargement and the expansion

ratio of 1:2. The two numerical and experimental predictions agreed to witness a symmetry breaking bifurcation of flow causing a short and long separation area for Re over 125, and on the basis of the altitude of the upstream channel as well as the highest flow velocity at the upstream. They witnessed a growth in the overall length of the long separation area. The short area remained stable with an increase in the Reynolds numbers to over 125. They applied a LDA to acquire the numerical predictions and empirical data that were conducted by using a finite volume method.

Mistrangelo and Bühler (2007) numerically had studied MHD flows in abrupt enlargements of rectangular channels, using an asymptotic-numerical technique. The mathematical utility comprises in an extended variant of the commercial code CFX, allowing for effective outcomes and for any Hartmann numbers up to 1000. The asymptotic technique was used for creeping MHD flow at magnetic fields that are very strong. The Numerical result was recorded for higher imposed magnetic fields and for a stable Reynolds number. They claimed that, for intermediate Hartmann numbers, eddies may appear underlying the enlargement. On the other hand, they were already suppressed at Ha value greater than 60. Additionally, areas with minimal velocities were recognized near the outer corners of the cross-sectional enlargement. In terms of intense magnetic fields, the internal layers were created at the enlargements that gather the flow from the upstream core and disseminate a relatively big portion to the side layers.

The extra pressure drop as a result of 3D induced currents was quantified, and so was the flow rate by the single internal layer and the side layer. Several tests on MHD flows within electrically conducting abrupt enlargements in rectangular channels were carried out by Bühler et al. (2007) for high Hartmann numbers. The overall distribution of wall potential and the distribution of pressure across the Hartmann wall were estimated up to the values over Ha = 5000. The reduction in pressure data comprised an inertial distribution that may be rather considerable for mild N, but it disappears asymptotically

with the increase of N up to the value of infinity. On the other hand, even for the peak result conducted in this study (N = 39,151), a relatively small inertial contribution was seen. In the case, where N moves to infinity the overall measurement shows that inertia has less asymptotic predictions for the pressure distribution. On the basis of the examination of the wall potential, it is likely to detect the reduced velocity at the core centres and the inclined velocity nearer to the side walls when moving towards the enlargement. The side wall potential profiles provided more information on the distribution of the flow rates of the local side layer. This suggested a side layer jet that was strong directly underlying the enlargement. An evaluation between calculated and measured surface potentials was carried out for the symmetrical plane and at the side wall, which displayed parallel conclusions.

Aloui and Madani (2008) investigated the features of flow of aqueous foam via a horizontal abrupt enlargement that is localized at the center of a horizontal channel. Using a square cross-section 21× 21 mm^2 for the upstream, as well as a rectangle cross-section 21× 42 mm^2 for the downstream, this uniqueness had an aspect ratio of 0.5. With the abrupt enlargement, they investigated wet foam flow dynamics near the singularity by using of PIV, regular pressure loss, static drainage, underlying liquid film thickness, as well as bubble sizes and local void fraction. Near the expansion, a singular pressure increase was seen by extrapolation with the use of the linear static pressure measurement evolutions acquired in the downstream and upstream at a remote distance from the singularity. On the other hand, the mean and fluctuating velocities with a PIV technique close to the singularity, were acquired from a set of 150 immediate snapshots for every selected quality of the low foam reorganization. They studied the impact of the existence of this singularity on the liquid film thickness values, for all the three scenarios under investigation (scenario A: U = 2 cm/s; scenario B: U = 3 cm/s; scenario C: U = 4 cm/s). Considering 1D flow and after the completion of the gravitational drainage, the liquid

film thickness value does not depend on the foam velocity. In a 2D flow, this thickness is reduced in the case where the foam velocity is inclined. With regards to the gravitational drainage, they had recorded that the overall volume of drained liquid was reduced with the quality of foam N, as well as with the foam velocity. Downstream of this backward-facing step, the local void fraction and the bubble size were both impacted by singularity pressure. These outcomes suggested that the existence of these singularities within the foam flow models may have a significant impact on the foam's end-of-duct layout.

Sousa et al. (2011) studied the 3D flow of viscoelastic and Newtonian fluids via square-square enlargements. Graphical representations of the flow patterns were created with the use of streak photography; the flow's velocity field was estimated in detail with the use of a particle image velocity-meter. Moreover, a pressure drop measurement was recorded. They studied the Newtonian fluid flow for several expansion ratios: 1:2.4, 1:4, and 1:8, and then provided a comparison of the numerical results and the experimental results. For all of the area ratios investigated, a corner vortex was seen downstream of the backward-facing step, and an inclined in the flow inertia causes an improvement in the vortex size. They came to a consensus for a comparison of the numerical and the experimental results. The two non-Newtonian fluids flow was studied practically for several expansion ratios 1:2.4, 1:4, 1:8 and 1:12. These were compared with other numerical simulations using FENE-MCR, Oldroyd-B and sPTT constitutive formulas. In case of shear-thinning viscoelastic and the boger fluids, a corner vortex was developed at the downstream of the enlargement, which was reduced in strength and size with the increase of the elasticity of the flow. The recirculation created downstream of the square-square enlargement for all of the investigated fluids and expansion ratios, it shows a 3D layout via a helical flow. It could be noted that this was also anticipated in the numerical simulations conducted earlier.

2.3 Nanofluids

Industrial processes involving heating and cooling of fluids flowing inside the conduits of all sorts are widespread and represent some of the most common and important processes found in engineering today (Kreith et al., 1997). Indeed, in thermal engineering, forced convection is probably the most effective and widely used means to transfer heat. Applications include various types of heat exchangers, heating and cooling units, impinging jets, and a multitude of other flow-induced heat transfer situations. As heat transfer is of course directly related to the fluid's thermophysical properties, the possibilities of increasing, in particular, a fluid's thermal conductivity is quite appealing. Increased demands for improved cooling and heat dissipation technologies as well as the growing need for more compact and energy-efficient thermal management systems are continuously challenging engineers to come up with innovative solutions. The high level of interest for nanofluids in recent years is directly related to its potential of becoming a next-generation heat transfer medium. Conventional coolants such as water, ethylene glycol, and oils typically have lacklustre heat transfer performances. Engineers have therefore considered adding various types of solid particles in suspension in these coolants in order to provide heat transfer enhancement.

Initial attempts using particle sizes in the micron range were less than successful due to considerable adverse effects. Recent advances in manufacturing technologies have made the production of particles in the nanometer scale possible. Initial studies revealed that the use of suspensions containing nanoscale particles having higher thermal performance as heat transfer mediums were very promising. In essence, high-performance coolants could provide more compact, energy efficient heat management systems and provide more efficient localized cooling. Examples of benefits could include smaller/lighter heat transfer systems, reductions of heat transfer fluid inventories, reductions in emissions, and so on. Engineers are therefore hopeful that these special

solid– liquid mixtures will offer opportunities for development and innovation in a wide range of technological sectors.

Nanofluids were created by Chol (1995), after realizing that the mixture of nanoparticles (1-100 nm) with a base fluid enhances heat transfer. Materials commonly used as nanoparticles include chemically stable metals (e.g. gold, copper), metal dioxides (e.g., alumina, silica, zirconia, titania), dioxide ceramics (e.g. Al_2O_3, CuO), metal carbides (e.g. SiC), metal nitrides (e.g. SiN), carbon in various forms (e.g., diamond, graphite, carbon nanochannels, fullerene) and functionalized nanoparticles (Cheng, 2009).

In the previous decade, scientists had tested different kinds of nanomaterials for making nanofluids. Al_2O_3, SiO_2, ZnO, CuO, zirconia and silver are more common metal and metalloid oxides for preparing nanofluids compared to other metal oxide nanofluids (Khoshvaght-Aliabadi, 2014; Peyghambarzadeh et al., 2014; Yarmand et al., 2014; Yarmand et al., 2015). Additionally, many researchers (S. Choi et al., 2001; Das et al., 2003; Karthikeyan et al., 2008; Turgut et al., 2009; Yarmand et al., 2015) have experimentally worked with Carbon based materials such as Graphene (Yarmand et al., 2016), graphene oxide (GO) (Sudeep et al., 2014) and carbon nanotubes (CNTs) (YJ Hwang et al., 2006; Z. Nikkhah et al., 2015). The material on the nanometer scale has special chemical and physical properties, so the nanofluids have been attractive to the scientists. Specifically, several nanofluids have demonstrated the improved thermal conductivity which makes them appropriate for use as working fluids. The previous experimental works showed that the nanofluid could increase the convective heat transfer compared to the pure base fluids.

Although effective thermal conductivity enhancement is very promising, it is certainly not the only factor weighing in on a nanofluid's potential as a heat transfer medium. Other important factors include some other thermophysical properties such as

viscosity and specific heat, as well as flow-related parameters and considerations such as particle clustering and migration, nanofluid stability, and, of course, flow conditions (Figure 2.11).

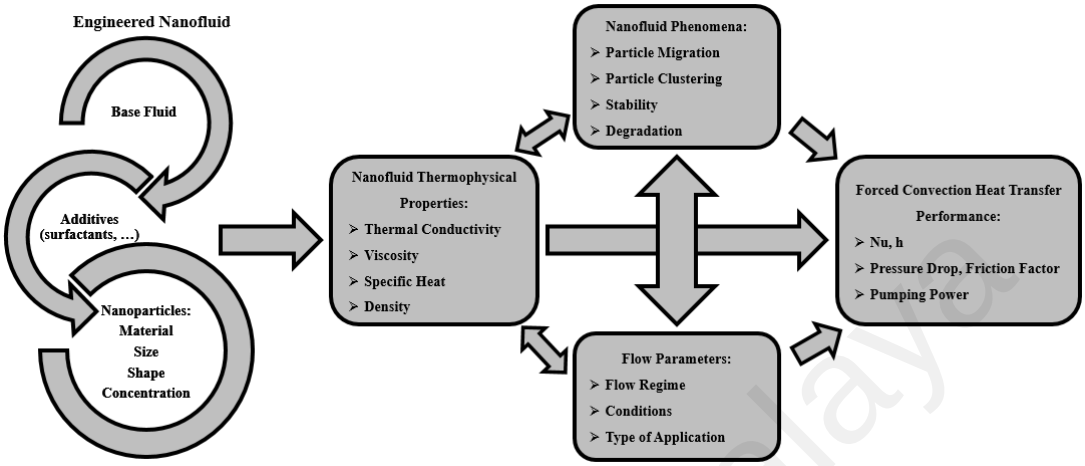

Figure 2. 11: Factors influencing nanofluid forced convection heat transfer performance.

2.4 Nanofluid Effective Properties

Obviously, the choice of nanofluid effective properties will have considerable effects on the obtained results for any forced convection problem. Indeed, contradicting results by various research groups can, at least to a certain extent, be blamed on the dispersion of experimental data on such properties as nanofluid effective thermal conductivity and viscosity. Furthermore, the multitude of theories and correlations that have been used and developed for these thermophysical properties will undoubtedly yield results, predictions, and conclusions that can be strikingly different.

Properties such as density and heat capacity are most commonly based on the basic mixing theory for a two-component mixture, whereas nanofluid effective thermal conductivity and viscosity are more complex to accurately model. Various approaches have been used by different authors; these include using relationships developed over the past century for conventional solid–liquid mixtures, simple correlations developed strictly

from experimental data obtained for specific types of nanofluids (e.g., as a function of particle volume fraction only), or correlations encompassing various important parameters (e.g., temperature, particle size, particle volume fraction, etc.). As more knowledge is gained on the behaviour of nanofluids, more adequate correlations encompassing various factors will be developed.

2.4.1 Density

Amongst the different thermo-physical properties of nanofluids, viscosity and thermal conductivity were more interested for the researchers (Chandrasekar et al., 2010; Mintsa et al., 2009; Papari et al., 2011; Ren et al., 2005). A few numbers of researchers worked on other properties such as specific heat and density. Viscosity and thermal conductivity are not enough to evaluate heat transfer coefficient theoretically. Specific heat and density are also essential for heat transfer information (E Montazer et al.). Since these properties have significant influence on nanofluid flow and heat transfer characteristics, so they should be determined accurately (Maiga et al., 2005). Although, experimental evaluation of nanofluid properties encounter a lot of limitations such as difficulties in preparing monodisperse suspensions, methodical problems in measuring particle size, concentration, and inhomogeneity of its solution. The ranges of the investigated variables are limited accordingly. Therefore, some density measurements have been presented for different nanofluids at various conditions (Pastoriza-Gallego et al., 2011), while suggesting the reported theoretical correlation for the estimation of nanofluids density is based on simple model (R. Vajjha et al., 2009). Nanoparticle concentration increment displays the role of the interaction on the fluid density since the effect of particle size and size distribution on density is almost negligible (Maiga et al., 2005; E Montazer et al.).

Nanofluid density is typically obtained by measuring the volume and weight of the mixture. The particle volume fraction ϕ can be estimated knowing the densities of both constituents (Equation 2.1) (Pak & Cho, 1998):

$$\rho_{nf} = (1 - \emptyset)\rho_{bf} + \emptyset\rho_{nP} \tag{2.1}$$

By rearranging the above equation, one can therefore determine the volume fraction ϕ of the mixture (Equation 2.2). Nanoparticle densities are usually values obtained in the available literature. This approach has been used by most nanofluid researchers to date.

$$\emptyset = \frac{\rho_{nf} - \rho_{bf}}{\rho_{nP} - \rho_{bf}} \tag{2.2}$$

2.4.2 Specific Heat

In some cases, considering nanofluid convective heat transfer flows, it was suggested that nanofluid specific heat be calculated using the following equation based on the simple mixing theory (Equation 2.3) (Y.-j. Hwang et al., 2007; Jang & Choi, 2007; Maiga et al., 2005; Pak & Cho, 1998):

$$C_{P,nf} = (1 - \emptyset)C_{P,bf} + \emptyset C_{P,nP} \tag{2.3}$$

Others, however, have used an alternate approach based on heat capacity concept (can be deduced from the first law of thermodynamics). Some have stated that this approach is more accurate (Buongiorno, 2006; Manca et al., 2012; Xuan & Roetzel, 2000):

$$(\rho C_P)_{nf} = (1 - \emptyset)\ (\rho C_P)_{bf} + \ \emptyset(\rho C_P)_{nP} \tag{2.4}$$

$$C_{P,nf} = \frac{\emptyset\ (\rho C_P)_{nP} + \ (1 - \emptyset)\ (\rho C_P)_{bf}}{\emptyset\ \rho_{nP} + (1 - \emptyset)\rho_{bf}} \tag{2.5}$$

Both of these formulations (Equations 2.4 and 2.5) will, of course, produce different results for specific heat. Available experimental results for nanofluid specific heat seem to confirm that the heat capacity concept does indeed yield more accurate predictions (Barbés et al., 2013; Zhou & Ni, 2008).

2.4.3 Thermal Conductivity

Most researchers seem to agree that various theories and correlations developed for conventional solid–fluid flows are not appropriate for nanofluids. A multitude of theories on the mechanisms responsible for the (according to some) anomalous increases in heat transfer capabilities of nanofluids and their corresponding relationships and correlations have been developed over the past 20 years. However, there does not seem to be a consensus on what is the most appropriate or accurate approach.

For example, in their literature review, X.-Q. Wang and Mujumdar (2008) identified over 20 different thermal conductivity models which could be potentially used for nanofluids. Undoubtedly, this number has considerably increased since then. Interestingly, some studies have shown that relationships originally derived for conventional liquid–solid particle mixtures appear to be reasonably adequate for liquid–nanoparticle mixtures, especially for low particle volume concentrations. Indeed, Maxwell (1881) original equation for particulate suspensions as well as subsequent extensions and developments, including the Hamilton and Crosser (1962) correlation, has been used by various authors for numerical modelling of confined flows using nanofluids (Equation 2.6):

$$\frac{k_{nf}}{k_{bf}} = \left[\frac{k_{np} + (n-1)k_{bf} - (n-1)\emptyset(k_{bf} - k_{np})}{k_{np} + (n-1)k_{bf} + \emptyset(k_{bf} - k_{np})}\right] \qquad (2.6)$$

$$n = 3/\psi$$

Where n is the empirical shape factor. For spherical particles $\psi = 1$, the Hamilton–Crosser equation reduces to the following equation (Equation 2.7) (Wasp et al., 1977):

$$\frac{k_{nf}}{k_{bf}} = \left[\frac{k_{np} + 2k_{bf} - 2\emptyset(k_{bf} - k_{np})}{k_{np} + 2k_{bf} + \emptyset(k_{bf} - k_{np})}\right] \qquad (2.7)$$

In various studies on convective nanofluid flows, this equation is often expressed, for example, in case of water–Al_2O_3 nanofluids (Equation 2.8):

$$k_{nf} = k_{bf}\,(4.97\,\emptyset^2 + 2.72\,\emptyset + 1) \quad (2.8)$$

Several authors found that results obtained with this approach can give results in relative agreement with their experimental results, at least in certain conditions (Barbés et al., 2013; Mintsa et al., 2009; Xuan & Li, 2000). The Hamilton–Crosser equation and derivatives have been used quite extensively in few studies, especially for early work on forced convection problems (Akbarinia & Behzadmehr, 2007; Khanafer et al., 2003). However, the most notable drawbacks of the Hamilton–Crosser model (and others of the same type) are some important physical parameters such as temperature and particle size which are not considered including other important parameters leading to different phenomena. As such other authors used various expressions developed over the past few years based on various experimental data sets. For example, some authors used experimental data obtained in-house in order to better compare numerical results with the corresponding experimental data. One such case is presented in the study on confined nanofluid radial flow by Gherasim et al. (2011), in which the data obtained by Mintsa et al. (2009) was used for nanofluid effective thermal conductivity.

Some of the most recent numerical research projects have used multivariable correlations, which can be used to predict nanofluid effective thermal conductivity. These include those developed by various groups (C. H. Chon et al., 2005; Koo & Kleinstreuer, 2004). The C. H. Chon et al. (2005) correlation has been used by C. T. Nguyen et al. (2007) in their study of heat transfer enhancement using nanofluids in an electronic liquid cooling system and by Abu-Nada (2009) in his study on heat transfer enhancement in natural convection. The correlation developed by Corcione (2011a) is similar in structure of the one developed by Chon et al. and it has also been used by some authors as it is based on a comprehensive set of experimental data obtained by several research groups (Equation 2.9):

$$\frac{k_{nf}}{k_{bf}} = 1 + 4.4Re_{np}^{0.4}Pr_{bf}^{0.66}\left(\frac{T}{T_{fr}}\right)^{10}\left(\frac{k_{np}}{k_{bf}}\right)^{0.03}\emptyset^{0.66} \quad (2.9)$$

Where Re_{np} is the nanoparticle Reynolds number, Pr is the Prandtl number of the base liquid, T is the nanofluids temperature, and T_{fr} is the freezing point of the base liquid. The Reynolds number is defined as $Re = (\rho_{bf} u_B d_{np})/\mu_{bf}$, where ρ_{bf} and μ_{bf} are the mass density and dynamic viscosity respectively of the base fluid and d_{np} and u_B are the nanoparticle diameter and Brownian velocity, respectively. Once u_B is calculated as the ratio between d_{np} and the time required to cover distance $\tau_D = (d_p)^2/6D$ (Keblinski et al., 2002) where D stands for the Einstein diffusion coefficient. The nanoparticle Reynolds number is given by Equation (2.10).

$$Re_{np} = \frac{2\rho_{bf}k_b T}{\pi\mu_{bf}^2 d_{np}} \quad (2.10)$$

Where $k_b = 1.38066 \times 10^{-23} J/K$, is the Boltzmann constant. All the physical properties in Equations (2.9) and (2.10) are calculated at nanofluids temperature *T*.

C. H. Li and Peterson (2006) documented the effect of particle size on thermal conductivity enhancement. They showed that 36 nm Al_2O_3 in water had larger thermal conductivity enhancement than 47 nm Al_2O_3 in water, especially at high temperatures (35.5 °C); however, the difference between these two nanofluids is indistinguishable at 28 °C. H. Chen et al. (2008) observed that aqueous suspension of titanate nanotubes (aspect ratio is approximately 10) have higher thermal conductivity enhancement than the data predicted by the Hamilton–Cross model. Timofeeva et al. (2009) reported that the effective thermal conductivity predicted by the Hamilton–Cross model is significantly diminished by interfacial effects proportional to the total surface area of nanoparticles; the results were consistent with the prediction of the Hamilton–Cross model for spherical particles.

Several studies have reported on the effect of temperature and on thermal conductivity of the nanofluids. H. Chen et al. (2008) reported that the thermal conductivity increases with the increase of the temperature of the nanofluid. This conclusion is similar with that presented by C. H. Li and Peterson (2006), who found that thermal conductivity significantly increases with small increases in temperature. A total of 6% volume fraction of CuO nanoparticle/distilled water suspension increased the effective thermal conductivity by 1.52 times that of pure distilled water, and 10% Al_2O_3 nanoparticle/distilled water suspension increased the effective thermal conductivity by a factor of 1.3 at 34 °C. However, some researchers documented that thermal conductivity increased only slightly as the temperature of nanofluids increased slightly. C. Chon and Kihm (2005) observed a lesser increase in thermal conductivity than that of Das at the same temperature range. Thermal conductivity increase at different temperatures is affected by particle size in the colloidal suspension system. Small particle size in the nanofluids result in large thermal conductivity increase at high temperatures, whereas large particles in the nanofluids result in small thermal conductivity increase at high temperatures. However, Timofeeva et al. (2007) argued that thermal conductivity enhancement of nanofluids relative to base fluids at elevated temperatures is independent of temperature by investigating both water- and EG-based nanofluids.

Nan's modified Maxwell's model was employed to predict the thermal conductivity ratio of nanofluids (Nan et al., 1997). The model determined the effects of particle geometry and finite interfacial resistance. The expression of the model is presented in Equation (2.11).

$$\frac{k_{nf}}{k_{bf}} = \frac{3 + j[2b_{11}(1 - L_{11}) + b_{33}(1 - L_{33})]}{3 - j(2b_{11}L_{11} + b_{33}L_{33})} \tag{2.11}$$

Where L_i represent particles shaped as prolate ellipsoids with principal axes $a_{11} = a_{22} < a_{33}$.

$$L_{11} = \frac{P^2}{2(P^2-1)}\frac{P}{2(P^2-1)^{3/2}}\cosh^{-1}P\ , L_{33} = 1 - 2L_{11}\ , P = a_{33}/a_{11}\ , b_{ii} = \frac{k_{ii}^c - k_f}{k_f + L_{ii}(k_{ii}^c - k_f)}$$

$$k_{ii}^c = \frac{k_{np}}{1+\gamma L_{ii} k_{np}/k_{bf}},\ \gamma = (2 + 1/P)R_{bd}\, k_{bf}/(a_{11}/2)$$

R_{bd} is the (Kapitza) interfacial thermal resistance. The upper bound of this prediction neglected interfacial thermal resistance (R_{bd} = 0), while the lower bound used a typical value of interfacial resistance (10^{-8} m^2 K/W). The final results showed that thermal conductivity enhancement of nanofluids is predicted by the lower bound theory with a < 17% error, while the upper bound theory predicts 90% of data with a < 18% error. Shape size has a key function in thermal conductivity enhancement of nanofluids. Thermal conductivity of nanofluids has been thoroughly investigated, but discrepancies still exist. The nature of particles, heat transfer of the fluid, and particle size and distribution affect the physical properties of the prepared nanofluids. The nanofluid synthesis process should be standardized and fully understood. Measurement methods also strongly influence the results of measured physical properties.

Theoretical mechanisms have been proposed to explain anomalous effective thermal conductivity enhancement. These mechanisms include the Brownian motion of particles, nanolayer structure at the interface nanoparticle medium, and nanoparticle clustering or agglomeration (Lamas et al., 2014). Keblinski et al. (2002) proposed to neglect the Brownian motion because the theoretical Brownian diffusion of nanoparticles is slower than thermal diffusion of the base fluid. Moreover, researchers observed from experimental studies that the dependence of thermal conductivity enhancement on Brownian mechanisms is negligible because they simply follow the temperature behavior of the base fluid. The nanolayer theory states that liquid molecules near solid surfaces become more organized than bulk liquids and form a solid-like layer that enhances heat conduction through the medium. However, Kapitza resistance at the nanoparticle medium interface could 49 negatively affect possible enhancements from the nanolayer structure.

A recent benchmark study suggested that effective thermal conductivity of nanofluids depends on the effective medium theory, which states that spatial distribution of particles in the medium is the key to observed enhancements (Lamas et al., 2014). The most commonly studied nanoparticles in thermal nanofluid engineering include Cu, CuO, Al_2O_3 , and CNTs (F.-C. Li et al., 2013; Ponmozhi et al., 2010). CNT-based nanofluids exhibit the highest enhancement on effective thermal conductivity under the same experimental conditions. This condition is explained by the high thermal conductivity and geometrical aspect of individual CNTs (Hasselman & Johnson, 1987; Lamas et al., 2014).

Phuoc et al. (2011) prepared the nanofluids by dispersing MWCNTs in deionized water (DW). Thermal conductivity enhanced from 2.3% to 13% for nanofluids with 0.5 wt% to 3 wt% MWCNTs (0.24 vol% to 1.43 vol%). S. Choi et al. (2001) reported significant enhancements for MWCNTs (mean diameter: 25 nm and length: 50 μm) in oil suspension at room temperature. Thermal conductivity increased by more than 160% at 1% volume fraction compared with that of the base fluid. Ding et al. (2006) reported a maximum enhancement of 79% at 1 wt% MWCNT dispersed in water with SDBS as surfactant. Assael et al. (2004) observed thermal conductivity enhancement of 38% for 0.6 vol% CNTs in water stabilized by SDS and CTAB. Ghozatloo et al. (2013) investigated the thermal conductivity of functionalized graphene nanofluids prepared via the alkaline method. Nanosheet graphene was synthesized using CVD. Thermal conductivity enhancement was 13.5% for sample 1 (0.05 wt%) and 12.5% for sample 2 (0.03 wt%) at 25 °C; sample 1 increased to 17% at 50 °C. F.-C. Li et al. (2013) prepared viscoelastic fluid-based nanofluids (VFBN) using viscoelastic aqueous solution of cetyltrimethyl ammonium chloride/sodium salicylate as base fluid and MWCNTs as nanoparticles. The experimental thermal conductivities of the tested VFBNs were significantly higher than those of corresponding base fluids. These thermal conductivities increased as particle volume fraction and fluid temperature increased, which

demonstrated potential for heat transfer enhancement. With significantly increasing thermal loads in microelectronics and higher-powered automobiles, the need for high performance cooling fluids increases each year. Conventional approaches that use extended surfaces require additional pumping power and have been assumed to have reached their limits. Various attempts have been made to increase the thermal conductivity of the fluid itself (D. Lee et al., 2006). Chol (1995) presented the possibility of using a new type of fluid-containing nanoparticles in 1995, and has also reported about the large enhancements that exceed 100% in effective thermal conductivity (K_{eff}) of these fluids. This prospect for fluids and nanofluid enhancement triggered researchers to determine the best combinations of particles and solvents (S. Choi et al., 2001; Eastman et al., 2001; S. Li & Eastman, 1999; Murshed et al., 2005; Patel et al., 2003; Timofeeva et al., 2007; Timofeeva et al., 2009; Tu et al., 2004; Wen & Ding, 2005; Xuan et al., 2003; Xuan & Roetzel, 2000; You et al., 2003) and to clarify governing mechanisms (Jang & Choi, 2004; Keblinski et al., 2002; Kumar et al., 2004; B.-X. Wang et al., 2003).

Different mechanisms have been proposed to explain thermal transport enhancement, including interfacial resistance, nanoparticle motion, liquid layering at particle liquid interface, and nanoparticle clustering (Eastman et al., 2004b). Nanoparticle motion (Brownian motion) (Bhattacharya et al., 2004; C. Chon & Kihm, 2005; Koo & Kleinstreuer, 2004; Krishnamurthy et al., 2006; Prasher et al., 2005; Wong & Kurma, 2008), and nanoparticle clustering (Hong et al., 2006; D. Lee et al., 2006; Prasher et al., 2006; B.-X. Wang et al., 2003; Xuan et al., 2003; Yu & Choi, 2004) have attracted the most attention.

Keblinski et al. (2002) proposed three conceivable mechanisms that are important for abnormal increases (i.e., Brownian motion, liquid layering, and ballistic phonon transport). These mechanisms provide insight into the most important factor that affects effective thermal conductivity (K_{eff}). Although the effect of Brownian motion was shown

to be negligible through a scaling analysis, a few researchers still argue its influence. For example, Jang and Choi (2004) and Kumar et al. (2004) derived their own formulas to consider the nanoconvection caused by Brownian motion. Both of the research groups predicted K_{eff} well using different equations (Kumar et al., 2004). Both of the groups also disregarded metal oxide particles to validate the high aggregation in the Brownian models (Jang & Choi, 2004; Kumar et al., 2004; D. Lee et al., 2006). Aggregate particles move more slowly than isolated particles. Thus, mobility equivalent size (often called hydrodynamic size) should be used instead of primary particle size.

2.4.4 Dynamic Viscosity

Several rheological studies have determined that at least certain types of nanofluids behave as Newtonian fluids for varying ranges of particle volume fractions (Halelfadl et al., 2013; Heris et al., 2006; Kulkarni et al., 2007). Generally speaking, a fluid is considered "Newtonian" if its viscosity is independent of shear rate. In probably the first investigation interested in this question, Pak and Cho (1998) considered 13 nm Al_2O_3 and 27 nm TiO_2 particles suspended in water. From their study, they determined that the viscosities of the dispersed fluids with Al_2O_3 and TiO_2 particles at a 10% volume concentration were, respectively, approximately 200 and 3 times greater than that of water. Furthermore, they found that mixtures containing Al_2O_3 and TiO_2 particles showed shear-thinning behavior at or above the volume concentration of 3% and 10% respectively. Similarly, Das et al. (2003) found that in their mixtures containing Al_2O_3 nanoparticles dispersed in water, the suspensions showed Newtonian behavior up to 4%. In the investigations carried out by Kulkarni et al. (2007), the results revealed that for nanofluids consisting of copper oxide nanoparticles dispersed in a 60:40 propylene glycol–water mixture, the fluids exhibited a Newtonian behavior for the considered range of $0 \leq \phi \leq 6\%$.

The effective dynamic viscosity of nanofluids can be approximated by various means. On one hand, it can be calculated using several existing theoretical formulas that have been derived for two-phase mixtures. One such relationship (Equation 2.12) was proposed by Brinkman based on Einstein's equation for viscous fluids containing diluted, small, rigid, and spherical particles in suspension (Brinkman, 1952):

$$\frac{\mu_{nf}}{\mu_{bf}} = \frac{1}{(1-\emptyset)^{2.5}} \tag{2.12}$$

This formulation was commonly used in the early work on nanofluids (Chein & Huang, 2005; Khanafer et al., 2003). In his theoretical analysis, Batchelor (1977) considered the effect of Brownian motion of particles on the bulk stress of an approximately isotropic suspension of rigid and spherical particles by developing the relationship of Equation 2.13:

$$\frac{\mu_{nf}}{\mu_{bf}} = 1 + 2.5\,\emptyset + 6.5\,\emptyset^2 \tag{2.13}$$

In general, both of these formulas have been found to be somewhat adequate in some cases for very low particle concentrations (i.e., $\phi \leq 1\%$), although they seem considerably underestimate this property compared to experimental data for cases with more particle concentrations (Kulkarni et al., 2007; Murshed et al., 2008a; Pak & Cho, 1998). Other developments for the viscosity of fluids containing suspended solid particles can be found in the works of Graham (1981) and Lundgren (1972). It should be noted that these correlations are for the general case of conventional fluids with suspended solid particles and were not specifically developed for nanofluids. The applicability of these formulas is therefore questionable. In order to get around the lack of developed theory that could accurately represent nanofluid effective viscosity for numerical forced convection studies, Maïga et al. (2004) performed a least-squares fitting of available experimental data. The data were collected from early studies on nanofluids (S. U. Choi

& Eastman, 1995; S. Lee et al., 1999; Masuda et al., 1993). For a water–Al_2O_3 nanofluid, the corresponding result is given as follows (Equation 2.14):

$$\frac{\mu_{nf}}{\mu_{bf}} = 123\ \emptyset^2 + \ 7.3\ \emptyset + 1 \tag{2.14}$$

As the above equation does not consider other important effects such as temperature, Palm et al. (2006) performed curve fitting of the temperature-dependent data published by Putra et al. (2003). The results of them illustrated the importance of considering fluid temperature in numerical simulations. As the temperature increases, so does the thermal conductivity. However, the effective viscosity decreases with temperature. Others have investigated rheological properties of nanofluids "in-house" and have used the collected data in their numerical models (P. Namburu et al., 2007; Namburu et al., 2009; P. K. Namburu et al., 2007). In the numerical work by Gherasim et al. (2011) on nanofluid heat transfer and fluid flow in a confined radial flow cooling system, the authors used viscosity data obtained in-house (C. Nguyen et al., 2007). The same nanofluids were used in their experimental work on radial flow systems (Gherasim et al., 2009) and therefore more accurate numerical– experimental comparisons were made possible. As in the case of the effective thermal conductivity of nanofluids, some of the most recent numerical studies have used multivariable correlations to predict nanofluid effective viscosity. The correlation developed by Corcione (2011b) is one such equation, Equation 2.15. This correlation is also based on a comprehensive set of experimental data by various authors.

$$\frac{\mu_{eff}}{\mu_{bf}} = \frac{1}{1 - 34.87\left(d_{nP}/d_{bf}\right)^{-0.3}\ \emptyset^{1.03}} \tag{2.15}$$

Where, d_{bf} is the equivalent diameter of a base fluid molecule:

$$d_{bf} = 0.1\left(\frac{6\ M}{N\ \pi\ \rho_{bf0}}\right) \tag{2.16}$$

Where, M and N are the molecular weight of the base fluid and the Avogadro number (6.022×10^{-23} mol^{-1}) respectively, and ρ_{bf0} is the mass density of the base fluid calculated at $T_0 = 293$ K.

2.5 Stability of nanofluids

The main challenge in preparing nanofluids is their poor stability caused by the formation of agglomerates, which are generated by high surface areas and strong van der Waals forces among nanoparticles. The stability of nanofluids is essential in practical applications because the thermo-physical properties of unstable fluids change with time (Bianco et al., 2014; Haghighi et al., 2013). Although various methods have been developed to prepare nanofluids, all of these methods have instability problems caused by particle agglomeration in base fluids. Stability requires uniformly dispersed nanoparticles in the base fluid. The thermal and electrical properties of nanofluids are enhanced when the nanofluids are stable (Philip & Shima, 2012; Ponmani et al., 2014). Nanoparticle agglomeration not only settles and clogs microchannels, but also decreases the thermal conductivity of nanofluids (Beck et al., 2010). Thus, the stability of nanofluids should be investigated because it significantly influences the properties of nanofluids for application; the influencing factors in the dispersion stability of nanofluids should also be studied and analysed (Sarkar et al., 2012; Sarkar et al., 2013).

Colloidal dispersions have been investigated through particle motion analysis under various flow conditions and sedimentation characteristics studies of suspended nanoparticles in base fluids to prepare stable nanofluids (Wasan et al., 2005). Colloidal stability in water is best studied using the Derjaguin–Landau–Verwey–Overbeek (DLVO) theory (Derjaguin & Landau, 1941; Overbeek, 1952; Rao, 2010). Although a recently proposed extended DLVO theory describes satisfactorily the stability of nanofluids, good theoretical framework and analytical tools that could develop stable

nanofluids are still lacking (El-Brolossy & Saber, 2013; Rao, 2010). Nanofluids have recently been recognized to be more stable than micrometer-sized particle suspensions because of vigorous Brownian motion of suspended nanoparticles in base fluids (Yujin Hwang et al., 2008; Tantra et al., 2010). Among the various nanofluid preparation methods, adding surfactants is efficient in making homogeneously dispersed nanoparticles in base fluids. Surfactants [e.g., sodium dodecyl sulfate (SDS)] cause electrostatic repulsion among surfactant-coated nanoparticles, which significantly decreases particle agglomeration caused by the van der Waals forces of attraction (Fendler, 2001; Tantra et al., 2010).

Low costs, long-term stability, and good fluidity are the three most significant preconditions for the nanofluids toward practical applications in the heat transport field (K. J. Lee et al., 2007).

Gravitational force causes particles to separate from the liquid and settle at the bottom. The settling theory of Stoke in Equation 2.17 explains particle settling when gravitational acceleration and viscous forces act on particles. For heat transfer applications, the nanoparticles are denser than the host liquids ($\rho_{np}>\rho$) and settle with time (Yujin Hwang et al., 2008; Kallay & Žalac, 2002; Witharana, 2011). However, this effect is counter-balanced by the smaller sizes of the nanoparticles (x), which result in low settling velocities (U_t) and large time scales. Problems occur when nanoparticles flock together and form aggregates, which are heavy and settle quickly.

$$U_t = \frac{x^2(\rho_{np} - \rho)g}{18\mu} \tag{2.17}$$

Settling is essential in various industrial sectors (e.g., petroleum, mining, and mineral). Fluids are either stationary or moving in heat transfer equipment. The probability of particles settling on the tube in circulating nanofluids (i.e., forced convection in tubes) is low because of mixing. However, the probability is high in natural

convection and pool boiling environments because of the stationary nature of the bulk fluid. Thus, settled particles clog fluid channels and add thermal wall resistance where wall materials are highly thermally conductive. Ultimately, nanofluids could diminish the system instead of enhancing it (Witharana et al., 2013). Therefore, the increase in critical heat flux is proven because of the systematic deposition of nanoparticles on heated surfaces. The question on how to stabilize nanofluids for heat transfer applications is still remains. A nanofluid collapses as a result of particle settling, which in turn could be a consequence of undesired aggregation. The interaction among suspended particles should be examined further explore this fact.

Y.-j. Hwang et al. (2007) evaluated the stability of nanofluids by using UV-vis, a spectro photometer where the multiwalled carbon nanotubes (MWCNT) and Fullerene/oil from absorption and particle concentration exhibited a linear relation. The relative nanofluid stability was estimated from this relation. X.-j. Wang et al. (2009) measured the stability of nanofluids using a Malvern ZS Nano S analyzer (DLS), alumina, and Cu/water. A well-dispersed suspension was obtained with high surface charge density. G. Chen et al. (2008) employed small angle X-ray scattering with Ludox. In X-ray scattering analysis, particles in the liquid are complicated by the interference among X-rays that are elastically scattered from individual particles (Wensel et al., 2008). They evaluated the stability of nanofluids by visually inspecting the dispersion stability of nanofluids with nanotubes and metal oxide particles. Chiesa and Simonsen (2007) utilized transmission electron microscopy (TEM) and alumina/oil, and obtained stable nanofluids when the nanoparticles were well distributed.

Meng et al. (2012) produced CNT glycol nanofluids, their sizes and morphologies were examined using TEM, JEM-2000EX at an acceleration voltage of 160 kV. UV-Vis-NIR spectroscopy of CNT glycol nanofluids was recorded on a Cary 500 spectrophotometer from 200 nm to 2500 nm. CNTs were treated by oxidation with HNO_3,

where they were broken into short and less twisted shreds after HNO_3 treatment, which resulted in high stability and enhanced dispersion. The prepared nanofluids could remain stable for more than two months without sedimentation.

2.6 Heat Transfer Correlations

2.6.1 Genius of Sudden Expansion Application

In 1970, DOUGALL (1970) published results of detailed experiments on the turbulent heat transfer at the downstream of an abrupt expansion in a circular pipe. In the early work of Boelter et al. (1948) they used air as the working fluid. They imposed a nearly constant heat flux boundary condition downstream of the abrupt expansion by using an electrically heated pipe. The primary instrumentation consisted of thermocouples mounted on the outer surface of the downstream tube. Zemanick and Dougall's results agree quite well with those of the earlier researchers as far as the axial variation of the local Nusselt number is concerned. Their peak Nusselt number, however, increased approximately as 0.8 power of the Reynolds number and appeared to have significant compressibility effects in some runs. Their carefully documented experimental results have been compared with numerical results based on a two-layer model of the near wall zone. They also represented the maximum Nusselt number data, Equation (2.18) of all the three geometries tested by them:

$$Nu_{max} = 0.2\, Re_d^{0.667} \tag{2.18}$$

Park and Ota (2010) presented the experimental results on study of turbulent separation flow and heat transfer in a symmetric expansion plane channel. The step used was 20 mm high and 200mm wide and the Reynolds number maintained from 5,000 to 35,000. From the experimental measurements of the mean and turbulent fluctuation of temperatures and velocities, they obtained that local Nusselt number profile was

significantly different at the lower and upper walls result the Coanda effect caused by instability between the lower and upper separated shear layers. These results show relevant agreement with the data of Yuki et al. (2004). In this study they used the empirical formulas (Equations 2.19 and 2.20) and obtained the difference between heat transfer from the lower and upper walls which increased with an increase in Re and reached up to about 45%.

$$Nu_{max} = 0.079\left(U_{ref}\frac{H}{\nu}\right)^{0.071} \quad (Upper\ Wall) \tag{2.19}$$

$$Nu_{max} = 0.053\left(U_{ref}\frac{H}{\nu}\right)^{0.0712} \quad (Lower\ Wall) \tag{2.20}$$

D. H. Lee et al. (2011) performed numerical and experimental study of heat transfer at axisymmetric sudden expansion followed by a sudden contraction called (cavity) in a circular channel with the uniform wall temperature. The main element of their test section was an electrically-heated Nickel-Chromium ribbon (0.01cm thick, 0.32cm wide). They reported that the ribbon was surrounded with epoxy which effectively insulated it thermally and electrically from the aluminium tube walls on both sides.

The experimental results revealed that the maximum Nusselt numbers appeared between 9 and 12 step heights from expansion step. They also obtained a good agreement with numerical results evaluated by using Equation (2.21) for local Nusselt numbers.

$$Nu(x) = \frac{h(x)D}{k_a} = \frac{V_s^2 D}{[A_s(T_s(x) - T_b(x))K_a R_s]} \tag{2.21}$$

Where V_s is the voltage across the ribbon and R_s is the ribbon resistance. Also, h (x) and k_a are the local heat transfer coefficient at axial position x of the gage from the upstream piston and the thermal conductivity of air, respectively. A_s is the ribbon surface area. $T_{s(x)}$ and $T_{b(x)}$ are, respectively, the ribbon temperature and bulk temperature of air flow at the ribbon location x from the upstream piston.

Zohir and Gomaa (2013) had focused on heat transfer properties and pressure drop for turbulent airflow within a sudden expansion pipe that is equipped with a propeller swirl generator or a spiral spring item with multiple pitch ratios. The study was carried out for the Reynolds number changing from 7500 to 18500, underlying uniform heat flux conditions. The experiments were carried out in three zones for the propeller fan (n = 15 blades; blade angle = 650), and in three independent pitch ratios for the spiral spring (P/D = 10, 15, 20). The effect of the utilization of the propeller rotating freely was discussed, as was the input spiral spring on heat transfer improvement and pressure drop. In these trials, the spiral spring and swirl generator were utilized to create a swirl within the tube flow. They considered both relative mean and mean Nusselt numbers and compared them with those acquired from different analogous scenarios. The results from experimentation suggest that the tubes with the propeller have shown a great development of heat transfer ratio compared to the plain tube, about 1.69 times for X/H=5. Regarding the tubes with spiral springs, the heat transfer rate compared to the plain tubes was about 1.37 times for the case of P/d = 20. This high drop in pressure with utilization of the propeller was shown to be 3 times, and for the case of the spiral spring it was 1.5 times compared to the plain tube. The researchers created correlations for the average Nusselt number, spiral spring pitch and fan location.

Table 2. 1. Correlations of experimental results and its constants with maximum deviation values.

Item correlated	Correlation form	Correlation constants				Error
		a	b	c	d	
Nusselt number	$Nu = aRe + b(tan\theta) + cS + d$	6.22E-8	0.98	-1.12	0.83	±17.5%
Pressure drop	$\Delta P = aRe + b(tan\theta) + cS + d$	1.5E-5	0.37	-0.086	-0.34	±11.9%
Enhancement factor	$\eta = aRe + b(tan\theta) + cS + d$	-6.87E-6	1.02	-1.18	1.03	±18.5%

2.6.2 Genius of Nanofluid Forced Convection

Among the earliest published results on forced convection of nanofluids, the work by Pak and Cho (1998) considered water-based nanofluids with Al_2O_3 and TiO_2 particles in turbulent flow in a circular pipe. Results showed that the Nusselt number for the dispersed fluids increased with particle volume concentration as well as with the Reynolds number. However, under a condition of constant average velocity, they noted that the heat transfer coefficient of the nanofluid was 12% lower than that of pure water. Therefore, they recommended that a better selection of particles having higher thermal conductivity and larger sizes be considered. For the types of nanofluids and ranges considered ($0 < \phi < 3\%$, $10^4 < Re < 10^5$, and $6.54 < Pr < 12.33$), Pak and Cho (1998) proposed the following correlation (Equation 2.22) for the Nusselt number. One can note the resemblance to the Dittus–Boelter equation for conventional fluids:

$$Nu = 0.021\, Re^{0.8} Pr^{0.5} \tag{2.22}$$

Dittus and Boelter (1930) presented equation 2.23 for evaluation of Nusselt number for water:

$$Nu = 0.023 Re^{0.8} Pr^{0.4} \tag{2.23}$$

The Dittus-Boelter equation is a good approximation where temperature differences between bulk fluid and heat transfer surface are minimal. But, their equation did not contain any dependence on the weight/volume concentration.

The equation presented by Gnielinski (1976) for liquids is (2.24):

$$Nu = 0.012(Re^{0.87} - 280) Pr^{0.4} \tag{2.24}$$

Where $1.5 < Pr < 500$, $3000 < Re < 10^6$.

Petukhov (1970) presented an equation (2.25) for evaluation of Nusselt number for water:

$$Nu = \frac{\left(\frac{f}{8}\right) Re\ Pr}{1.07 + 12.7\left(\frac{f}{8}\right)^{0.5} (Pr^{2/63} - 1)} \quad (2.25)$$

Equation 2.25 is applicable for the range of 0.5 < Pr < 2000 and 3000 < Re < $5*10^6$.

Gnielinski (1975) presented equation for evaluation of Nusselt number for water:

$$Nu = \frac{\left(\frac{f}{8}\right) (Re - 1000)\ Pr}{1 + 12.7\left(\frac{f}{8}\right)^{0.5} (Pr^{2/3} - 1)} \quad (2.26)$$

Where, $f = (0.79 \ln Re - 1.64)^{-2}$. Equation 2.26 is valid for the range of 2300 < Re < 106 and 0.5 < Pr < 2000.

Early numerical work on the application of nanofluids in tube flow has shown that considerable heat transfer enhancements are possible in applications (El Bécaye Maïga et al., 2006; Maiga et al., 2005). The nanofluids that were considered consisted of Al_2O_3 nanoparticles in water or ethylene glycol. In these early studies, the authors used the single-phase approach using the Hamilton–Crosser equation for the evaluation of effective thermal conductivity and a curve-fitting equation based on the available experimental data for the effective viscosity. In the specific case of tube flow, El Bécaye Maïga et al. (2006) , presented the correlations, equations (2.27-2.29):

For laminar flow, constant wall heat flux,

$$Nu_{nf} = 0.086\ Re_{nf}^{0.55}\ Pr_{nf}^{0.5} \quad (2.27)$$

For laminar flow, constant wall temperature,

$$Nu_{nf} = 0.28\ Re_{nf}^{0.35}\ Pr_{nf}^{0.36} \quad (2.28)$$

For turbulent flow,

$$Nu_{nf} = 0.085\ Re_{nf}^{0.71}\ Pr_{nf}^{0.35} \quad (2.29)$$

The work by Xuan and Li (2003) also provided empirical correlations for computing Nusselt numbers in laminar and turbulent tube flows using water-based nanofluids consisting of Cu and TiO_2 nanoparticles (Equations 2.30 and 2.31). These correlations are valid for concentrations of up to 2%. Results show an increase in heat transfer performance with an increase in particle volume fraction for the same Reynolds numbers.

For laminar flow,

$$Nu_{nf} = 0.4328\,(1.0 + 11.28\,\emptyset^{0.745}\,Pe_d^{0.218})\,Re_{nf}^{0.333}Pr_{nf}^{0.4} \qquad (2.30)$$

For turbulent flow,

$$Nu_{nf} = 0.0059\,(1.0 + 7.6286\,\emptyset^{0.6886}\,Pe_d^{0.001})\,Re_{nf}^{0.9238}Pr_{nf}^{0.4} \qquad (2.31)$$

Xuan and Li (2003) presented their correlation in which Nusslet number was a function of Reynolds number, Prandtl number, concentration and particle size. R. S. Vajjha et al. (2010) mentioned that particle size had insignificant effect on the heat transfer coefficient. The Nusselt number, by definition, is a function of the heat transfer coefficient (h) and the thermal conductivity (k) of the nanofluid. Both heat transfer coefficient and thermal conductivity vary with the particle concentration of the nanofluid. Consequently, Nu must be a function of the particle concentration of the nanofluid. With this argument they developed a Nusselt number correlation (Equation 2.32) as a function of Pr, Re and ∅.

$$Nu_{nf} = 0.065(Re^{0.65} - 60.22)(1 + 0.0169\emptyset^{0.15})Pr^{0.542}\,; \quad R^2 = 0.97 \qquad (2.32)$$

This equation has maximum deviations of ±10% and an average deviation of 2% when compared with the experimental data points. The correlation is valid for $3000 < Re < 16{,}000$, $0 < \emptyset < 0.06$ for CuO and SiO_2 nanofluids and $0 < \emptyset < 0.1$ for the Al_2O_3 nanofluid.

Recently, two correlations of average Nusselt number of different nanofluids flow through an abrupt expansion pipe were proposed by Kimouche et al. (2017). The first one represents the average Nusselt number as a function of Reynolds number, volume fraction and the ratio of densities of the nanoparticles to that of the base fluid equation (2.33):

$$\overline{Nu} = (0.494\, Re^{0.763}) \times \left(0.854 + \left(0.362 + 0.375\left(\frac{\rho_s}{\rho_f}\right)^{0.0738}\right)\emptyset^{0.909}\right) \quad (2.33)$$

Likewise, a second correlation was developed considering Reynolds number, volume fraction and conductivity ratio of solid particle to the base fluid conductivity as shown by equation (2.34).

$$\overline{Nu} = (0.494\, Re^{0.763}) \times \left(0.854 + \left(0.622 + 0.119\left(\frac{K_s}{K_f}\right)^{0.0754}\right)\emptyset^{0.909}\right) \quad (2.34)$$

2.7 Introduction to Regression Analysis

Regression analysis is a form of predictive modelling technique which investigates the relationship between a dependent (target) and an independent variable (s) (predictor). Regression analysis is an important tool for modelling and analysing data. There are multiple benefits of using regression analysis. They are as follows:

- It indicates the significant relationships between dependent variable and independent variables.
- It indicates the strength of impact of multiple independent variables on a dependent variable.

2.7.1 Modelling a Response

In regression, the variable y to be modelled is called the dependent (or response) variable and its true mean (or expected value) is denoted by E(y). In fact, y is equal to E(y) plus or minus some random amount, which is unknown.

$$y = E(y) + Random\ error \tag{2.35}$$

This model is called a probabilistic model for y. The adjective *probabilistic* comes from the fact that, when certain assumptions about the model are satisfied, we can make a probability statement about the magnitude of the deviation between y and E(y).

The variables used to predict (or model) y are called independent variables and are denoted by the symbols x_1, x_2, x_3, etc. The process of finding the mathematical model that relates y to a set of independent variables and best fits the data is part of the process known as regression analysis. Flowchart of the regression process is represented briefly in Figure 2.12.

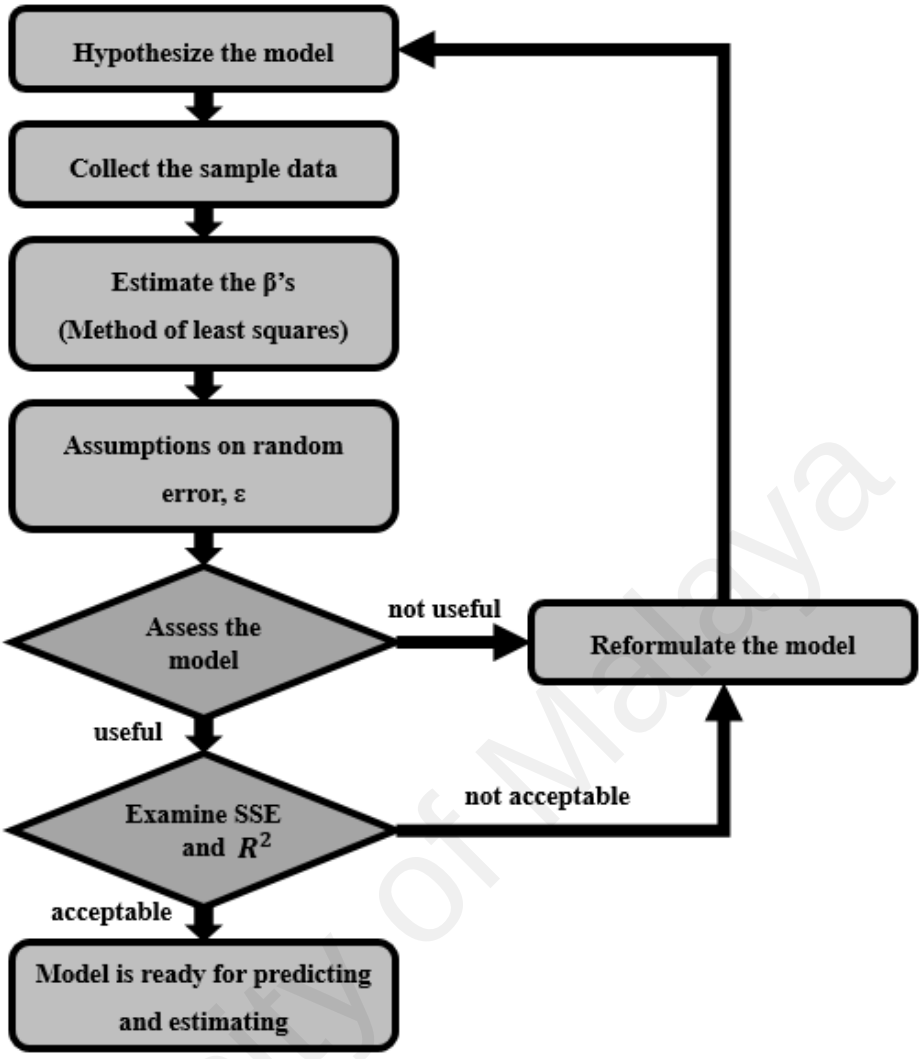

Figure 2. 12: Flowchart of regression process

The response surface is a convenient method for modeling a response (y) which is a function of quantitative independent variables.

2.7.2 Response Surface Methodology (RSM)

Response surface methodology (RSM) is a collection of mathematical and statistical techniques for empirical model building. With the careful design of experiments, the objective involves in the development of a response (output variable) which is influenced by several independent variables (input variables). An experiment is a series of tests, called runs, in which changes are made in the input variables in order to identify the reasons for changes in the output response (E Montazer et al., 2016).

Originally, RSM was developed to model experimental responses (Box & Draper, 1987), and then shifted into the modelling of numerical experiments. The difference is in the type of error generated by the response. In physical experiments, inaccuracy can be due to measurement errors while, in computer data generation the numerical noise is a result of incomplete convergence of iterative processes, round-off errors or the discrete representation of continuous physical phenomena (Giunta et al., 1996; Vassili Toropov et al., 1996; Van Campen et al., 1990). In RSM, the errors are assumed to be random.

The application of RSM to design optimization is aimed at reducing the cost of expensive analysis methods (e.g. finite element method or CFD analysis) and their associated numerical noise. Venter et al. (1996) have discussed the advantages of using RSM for design optimization applications.

The response can be represented graphically, either in the three-dimensional space or as contour plots that help visualize the shape of the response surface. Contours are curves of constant response drawn in the x_i, x_j plane keeping all other variables fixed. Each contour corresponds to a particular height of the response surface, as shown in Figure 2.13.

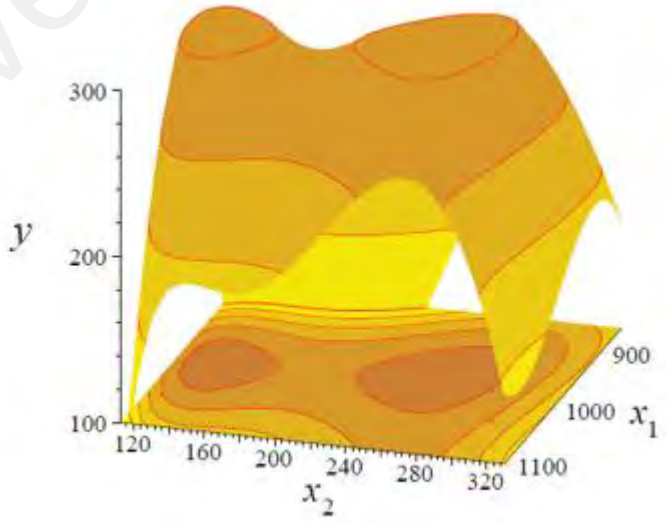

Figure 2. 13: Three-dimensional response surface and the corresponding contour plot.

This section reviews the two basic concepts in RSM, first the choice of the approximate model and, second, the plan of experiments where the response has to be evaluated.

2.7.2.1 Approximate model function

Generally, the structure of the relationship between the response and the independent variables is unknown. The first step in RSM is to find a suitable approximation to the true relationship. The most common forms are low-order polynomials (first, second or third-order).

The regression coefficients included in the approximation model are called the tuning parameters and are estimated by minimizing the sum of squares of the errors (SSE) (Box & Draper, 1987):

$$SSE(a) = \sum_{p=1}^{P} \left\{ w_p \left(F_p - \tilde{F}_p(a) \right)^2 \right\} \rightarrow min \qquad (2.36)$$

Where w_p is a weight coefficient that characterizes the relative contribution of the information of the original function at the point p, $p = 1 \ldots P$.

The construction of response surface models is an iterative process. Once an approximate model is obtained, the goodness-of-fit determines whether the solution is satisfactory or not. If this is not satisfactory, the approximation process is restarted and further experiments are made.

To reduce the number of analyses in computer simulations, sensitivity data may be used in the model fitting, although this information is not always available at low cost. If in addition to the values of the original function $Fp = F(x_p)$ their first order derivatives at point p, $F_{P,i} = \frac{\partial}{\partial x_i} F_P \ (i = 1, \ldots, N, \ p = 1, \ldots, P)$ are known, the equation (2.36) is replaced by the following equation (2.37) (VV Toropov et al., 1993):

$$SSE(a) = \sum_{p=1}^{P} \left\{ w_p \left[\left(F_p - \tilde{F}_p(a)\right)^2 + \gamma \frac{\sum_{i=1}^{N} \left(F_{p,i} - \tilde{F}_p(a)_i\right)^2}{\sum_{i=1}^{N} F_{P,i}^2} \right] \right\} \rightarrow min \qquad (2.37)$$

Where $\gamma>0$ and is the parameter characterizing a degree of inequality of the contribution of the response and the sensitivity data. In this thesis, following the recommendations by VV Toropov et al. (1993).

Later, van Keulen et al. (2000) have presented a methodology for the construction of responses using both function values and derivatives on a weighted least-squares formulation. The authors concluded that the use of derivatives could provide a better accuracy and it requires a reduced number of data.

2.7.2.2 Design of experiments

An important aspect of RSM is the design of experiments (Box & Draper, 1987), usually abbreviated as DoE. These strategies were originally developed for the model fitting of physical experiments, but it can also be applied to numerical experiments. The objective of DoE is the selection of the points where the response should be evaluated.

Most of the criteria for optimal design of experiments are associated with the mathematical model of the process. Generally, these mathematical models are polynomials with an unknown structure, so the corresponding experiments are designed only for every particular problem. The choice of the design of experiments can have a large influence on the accuracy of the approximation and the cost of constructing the response surface.

In a traditional DoE, screening experiments are performed in the early stages of the process, when it is likely that many of the design variables initially considered have little or no effect on the response. The purpose is to identify the design variables that have large effects for further investigation. Genetic Programming has shown good screening

properties which suggests that both the selection of the relevant design variables and the identification of the model can be carried out at the same time.

A detailed description of the design of experiments theory can be found in the publications of Box and Draper (1987), Montgomery and Myers (1995) and Montgomery (1997), among many others. Schoofs et al. (1987) have reviewed the application of experimental design to structural optimization, Unal et al. (1996) discussed the use of several designs for response surface methodology and multidisciplinary design optimization and Simpson et al. (1997) presented a complete review of the use of statistics in design. As introduced earlier, a particular combination of runs could support to define an experimental design. The possible settings of each independent variable in the N-dimensional space are called levels. A comparison of different methodologies is given in the next section.

A. Full Factorial Design

To construct an approximation model that can capture interactions between N design variables, a full factorial approach (Montgomery, 1997) may be necessary to investigate all possible combinations. A factorial experiment is an experimental strategy in which design variables are varied together, instead of one at a time.

The lower and upper bounds of each of the N design variables in the optimization problem needs to be defined. The allowable range is then discretized at different levels. If each of the variables is defined at only the lower and upper bounds (two levels), the experimental design is called 2^N full factorial. Similarly, if the midpoints are included, the design is called 3^N full factorial and shown in Figure 2.14.

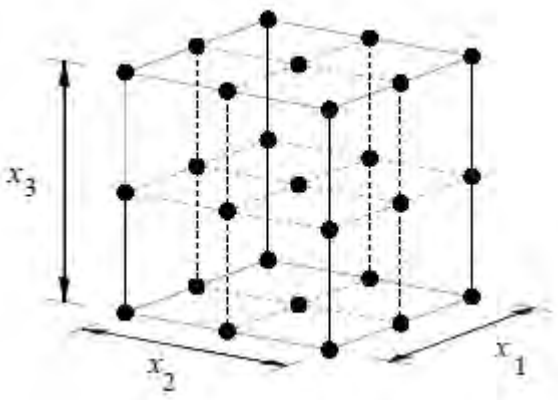

Figure 2. 14: A 3^3 full factorial design (27 points)

Factorial designs can be used for fitting second-order models. A second-order model can significantly improve the optimization process when a first-order model suffers lack of fit due to interaction between variables and surface curvature. A general second-order model is defined as

$$y = a_0 + \sum_{i=1}^{n} a_i x_i + \sum_{i=1}^{n} a_{ii} x_i^2 + \sum_{j=1}^{n} \sum_{i=1}^{n} a_{ij} x_i x_j \quad (i < j) \tag{2.38}$$

Where x_i and x_j are the design variables and values of a_i are the tuning parameters.

The construction of a quadratic response surface model in *N* variables requires the study at three levels so that the tuning parameters can be estimated. Therefore, at least (*N*+1) (*N*+2) / 2 function evaluations are necessary. Generally, for a large number of variables, the number of experiments grows exponentially (3^N for a full factorial) and becomes impractical. A full factorial design typically is used for five or fewer variables. If the number of design variables becomes large, a fraction of a full factorial design can be used at the cost of estimating only a few combinations between variables. This is called fractional factorial design and is usually used for screening important design variables. For a 3^N factorial design, a $\left(\frac{1}{3}\right)^P$ fraction can be constructed, resulting in 3^{N-P} points. For example, for p=1 in a 3^3 design, the result is a one-third fraction, often called 3^{3-1} design, as shown in Figure 2.15 (Montgomery, 1997).

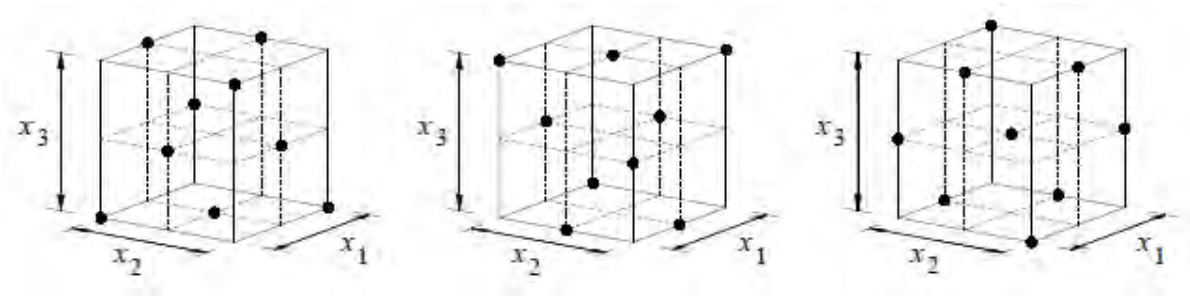

Figure 2. 15: Three one-third fractions of the 3^3 design

B. Box-Behnken Design

In the Box-Behnken design shown in Figure 2.16, the design points are at the midpoint of the edge and at the centre. The convergence of the predicted function to real function is faster. However poor coverage of the corners of the design space is a disadvantage for the calculation of the surfaces with a badly estimated design space. The ratio of number of experiments to the number of coefficients should be in the range of 1.5 to 2.6.

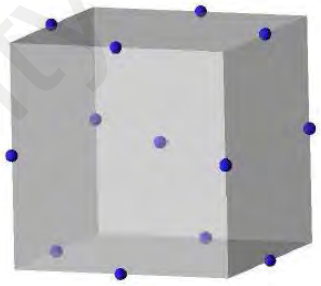

Figure 2. 16: Box-Behnken designs for 3 parameters

The design points for the Full-Factorial and the Box-Behnken designs are shown in the same cube in Figure 2.17. The corners and face centres of the cube are not included in the Box- Behnken design. The number of computational evaluations required for N variables are shown in Table 2.2. It is observed that the Full-Factorial design requires significantly more computational evaluations as the number of variables increases.

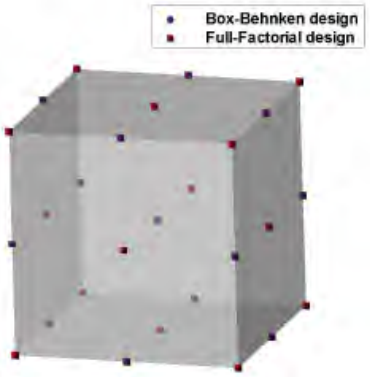

Figure 2. 17: Box-Behnken and Full-Factorial designs

Table 2. 2: Number of computational evaluations required for Box-Behnken and Full-Factorial designs

Number of computational evaluations for N variables	Box-Behnken	Full-Factorial
3	13	27
4	25	81

C. Central Composite Design

A second-order model can be constructed efficiently with central composite designs (CCD) (Montgomery, 1997). CCD are first-order (2*N*) designs augmented by additional centre and axial points to allow estimation of the tuning parameters of a second-order model. Figure 2.18 shows a CCD for 3 design variables.

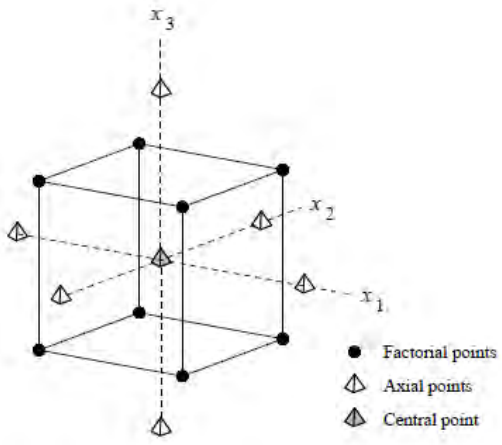

Figure 2. 18: Central composite design for 3 design variables at 2 levels

In Figure 2.18, the design involves 2^N factorial points, $2N$ axial points and 1 central point. CCD presents an alternative to 3^N designs in the construction of second-order models because the number of experiments is reduced as compared to a full factorial design (15 in the case of CCD compared to 27 for a full-factorial design). CCD have been used by Lautenschlager et al. (1997) for the multi objective design of a flywheel. In the case of problems with a large number of designs variables, the experiments may be time-consuming even with the use of CCD.

D. D-Optimal Designs

The D-optimality criterion enables a more efficient construction of a quadratic model (Montgomery & Myers, 1995). The objective is to select P design points from a larger set of candidate points. Equation 2.39 can be expressed in matrix notation as:

$$Y = X * B + e \tag{2.39}$$

Where Y is a vector of observations, e is a vector of errors, X is the matrix of the values of the design variables at plan points and B is the vector of tuning parameters. B can be estimated using the least-squares method as:

$$B = (X^T * X)^{-1} X^T Y \tag{2.40}$$

The D-optimality criterion states that the best set of points in the experiment maximizes the determinant $| X^T X |$. "D" stands for the determinant of the $X^T X$ matrix associated with the model. From a statistical point of view, a D-optimal design leads to response surface models for which the maximum variance of the predicted responses is minimized. This means that the points of the experiment will minimize the error in the estimated coefficients of the response model.

The advantages of this method are the possibility to use irregular shapes and the possibility to include extra design points. Generally, D-optimality is one of the most used criteria in computer-generated design of experiments.

Several applications are described in the publication of Giunta et al. (1996) for the wing design of a high-speed civil transport. Later, Unal et al. (1996) conducted a multidisciplinary design optimization study of a launch vehicle. Haftka et al. (1998) have reviewed the use of D-optimality criteria for the optimization of experimental designs.

2.8 Summary

Fluid flow via sudden expansions are among the basic topics within the discipline of fluid mechanics. The comprehension of these types of flows has attracted a great volume of research, attributable to their wide usage in numerous applications such as heat exchangers, dump combustors, nuclear reactors and diffusers; as well as pipe-flow systems within the chemical and petroleum industries, pharmaceutical, medical science, air-conditioning ducts, and fluidic devices. In addition, improvement of thermal transport properties of heating fluids has been found to enhance the efficiency of heat exchangers, shrink the size of the systems and reduce the operational cost.

Recently, suspension of the solid particles among the fluid has been shown to enhance thermal conductivity of the fluid. It has been reported in a number of studies (Abu-Nada, 2008; Roy et al., 2004; Xuan & Roetzel, 2000) that the dispersion of the solid nanoparticles in a base fluid significantly changes the thermo-physical properties of conventional fluids. Because the nanoparticles are so fine, gravity becomes less important and thus chances of sedimentation are also less, which makes the nanofluids more stable.

The primary purpose here is to provide a summary of the recent research progress on the fluid flow and the heat transfer performance of the nanofluids in abrupt enlargement configurations in order to suggest several potential explanations about implementation of these configurations in industries. In general, none of the existing correlations appear entirely satisfactory for the general use in the sudden expansion of

pipe. This study was undertaken for developing more generally applicable correlations, based on the research concepts.

CHAPTER 3: METHODOLOGY

3.1. Experimental Apparatus Process and Repeatability

3.1.1. Test Rig

Figure 3.1 shows the schematic view of overall experimental set-up for the present work which consists of a flow loop, heated test section, cooling section, measuring instruments, data acquisition and control units. The flow loop includes a pump, a magnetic flow meter, a reservoir tank, a differential pressure transmitter, and a test section. This configuration closely resembles heat transfer in most heat exchangers to enable much clear representative of real engineering application. The nanofluids were pumped from a 20 L capacity stainless steel jacketed tank by a Cole-ParmerTM magnetic drive pump at a flow rate of 0-4 l/m, and the pump flow was controlled by a Hoffman MullerTM inverter. The flow rate and the pressure loss were measured using a NFLO-25 Electromegnetic flow meter and a FoxboroTM differential pressure transmitter, respectively. In this experiment PLC control system was used and WINCC software was used for recording and analysis of the data. The uncertainties of the flow meter and differential pressure transmitter were ± 0.5 % and ± 0.075 %, respectively.

The experimental parameters set on the basis of comparison of the results obtained from previous researchers and the limitations of the experimental setup. The flow region has been influenced by the reattachment point, which enhances with the increase of Reynolds number. So, the present parameters were specifically set on the basis of availability of length of the extended section after step. Insulation, power supply, piping and fitting etc. were considered following international standard codes. Line losses, thermal losses etc. were evaluated following standard equations.

A straight stainless-steel sudden expansion flow passage test section with a 0.8 m upstream length and 0.62 m downstream length, 0.0127 m (0.5 inch) upstream inlet and 0.0254 (1 inch) downstream outlet diameters, for an expansion ratio (ER) of 2 was used in the present investigation. The schematic diagram of flow configuration and boundary conditions of this study is shown in Figure 3.2.

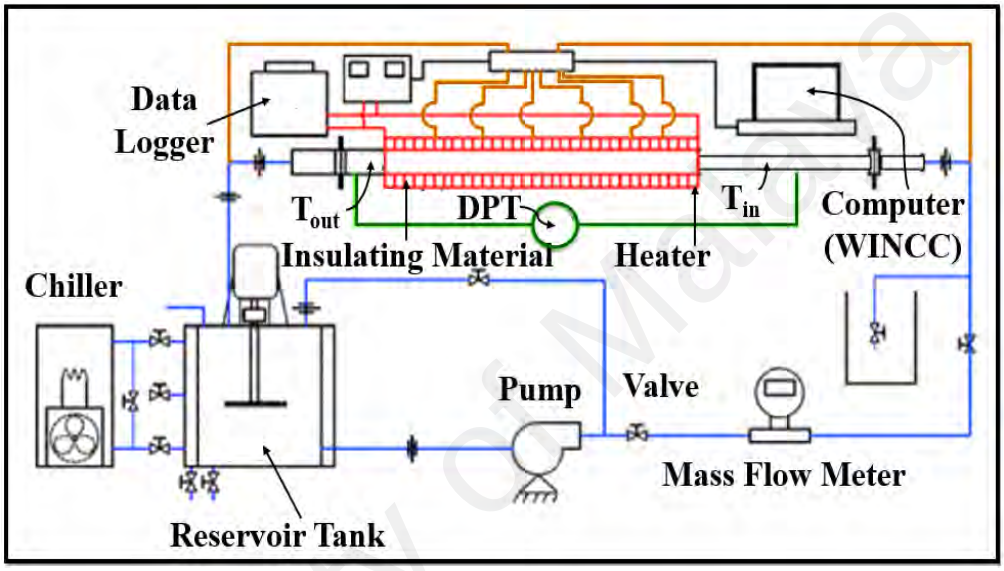

Figure 3. 1: Schematic view of the test rig

In the test section, the downstream walls were heated by using two units of programmable DC power supply with output voltage of 8 V and current 400 A, while whole of the walls were insulated. The boundary conditions of the experiments were maintained as follows: After expansion, there was a constant heat flux of 600 W provided by DC power supplies. Also, the inlet fluid rate was in the range of 3 to 16 Lit/min.

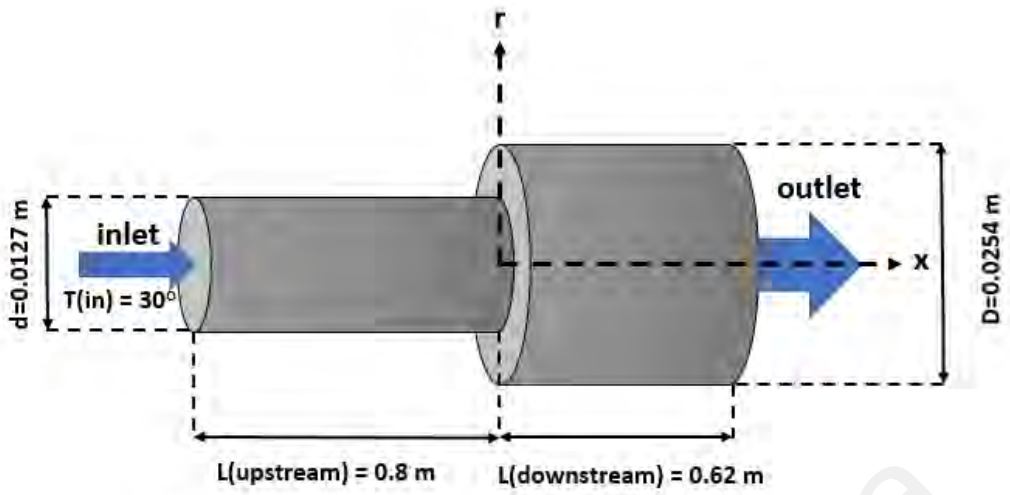

Figure 3. 2: A 3D view of schematic configuration of abrupt expansion of the present study.

Sixteen K type thermocouples were purchased from Omega then they were installed on the test section by using high temperature epoxy glue on the outer surface of the test section. The positions of the thermocouples, which are schematically presented in Figure 3.3, where they were placed on the outer surface or away from the inner surface of the cylindrical tube alternatively at the top and bottom surfaces to avoid boundary layer interruption originating from the thermocouple probe protruding into the conduit inner surface. As shown in Figure 3.4, there exists a gap between the outer and the inner surface corresponding to the thickness of the conduit.

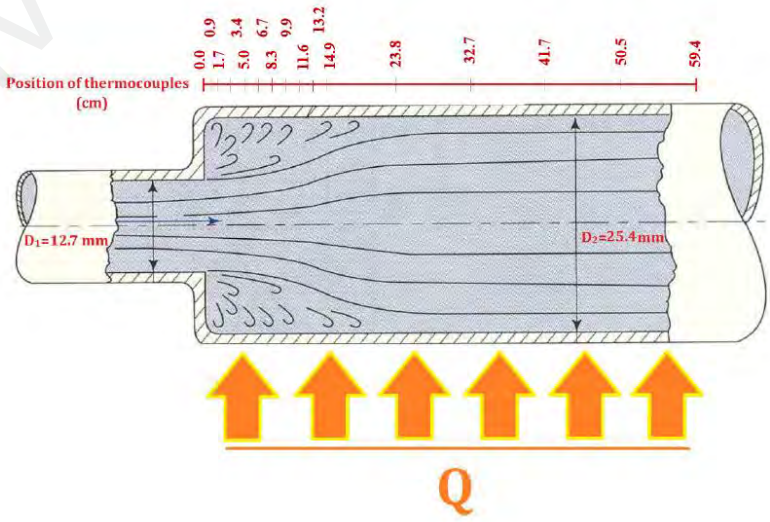

Figure 3. 3: Schematic view of the test section and the thermocouples position

In a pure conduction heat transfer, the inner surface can be described via the classical heat conduction equation. Besides the surface thermocouples, two RTD (PT-100) sensors (From Omega) were installed in input and output to measure and record the inlet and outlet temperatures of the working fluids. Note that all of the thermocouples as well as RTDs were calibrated by Ametek temperature calibrator (AMETEK Test & Calibration Instruments, Denmark). The RTDs and thermocouples were connected to the PLC and SCADA system for the continuous monitoring and recording of the temperature data by a WINCC software in a computer.

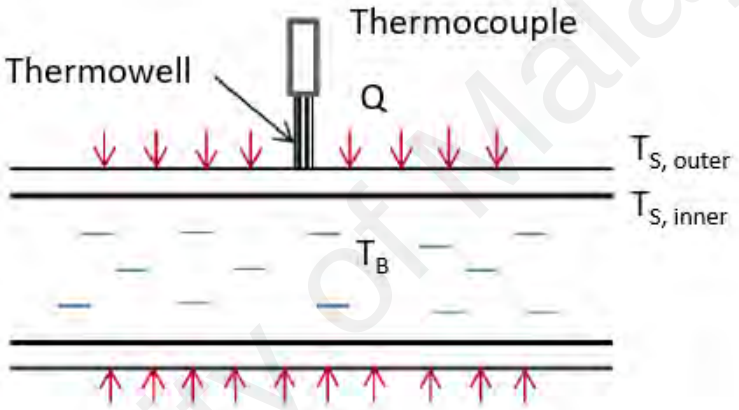

Figure 3. 4: Schematic view of temperature variation through the heated wall

To minimize radial conduction losses to the ambient air, the tube was covered with 5.1 cm of polyurethane foam and, to minimize radiation losses to the room, the foam was wrapped in an aluminized mylar jacket as shown in Figure 3.5. Two K-type thermocouples were installed on the outermost surface of the insulation to measure the amount of heat loss.

The comparative assessment between the input and output energy at different *Re* by using conventional expression for total heat flow and the heat recovered, ($Q = VI = \dot{m} C_p(T_{in} - T_{out})$) showed the average loss of approximately 3.96%, which is

reasonable. It is believed that this low percentage of heat loss would not affect the overall heat transfer calculation process.

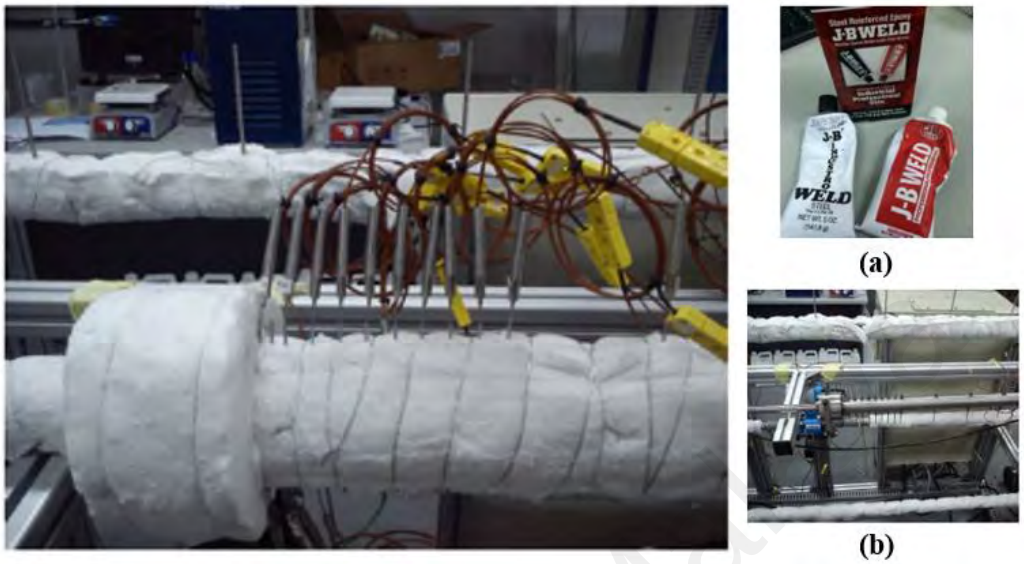

Figure 3. 5: Thermocouple installation in the test section; (a) High temperature Epoxy up to 200°C and (b) Thermo-wells.

During the pipe flow experimental process, each sample was first poured into the stainless-steel jacketed tank and circulated along the piping networks and measuring instruments using magnetic driven pump. The flow rate was maintained to correspond to the previous water run value in order to minimized the effect of pumping power and to reflect the actual contribution of the material property on the overall enhancement (if any) into the system. The cooling bath circulator was connected to the jacketed tank and its temperature was adjusted until the bulk temperature complied with the predetermined criteria.

The relevant data were recorded after steady state condition was reached. The acquired raw data underwent series of rigorous analysis to obtain relevant property to describe the heat transfer performance. The surface, inlet, outlet and bulk temperature measurements were used along with the thermos-physical properties data to calculate heat transfer coefficient and Nusselt number which were plotted with respect to fluid bulk velocity/Reynolds Number for comparative assessment. The pressure drops over the test

pipe was measured by which the friction factor was calculated and plotted against flow velocity. To assess the reproducibility of the results the test section was thoroughly cleaned by using filtered and distilled water at the end of the sample test run and the experiment was repeated using distilled water at similar condition. Uncertainty analysis was conducted for both raw and derived parameters to ascertain the actual improvement in heat transfer under the present approach. However, considering the conduction and convective heat transfer process which occurred simultaneously in the present case, the further calibration test was needed to determine the exact temperature at the inner surface.

The inlet temperature of bulk fluid and heat flux at different locations "x" of the duct were formulated as mentioned in the data processing section. The specifications and the accuracy of the measuring instruments and sensors used in the present experimental setup are presented in Table 3.1.

Table 3. 1: Specifications and errors of the measuring instruments and sensors used in the present experiment.

Measured Parameter	Instrument and sensor type	Operating condition	Error
Surface Temperature	Type K thermocouple	0-300°C	±0.1°C
Bulk Temperature	RTD (PT-100) Sensor	0-200°C	±0.1°C
Fluid Flow Rate	N-FLO-25 Electromagnetic flow meter	0.03 m/s ~ 12 m/s	±0.5%
Fluid Pressure Drop	Foxboro™ differential pressure transmitter	0-25 kPa	±0.75%
Cooling Unit	WiseCircu, DAIHAN Scientific, Refrigerated circulating bath	2.2 kW	±0.1°C

3.1.2. Design and Construction

Some basic requirements are developed as design considerations for the convection loop. These requirements are generated in order to meet certain goals: some to mimic heat

exchanger conditions, some to meet existing equipment and lab requirements, and finally some arbitrary conditions.

3.1.2.1 Test Section

A straight stainless-steel sudden expansion pipe configuration with a 0.8 m upstream length and 0.62 m downstream length, 0.0127 m (0.5 inch) upstream inlet and 0.0254 m (1 inch) downstream outlet diameters, for an expansion ratio (ER) of 2 was used as the test section (Figure 3.6).

Figure 3. 6: Test section parts

3.1.2.2 Reservoir Tank

The reservoir tank is a Jacketed Stainless steel of cylindrical shape with a capacity of 20 litters. The reservoir is kept 30 cm above the gear pump so that the gear pump will have adequate inlet flow to avoid cavitation. At the bottom of the reservoir a piping connects the gear pump while at the top a bypass line, return line and top stirrer for mixing fluid inside the tank are installed as presented in Figure 3.7.

Figure 3. 7: Photograph of the reservoir tank

3.1.2.3 Gear Pump

The gear pump used for the experiment is a Liquid flow sealed gear pump (Cole-Parmer magnetic drive pump), (Figure 3.8). It is rated for a maximum flow of 120 LPM and Max Head is 8 M. This pump is capable of operating at variable speed with the maximum rated speed of 3200 RPM. The suction side of the pump is connected to the reservoir.

The pump is capable of operating with water up to 80℃, due to the shaft seal limitations. After rough estimation of the total loop pressure losses, assuming maximum 15mm inner diameter tubing, and from knowledge of the pump characteristic curve, it is found that the pump should be capable of producing around 52LPM.This will deliver a significantly turbulent flow rate for water at room temperature, up to Reynolds of 30,000. Therefore, the pump is deemed usable for the experiment.

Figure 3. 8: photograph of the magnetic gear pump

3.1.2.4 Inverter

A Hoffman Muller inverter was used to control the speed of the pump as shown in Figure 3.9.

Figure 3. 9: Photograph of the Hoffman Muller inverter

The specifications of the inverter are presented in Table 3.2.

Table 3. 2: Technical specifications for V8 series inverters

Items	Contents
Model	HM-V8A11P5B
Input	AC, 1PH, 230V, 50/60HZ
Output	3PH, 1.5KW, 7A, 0-650HZ

3.1.2.5 Electromagnetic Flow Meter

N-FLO-25 Electromagnetic flow meter was used to measure fluid flow rate (Figure 3.10). A magnetic flow meter (mag flowmeter) is a volumetric flow meter which does not have any moving parts and is ideal for wastewater applications or any dirty liquid which is conductive or water based. Magnetic flowmeters will generally not work with

hydrocarbons, distilled water and many non-aqueous solutions. Magnetic flowmeters are also ideal for applications where low pressure drop and low maintenance are required.

Figure 3. 10: Photograph of the electromagnetic flow meter

The operation of a magnetic flow meter or mag meter is based upon Faraday's Law, which states that the voltage induced across any conductor as it moves right angles through a magnetic field is proportional to velocity of that conductor. The technical specifications are presented in Table 3.3.

Table 3. 3: Technical specifications of electromegnetic flow meter

Items	Contents
Model	N-FLO-25 Electromagnetic flow meter
Sensor range	DN10-DN3000
Operational pressure	PN 10 (1.0 MPa) for DN 15 to 300. Tri Clover
Measurement flow range	8 m^3/h
Measurement accuracy	±0.5%
Repeatability	0.1%
Environment temperature	-20°C to 50°C
Minimum conductivity of measured liquid	5 μs/cm

Lining	Teflon (PTFE)
Measuring electrodes	Hastelloy C4 standard

As stated above, the flow meters were supplied after calibration by the manufacturer, as shown in Table 3.4. Fluid viscosity can become an issue if the viscosity is higher than that of water. The deviation of the flow meter reading becomes an issue when the meter is running in the lower 25% of its operating range for fluids of viscosity less than 30 times that of water. Nanofluids used in the experimental investigation were typically only 5 times more viscous than that of water, therefore the calibration had not been an issue.

Table 3. 4: Flow meter calibration data

Flow (m^3/hr)	Volume (L)	Actual (L)	Error (%)	Repeatability (%)
0.5	5.201	5.214	0.24	0.062
0.8	12.374	12.368	-0.05	0.105
1.6	20.871	20.787	-0.40	0.019

3.1.2.6 Differential Pressure Transducers

The smart FoxboroTM differential pressure transmitter (Model: IDP10-T22D21D-LIT) with accuracy of ±0.075% of span connected to the inlet and outlet of the test section was used in this investigation (Figure 3.11).

Figure 3. 11: Photograph of the Differential Pressure Transducers

The standard specifications of the Differential Pressure Transducers are presented in Table 3.5. The calibration condition, static pressure test and differential pressure test are presented in Table 3.6 to Table 3.8, respectively.

Table 3. 5: Standard specifications of the Differential Pressure Transducers

Items	Contents
Model	IDP10-T22D21D-LIT
Process Fluid	Liquid, Gas of Vapor
Application	Differential Pressure, Gauge Pressure, Absolute Pressure
Measuring Range	0 - 0125 Kpa ~ 0 - 1.5 Kpa (Minimum) 0 - 4.0 Mpa ~ 0 – 1500.00 Kpa (Maximum)
Accuracy	± 0.075% of span
Stability	± 0.15% of URL for 2 years
Working Temperature	-25 to 95°C
Max. Pressure	1500 Kpa
Body material	SS 304
Diaphragm	SS 316L

Table 3. 6: Calibration conditions for Differential Pressure Transducers

Ambient temperature	20°C
Relative humidity	60%
Grounding resistance	>200 MΩ
Calibration range	0 ~ 50 KPa

Table 3. 7: Static pressure test

Differential pressure value	Static pressure = 4.00 MPa			
	1 ATM	Error (%)	4 MPa	Error (%)
0.0 KPa	4.000 mA	0.000	4.012 mA	0.075
50.0 KPa	20.003 mA	0.019	20.000 mA	0.000

Table 3. 8: Differential pressure test

D/P Value	Output	Zero to F.S.	Error (%)	F.S. to Zero	Error (%)
0.0	4.000 mA	3.998 mA	-0.012	4.009 mA	0.056
12.5	8.000 mA	7.991 mA	-0.056	7.997 mA	-0.019
25.0	12.000 mA	11.992 mA	-0.050	11.992 mA	-0.050
37.5	16.000 mA	15.990 mA	-0.062	15.999 mA	-0.006
50.0	20.000 mA	19.997 mA	-0.019	19.992 mA	-0.050

3.1.2.7 Cooling Unit

A Refrigerated Bath Circulator (DAIHAN-brand, WCR- P30) was used to balance the heat input and it is inside the jacketed tank (Figure 3.12). This refrigerated bath has:

- RS232C Interface for Remote Monitoring and Controlling with PC
- Stainless steel Bath (#304) for Superior Durability & High Thermal Efficiency.
- Powerful Circulation Pump ensures temperature Uniformity: Internal and External Circulation.

- Locking Mode Supported for Experimental Safety (Input to Jog-Shuttle can be Disabled)

The specifications of the Refrigerated Bath are enlisted in Table 3.9.

Figure 3. 12: Photograph of the Refrigerated Bath Circulators

Table 3. 9: Specifications of refrigerated bath

Items		Contents
Capacity & Models		30 L, WCR-P30
Temp. Range & Accuracy		-25°C ~ +150°C, ±0.1°C
Temp. Resolution		0.1°C-Display, 0.1°C-Control
Temp. Uniformity & Probe		±0.2°C at -10°C, PT100
Heating Power		2.2 kW
Refrigerator		7/8 HP
Cooling Capacity	at +20°C	631 W
	at 0°C	429 W
	at -20°C	284 W
Refrigerant		CFC System-Free(R-404A) Refrigeration

3.1.2.8 DC Power Supply

The test section was heated by using two programmable DC power supply units with outputs of 8 V and output current of 400 A (Figure 3.13). The specifications of the DC power supply are enlisted in Table 3.10.

Figure 3. 13: Photograph of the DC power supply

Table 3. 10: Specifications of the DC power supply

Items	Contents	
DC Output Ratings	Voltage	8V
	Output Current	400A
	Output Power	3200W
Programming Accuracy	Voltage	0.05% + 4mV
	Current	0.1%+800mA
Output Ripple and Noise	CV p-p	60 mV
	CV rms	8 mV

3.1.2.9 Thermocouples

There were two different type of thermocouples used for the experiment. The thermocouples used for the bulk fluid inlet and outlet (bulk) temperatures in respect to

the test section are thermocouples from Omega (Model: PR-12-2-100-1/8-6-E-RP) with Temperature Range -50 to 250 °C. These are RTD sensor (PT-100) thermocouples with 3mm sheath diameter and 100 mm length. The tips of the thermocouples were inserted into the middle of the flow path of the fluid. The thermocouple was then attached to the data acquisition unit where the bulk temperatures were recorded and analyzed.

Another kind of thermocouples used for surface temperature measurement was type-K from Omega with Liquid Crystal Polymer Molded Transition Junction Rated to 260°C. This type-K thermocouple has 1mm sheath diameter and 5mm length. The thermocouples were supplied with specification from the manufacturer as ±0.1 °C accuracy.

All the thermocouples are not calibrated in the technical sense and they are tested with standard temperatures to ensure no manufacturing or connection flaws are creating erroneous readings. The heat transfer results are directly affected by the temperature measurements. Thus, all the thermocouples (Type-K and RTD sensor) used in this experiment must be calibrated to determine their accuracy. The thermocouples are calibrated by two ways:

1. 650SE - Reference Temperature Calibrator

   The system provides significant improvement in the calibration accuracy up to ±0.04°C with the use of an external reference sensor. Axial homogeneity in the calibration well is important, as the typical thermo-sensitive element of a sensor can vary from 5mm to 60mm. The actual temperature in the well inherently deviates from the ideal temperature as a function of the proximity to the bottom of the well (Figure 3.14).

Figure 3. 14: Photograph of the Thermocouple calibrator.

2. The thermocouples were immersed in well mixed boiling-water bath which was at 100.16°C for the laboratory pressure and a well-mixed ice-water bath was maintained at 0°C (Figure 3.15).

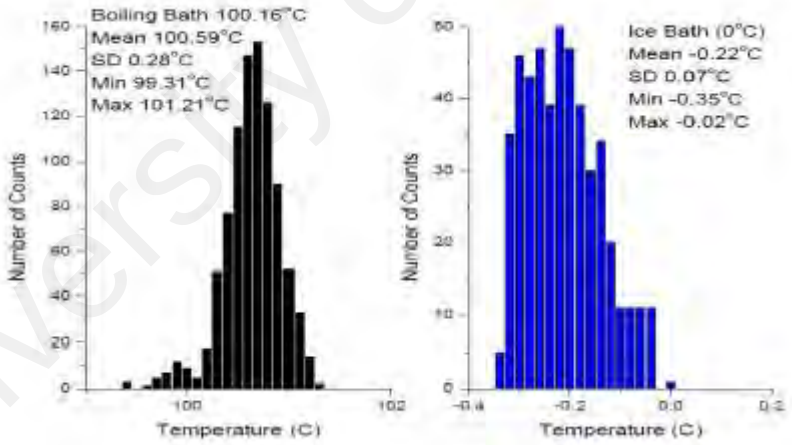

Figure 3. 15: Thermocouple testing

3.1.2.10 Data Acquisition Instrument

Graphtec (midi logger gl220) data acquisition systems were used in this study (Figure 3.16). Meanwhile, data loggers were connected to a PC for continuous data logging and monitoring. All the type-K thermocouples were attached to the channels of

Graphtec data logger. This multi-channel data logger provides 10 analog measurement channels, in addition to four channels each of discrete logic and pulse inputs. The GL220 supports one external trigger input and four alarm outputs. The GL220 connected to a PC to allow data upload in real time as well as remote configuration and real time data acquisition.

Figure 3. 16: Photograph of the data acquisition instruments

3.2 Materials

3.2.1 F-GNP Nanofluids

Graphene nanoplatelets are two-dimensional (2D) with an average thickness of 5–10 nanometers and a specific surface area of 50-750 m^2/g and it can be produced of different sizes, 1 to 50 microns. These interesting nanoparticles, including short stacks of platelet-shaped graphene sheets which are identical to those found in the walls of carbon nanotubes, but in a planar form. The Graphene nanoplatelets (GNPs) have drawn a lot of interest due to their excellent electrical conductivity, high mechanical properties and the in-plane thermal conductivity of GNPs is reported to be as high as 3000-5000 W/m. Further, as this is a 2D material, the heat transfer properties were expected to be much different from the zero-dimensional nanoparticles and one-dimensional carbon nanotubes. Moreover, GNPs itself being an excellent thermal conductor, the graphene based nanofluids are normally expected to display significant thermal conductivity

enhancement (Fang et al., 2013). The graphene nanoplates were also offered in granular form which could be dispersed in water, organic solvents and polymers with the right choice of dispersion aids, equipment and techniques.

Graphene nanoplatelets (GNPs) have special properties dependent on the number of layers, such as the saturable absorption, linear monochromatic optical contrasts and electric field assisted band gaps, which are not found in previously produced materials.

Polycarboxylate Functionalized Graphene Nanoplatelets (*F*-GNPs) with particle diameter of 2 μm, average thickness of 6-8 nm and surface area of 500 m^2/g were purchased from Sigma-Aldrich Co., Selangor, Malaysia. An ultrasonic disruptor has used to produce nanofluids from the specific nanoparticles and the selected base fluids. In the present case after 40 minutes of intensive sonication, the stable suspensions with the base fluid of distilled water were obtained according to the desired mass concentrations (wt. %) of *F*-GNP.

In this study, the low range of nanoparticle concentration in the colloidal suspension were considered. Results revealed that the enhancement of thermos-physical properties of nanofluids were significant without the remarkable loss in pumping power. However, enhancement of concentration could provide more effect on pumping power losses with increase of viscosity and erosion on the instrument and equipment surfaces. Stability of nanoparticles in the fluid is a challenging issue, where the carbon-based nanoparticles were dispersed in the nanofluids by covalent functionalization. Above all, the achievement from the application of nanoparticles could not be highly appreciable due to the adverse effect on stability. So, the present research was limited to the low range of concentration.

3.2.2 MWCNT-COOH Nanofluids

Carbon nanotubes (CNT) has attracted wide interest in many areas of science, technology, and medicine. Carbon nanotubes are molecular-scale tubes of graphitic carbon with outstanding properties. The simplest carbon nanotube is composed of a single sheet of honeycomb network of carbon atoms, called graphene, it is rolled up seamlessly into a tubular form. Single-wall carbon nanotube (SWCNT) was discovered by Iijima and Ichihashi (1993), however carbon nanotubes as multi-tubes (MWCNT) nesting in a concentric fashion were discovered already in 1991 (Iijima, 1991). SWCNT have diameter from 0.4 to 2.0 nm and length in the range of 20–1000 nm, while MWCNT are bigger objects with diameter in the range of 1.4–100 nm and length from 1 to several μm. The exact structure of a nanotube depends on the different angles and curvatures in which a graphene sheet can be rolled into a tube and is determined by a vector, which is called a chiral vector and discriminates CNTs into “zigzag", "armchair”, and “chiral” forms. The electronic properties of a nanotube change in correspondence to its structure; thus armchair nanotubes are metallic, while zigzag and chiral can be either metallic or semiconducting (Harris, 2009). In general, SWCNT are a mixture of metallic and semiconducting material, depending sensitively on their geometrical features, while MWCNT are regarded as metallic conductors (Mitróová et al., 2010).

In the study, CNT-based nanofluids were prepared using polyacrylamide and different concentrations of multi-walled carbon nanotubes that were functionalized with carboxyl groups (MWCNT-COOH). Functionalized Multiwalled Carbon Nanotubes (MWCNT-COOH) with purity 95%, maximum diameter of 8 nm and length ranges from 10 to 30 μm were purchased from Nanostructured & Amorphous Materials Inc, Houston, TX, USA. An ultrasonic disruptor has used to produce nanofluids from the specific nanoparticles and the selected base fluids. In the present case after 40 minutes of intensive

sonication, the stable suspensions with the base fluid of distilled water were obtained according to the desired mass concentrations (wt.%) of MWCNT-COOH.

3.2.3 Metal Oxide Nanofluids

Silicon dioxide (SiO_2) nanopowder with assay 99.5% and particulate size ranges from 10 to 20 nm were purchased from Sigma-Aldrich Co., Selangor, Malaysia. SiO_2 nanofluid has been prepared by dispersing nanoparticles in base fluid. Distilled water was used as a base fluid for the preparation of SiO_2 nanofluids. An ultrasonic disruptor has used to produce nanofluids from the specific nanoparticles and the selected base fluids. No surfactant additives were added during the preparation process. In the present case after 30 minutes of intensive sonication, the stable suspensions were obtained according to the desired mass concentrations (wt.%) of SiO_2.

Zinc oxide (*ZnO*) spherical shaped nanopowder with assay 97% and particulate size was less than 50 nm were purchased from Sigma-Aldrich Co., Selangor, Malaysia. The *ZnO* nanoparticles sedimented within several minutes as zinc oxide is insoluble in water and also, the particles remained within the clusters without being dispersed. Enhanced stability of the *ZnO* nanofluids is observed with sodium hexametaphosphate (*SHMP*). *SHMP* with purity 96% was purchased from Sigma-Aldrich Co., Selangor, Malaysia. After 60 minutes of intensive sonication, the stable suspensions were obtained according to the desired mass concentrations (wt%) of *ZnO*. The most stable suspension as per our sedimentation studies contained surfactant and nanoparticles in wt% ratio 1:10 (*SHMP: ZnO*). Table 3.11 presents the properties of nanoparticles used in this research.

Table 3. 11: Specifications of nanoparticles used in the present research

Nanoparticle	GNP	MWCNT	SiO_2	ZnO
Average size	Dia: 2 μm Average thickness: 5-10 nm	Dia: 8 nm Length: 10-30 μm	10 – 20 nm	< 50 nm

Purity	95%	95%	99.5%	97%
Thermal conductivity ($Wm^{-1}K^{-1}$)	3000	> 3000	1.38	50
Specific heat ($J\ kg^{-1}K^{-1}$)	790	480	680	494
Density ($gr\ cm^{-3}$)	2.3	2.17	2.2 – 2.6	5.61
Colour	Black	Black	White	White
Surface area (m^2gr^{-1})	750	500	175-225	>10.8

3.3 Thermo-Physical Characterization of Nanofluids

In this investigation, the thermo-physical properties of distilled water (Table 3.12) and nanofluids are based on experimental data. For this purpose, nanofluids were prepared using two-step method. *F*-GNP and MWCNT-COOH Nanofluids were prepared at 0.025%, 0.05%, 0.075% and 0.1% wt. %. Also, SiO_2 and ZnO nanofluids were prepared at 0.05%, 0.1%, 0.15% and 0.2% wt.%.

Figure 3. 17: Water distilling plant

Preparing deionized water by using water distillation W4L FAVORIT (Model WCS4L / W4L favorit Distillate output: 4 L per hour single distillation Power Supply: 220 / 240 V, 1.5 Watt, single phase) before using it in the experiments, see Figure 3.17.

After preparation of nanofluids, post-treatments including pH control and sonication were applied to the prepared nanofluids to improve the stability of nano-suspensions. Noticeably, in liquid suspensions, dispersed nanoparticles can attract or repel the neighbouring particles. These interactions depend on the distance between nanoparticles and the total interface energy that is the sum of the van der Waals attraction and the electrostatic repulsion internal forces. This relationship can be interpreted using DLVO theory (Chang et al., 2007). When nanoparticles are well-dispersed within the base fluid, high surface charge densities can be expected for nanoparticles, thus, strong repulsive forces can help to stabilize the nanofluids. According to the literature, the isoelectric point (IEP) is the concentration of potential controlling ions at which the zeta potential is exactly equal to zero. So, at the IEP, the value of surface charge density is identical to the charge density, which is the start point of the diffuse layer. Therefore, the charge density in this layer is zero. Critical to nanoparticle nucleation and stabilization in solution is that the repulsive energy is smaller for small particles, so a larger zeta potential is required for suspension stability. Note that, in this work, experimental measurement of IEP was not performed. However, using trial and error pH setting, the best condition for pH is experimentally obtained. As the pH of the solution departs from the isoelectric point of nanoparticles, the colloidal particles are more stable and subsequently, drastically modify the thermal conductivity of the fluid. Visual observations demonstrated that pH control has a strong influence on the stability of nanofluids. When pH of nanofluid is adjusted, the height of sedimentation layer of particles inside the vessel is minimized and clustering as well as agglomeration inside the bulk of nanofluid can barely be seen (V. Nikkhah et al., 2015). Time-settlement experiments were then employed to ensure about the stability of nanofluids over the time. Results demonstrated that nanofluids can be stable up to 21 days without formation of any settlement layer.

The thermo-physical properties of the nanofluids were deduced from those of fluid, nanoparticles, nanofluid and nanoparticle volume concentration ∅. The Thermo physical properties of the nanofluid are evaluated by using well-known empirical correlations (Abu-Nada, 2008; Alawi et al., 2015; Rashidi et al., 2014). The effective density is given by Equation 3.1 as:

$$\rho_{nf} = (1 - \emptyset)\rho_{bf} + \emptyset\rho_{np} \tag{3.1}$$

Where, ρ_{bf} and ρ_{np} are the densities of the base fluid and the solid nanoparticles, respectively. Additionally, ∅ is percentage of the volume concentration. Therefore, in the present study, the volume concentration was determined from the mass concentration of the dispersed fluid by the following equation (Equation 3.2) which was introduced by Pak and Cho (1998):

$$\emptyset = \frac{1}{\left(\frac{100}{\emptyset_m}\right)\left(\frac{\rho_{np}}{\rho_{bf}}\right) + 1} \times 100\% \tag{3.2}$$

Where, $\emptyset_m$ is the mass concentration of the dispersed fluid.

The heat capacitance of nanofluid is given by Equation 3.3 (Khanafer et al., 2003).

$$C_{P_{nf}} = \frac{(1 - \emptyset)(\rho C_P)_{bf} + \emptyset(\rho C_P)_{np}}{\rho_{nf}} \tag{3.3}$$

The effective thermal conductivity of nanofluid has been approximated by Maxwell-Garnetts (MG) model and given by Equation 3.4 (Khanafer et al., 2003).

$$K_{nf} = K_{bf}\left[\frac{K_{np} + 2K_{bf} - 2\emptyset(K_{bf} - K_{np})}{K_{np} + 2K_{bf} + \emptyset(K_{bf} - K_{np})}\right] \tag{3.4}$$

The viscosity of nanofluid is given by Brinkman (1952) expression, Equation (3.5).

$$\mu_{nf} = \frac{\mu_{bf}}{(1 - \emptyset)^{2.5}} \tag{3.5}$$

Table 3. 12: Experimental thermo-physical properties of distilled water

Temperature (°C)	20	25	30	35	40
Density (Kg m^{-3})	998.07	997.04	995.6	994.05	992.2
C_p (J kg^{-1} K^{-1})	4184.1	4180.9	4178.8	4177.7	4177.6
Viscosity (Pa s)	1.0017	0.8904	0.7972	0.7185	0.6517
Thermal Conductivity ($Wm^{-1}K^{-1}$)	0.6034	0.6110	0.6182	0.6251	0.6351

3.3.1 Density

In this study, the densities of distilled water and nanofluids were measured experimentally by KEM Density/Specific Gravity Meter DA-645 (Figure 3.18). The accuracy of density measurement and temperature are 0.00005 g/cm^3 and 0.3°C respectively. The experimental measurements were recorded 3 times at each temperature and the average was considered in the calculations.

Figure 3. 18: Photograph of the KEM Density/Specific Gravity Meter DA-645.

3.3.2 Specific Heat

A heat flux type differential calorimeter (TA DSC Q20) which is shown in Figure 3.19, was used to measure the specific heat capacity of the nanofluids. DSC, is a thermal analysis technique that looks at material's heat capacity (Cp) change with temperature. A sample of known mass is heated or cooled there and the changes in its heat capacity are tracked as changes in the heat flow. The term differential scanning calorimeter refers to

both the techniques of measuring calorimetric data while scanning as well, which is a specific instrument design. The technique can be carried out with other types of instruments. Range of DSC is (-50 to 350°C).

Figure 3. 19: Photograph of the heat flux type differential calorimeter TA DSC Q20.

3.3.3 Thermal Conductivity

KD2 Pro thermal analyser (KD2 Pro, Decagon Devices, Inc., Pullman, WA, USA) has been used for a long time to measure thermal conductivity of nanofluids. A schematic of the KD2 setup with the isothermal bath is shown in Figure 3.20. The main working principle of KD2 Pro thermal analyser is based on a transient hot wire method with 2-4% accuracy. A single needle sensor (1.3-mm diameter × 60-mm long) was used for measuring thermal conductivity and was installed in a jacketed beaker connected to a water bath. In order to get high accurate measurements, the experimental set-up ensures temperature stability. To keep the temperature at 20°C, 25°C, 30°C, 35°C, 40°C when measuring the thermal conductivity of nanofluid samples water bath (WiseCircu, Witeg Labortechnik GmbH, Wertheim, Germany) with 0.1°C accuracy was used. Nanofluids were employed into the jacketed beaker, and the temperature was kept constant for each test run. The water bath contains inlet and outlet tube for flowing and circulating water at a specific temperature for maintain temperature stability. Every 30 min the measurements

for each sample were recorded where the thermal conductivity of the sample was calculated as the mean of ten readings at the same temperature.

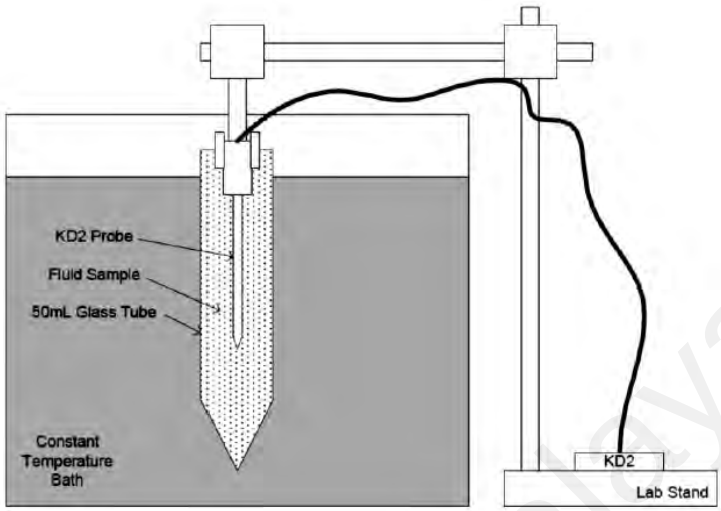

Figure 3. 20: Schematic setup of KD2 thermal properties analyser.

3.3.4 Viscosity

The viscosities of the nanofluids at different volume fractions were measured by using a HR-1 Discovery Hybrid Rheometer manufactured by TA Instrument Inc. (Figure 3.21). The HR-1 shares the cutting-edge technology of the Discovery Hybrid Rheometer family in a platform that is ideal for production control, asphalt manufacture, and a wide range of general measurements of viscosity and viscoelasticity at different temperatures. The bob is connected to the spindle drive and the sample needs to pour into the cup below the bob, and while rotating the bob, the different drag of the nanofluid is measured. This device was connected to the software Trios V.3.3.1.4246 in a computer to store data; it has its own calibration before starting any tests. The viscosities of the nanofluids were measured by varying temperatures and volume fraction of the nanofluids.

Figure 3. 21: A photograph of the HR-1, *Discovery Hybrid Rheometer*

3.4 Stability Analysis

The UV–Vis spectroscopy is a common method, which is utilized for the investigation of the stability of nanofluids including solid particles. According to the Beer–Lambert's law, there is a direct connection between the absorbance of a solution and the concentration of the absorbing species such as particles in the solution. Considering this law, the absorption spectrum of the prepared nanofluids exhibited a maximum peak at around 265 nm corresponding to π–π transition of conjugation system in the polyaromatic structures. The band gap energy, *Eg*, can be measured from UV–Vis absorption by Tauc's Equation, Equation (3.6) (Hadadian et al., 2014).

$$(\alpha h_\vartheta)^n = B\,(h_\vartheta - Eg) \tag{3.6}$$

Where α, h_ϑ, *n, Eg* and *B* are absorption coefficient, photon energy, the nature of optical transition, band gap energy and a material constant respectively. Plotting $(\alpha\, h_\vartheta)^n$ against the photon energy and extrapolating the linear region of the curve to the x-axis give the optical band gap. Regarding the dispersion state and the long-term stability, the colloidal stability of the carbon-nanostructures in base fluid is investigated quantitatively by UV–Vis spectroscopy.

The light transmission of all samples were measured with a Shimadzu UV spectrometer (UV-1800) operating between 190 and 1100 nm. The nanofluid solution was diluted with distilled water to allow sufficient transmission while each measurement was repeated three times to achieve a better accuracy.

3.5 Measurements and Data Reduction

Measurement of the thermo-physical properties containing density, viscosity, thermal conductivity and specific heat capacities at different volume fractions were done experimentally. An investigation of the heat transfer behavior of the nanofluids was performed by evaluating the heat transfer coefficient. The measurements were performed in the Reynolds number range of 4,000 to 16,000 for the distilled water, MWCNT-COOH, F-GNP, SiO2 and ZnO nanofluids. Data were compared for a variety of nanofluid concentrations up to 0.2 wt. % and 0.1 wt. % for metal oxide nanofluids and carbon based nanofluids, respectively.

The convective heat transfer coefficients (h) could be determined by measuring the wall temperatures at different axial dimensional ratios and the temperature of bulk fluid along with the flow rate of the working fluids, and the inlet and outlet temperatures. The Reynolds number can be calculated from Equation 3.7.

$$Re = \frac{\rho\, U_{ave}\, D}{\mu} \tag{3.7}$$

Where ρ and μ are density and viscosity of the working fluid and D is the downstream diameter. U_{ave},is the average flow velocity which can be calculated from Equation (3.8).

$$U_{ave} = \frac{\dot{m}}{\rho\, A_c} \tag{3.8}$$

Where, ṁ and A_c are mass flow rate and surface area of the cross section.

The DC power supplies provided a total power (Q) to the heated section which equals to 600 W. Accordingly, the local heat transfer coefficient ($h_{(\frac{X}{H})}$) could be determined from equation 3.11 at constant wall heat flux (q) of 12,128.56 W/m^2. The experiments were conducted at the Reynolds number range of 4,000–16,000.

$$Q = \dot{m}\, C_p\, (T_{out} - T_{in}) \tag{3.9}$$

$$q = \frac{Q}{A_w} \tag{3.10}$$

$$h_{(\frac{X}{H})} = \frac{q}{T_{s\,(\frac{X}{H})} - T_{b\,(\frac{X}{H})}} \tag{3.11}$$

Where $T_{s\,(\frac{X}{H})}$ is the temperature of pipe surface at the distance of axial ratio ($\frac{X}{H}$) and the stream-wise distance (X) is normalized by the step height H ($H = 0.5(D-d)$). Further, the temperature of the bulk fluid ($T_{b\,(\frac{X}{H})}$) at the distance of axial ratio is calculated by Equation (3.12) [32]:

$$T_{b\,(\frac{X}{H})} = T_{in} + \frac{Q\,(X/L)}{\dot{m}\, C_p} \tag{3.12}$$

Where L is a length of the corresponding wall and C_p is specific heat capacity of the working fluid.

The local Nusselt number ($Nu_{(\frac{X}{H})}$) could be evaluated from Equation (3.13).

$$Nu_{(\frac{X}{H})} = \frac{h_{(\frac{X}{H})}\, D}{K} \tag{3.13}$$

Where, K is thermal conductivity of the working fluid.

In order to calculate the friction factor, "*f*", the pressure drop across the test section was measured by a Foxboro™ differential pressure transmitter and Equation (3.14) was used.

$$f = \Delta P \frac{D}{L} \frac{2}{\rho U_{ave}^2} \tag{3.14}$$

3.6 Data Accuracies and Uncertainties

No experimental study is completely faultless. Overall, these errors make a difference between the observed and actual values of parameters. Thus, it is worthwhile to estimate the prevailing experimental errors. The error analysis was done based on the Taylor (1997) and Moffat (1988) guides.

3.7 Regression Process

High on the list of problems that experimenters most frequently need to deal with is the determination of the relationships that exist among the various components of a complex system. If those relationships are sufficiently understood, there is a good possibility that the system's output can be effectively modelled, maybe even controlled.

3.7.1 Overview of Regression Analysis

Regression analysis is a branch of statistical methodology concerned with relating a response y to a set of independent, or predictor, variables x_1, x_2, . . ., x_i. The goal is to build a good model for a prediction of equation relating y to the independent variables that will enable the researchers to predict y for the given values of x_1, x_2, . . . , x_i, and to do so with a little error of prediction. When using the model to predict y for a particular set of values of x_1, x_2, . . ., x_i, present author will expect a measurement of the reliability of prediction by the present authors. Thus the current author wants to know how large the error of prediction might be. All these elements are parts of a regression analysis, and the

resulting prediction equation is often called a regression model. Figure 3.22 explains the six steps of regression modeling procedure. The response surface is a convenient method for modeling a response which is a function of quantitative independent variables.

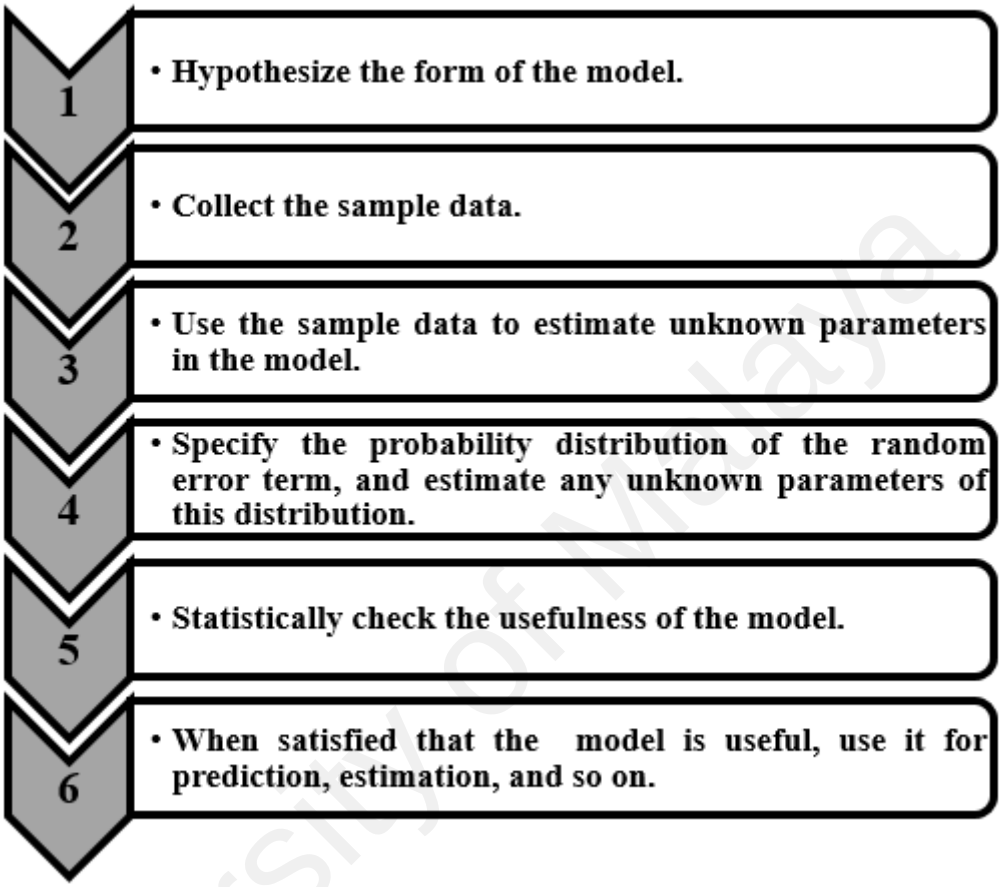

Figure 3. 22: Regression modelling, Six-step procedure

3.7.2 Collecting the data for regression

According to Figure 3.22, the initial step in regression analysis is to hypothesize a deterministic model for the mean response, E(y), as a function of one or more independent variables. Once a model for E(y) has been hypothesized, the next step is to collect the sample data that will be used to estimate the unknown model parameters (β's). This entails collecting observations on both the response y and the independent variables, $x_1, x_2, \ldots, x_i$, for each of the experimental units in the sample. Thus, a sample to be analyzed by regression includes observations on several variables ($y, x_1, x_2, \ldots, x_i$), not just a single

variable. The data for regression can be of two types: observational or experimental. Observational data are obtained if no attempt is made to control the values of the independent variables (x's). The second type of data in regression, experimental data, are generated by the designed experiments where the values of the independent variables are set in advance (i.e., controlled) before the value of y is observed.

3.7.2 Response Surface Methodology

RSM is a collection of mathematical and statistical techniques that are useful in the modelling of a problem (Montgomery, 1991). The RSM is based on the generation of response surfaces for a set of design variables. The response can be function of several variables and it can be obtained by using experimental or numerical methods (E Montazer et al., 2016). While generating the response surfaces, the method of Least Squares is employed. Once the response surfaces are determined, the best values of the response based on the corresponding values of independent variables can be evaluated.

In the definition of response surface methodology, some terminologies are encountered frequently, such as independent variable, response, response function etc. Independent variables are process/experimental inputs whose values or settings can be controlled by the experimenter.

The response is the measured quantity whose value assumed to be dependent on the values of independent variables. The true value of the response, corresponding to any particular combination of independent variables in the absence of any experimental error is denoted by E(y). Therefore, the response is function of independent variables and mathematically it can be shown by Equation (3.15):

$$E(y) = f(x_1, x_2, x_3, \dots x_k) \tag{3.15}$$

The function *f* is called the response function and it is assumed to be a continuous function of x_i. The function *f* that fits perfectly to the real response is usually unknown therefore it

must be approximated using a polynomial or some other type of function (Khuri & Cornell, 1996).

The response surfaces are approximated by fitting a second order model to the response values. The model equation is a linear function of unknown parameters forming coefficient vector β. For example, the quadratic model with 2 optimization variables is given by:

$$E(y_i) = \beta_0 + \beta_1 x_{1i} + \beta_2 x_{2i} + \beta_{11} x_{1i}^2 + \beta_{22} x_{2i}^2 + \beta_{12} x_{1i} x_{2i} + \varepsilon_i \tag{3.16}$$

Where i = 1, 2, ... $n \geq 6$ and β_0, β_2, β_{11}, ... are constant coefficients, y is the measured response, and ε is a random error vector used primarily to account for model's inability to approximate the real response. The matrix X and vector β can be written as:

$$X = \begin{bmatrix} 1 & x_{11} & x_{21} & x_{11}^2 & x_{21}^2 & x_{11}x_{21} \\ 1 & x_{12} & x_{22} & x_{12}^2 & x_{22}^2 & x_{12}x_{22} \\ \cdots & \cdots & \cdots & \cdots & \cdots & \cdots \\ 1 & x_{1n} & x_{2n} & x_{1n}^2 & x_{2n}^2 & x_{1n}x_{2n} \end{bmatrix} \tag{3.17}$$

$$\beta = \begin{bmatrix} \beta_0 \\ \beta_1 \\ \beta_2 \\ \beta_{11} \\ \beta_{22} \\ \beta_{12} \end{bmatrix} \tag{3.18}$$

In the second order model equation, the values of y_i and matrix X are known. The model is therefore fully described if the values of vector β can be estimated. The Method of Least Squares is used in the estimation of vector β. Consider the matrix X, a function of the independent variables (x) and the vector y as their responses, the vector β is estimated by the method of Least Squares by the Equation (3.19):

$$SSE = \sum_{i=1}^{n} \varepsilon_i^2 = \varepsilon' \varepsilon \tag{3.19}$$

Where ε' is the transpose of ε. The sum of the squares of the errors, *SSE* can be written as, Equation (3.20):

$$SSE = (y - X\beta)'(y - X\beta) \tag{3.20}$$

Then expanding the right-hand side of that Equation (3.20), such as Equations (3.21 to 3.23),

$$SSE = y'y - (X\beta)'y - y'X\beta + (X\beta)'X\beta \tag{3.21}$$

$$SSE = y'y - \beta'X'y - y'X\beta + \beta'X'X\beta \tag{3.22}$$

$$SSE = y'y - 2\beta'X'y + \beta'X'X\beta \tag{3.23}$$

The vector β can be found by minimizing the SSE. The derivative of SSE with respect to vector β is calculated. Then partial derivative set equal to zero and solved for β, Equations (3.24 to 3.25);

$$\frac{\partial SSE}{\partial \beta} = -2X'y + 2(X'X)\beta \tag{3.24}$$

$$(X'X)\beta = X'y \tag{3.25}$$

Assuming X' X is non-singular, we have the following least squares estimators, Equation (3.26).

$$\beta = (X'X)^{-1}X'y \tag{3.26}$$

It is clear that X' X is a square matrix and X' y is a column vector (Myers, 1971). Therefore, the system of equations can be solved for β by using a matrix solver.

The regression process starts with the definition of the problem. The variables that have the primary effect on the response are determined and the proper ones are chosen as the design variables. Then the design space is constructed using a Design of Experiments (DoE) approach.

In this study, the recognition of relationship between the controllable input parameters and the response variable was conducted using Box–Behnken design (BBD) technique under RSM. In order to evaluate the influences of axial ratio, Reynolds number, Prandtl number and volume fraction of nanoparticles on the heat transfer performance were considered.

Database is generated using experimental or numerical methods. In this study, the database required for RSM is generated by performing a series of experimental data. RSM is employed for the generated database and the response surfaces are approximated. The optimum values of the design variables that maximize the response are evaluated on approximated response surfaces. Real value of the response is calculated for the optimum values of the independent variables using experimental and numerical techniques. The average error between predicted and calculated responses is estimated. The regression process is terminated if the relative error is less than 5%. If the convergence criterion is not satisfied, a new RSM model is performed around the optimum points. The regression process is carried out until the average deviation is less than 5%. The quality of the proposed models is evaluated by analysis of variance (ANOVA), mentioned ahead in details.

Once the model is created, it is required to check the goodness of the model (Mavris, 2006). The accuracy of the RSM is validated by calculating RSM residuals which are the difference between the predicted and calculated responses. In regression analysis, the multiple coefficient of determination (R^2) is used to measure the strength of the relation which is evaluated by Equation 3.27. R^2 can take any value between 0 and 1 (Magee, 1990).

$$R^2 \cong 1 - \frac{SS_{res}}{SS_{tot}} \tag{3.27}$$

Where, SS_{tot} and SS_{res} respectively are the total sum of squares and the sum of square of residuals which can be calculated by Equations 3.28 and 3.29:

$$SS_{tot} = \sum_{i=0}^{i=n} (y_i - \bar{y})^2 \quad (3.28)$$

$$SS_{res} = \sum_{i=0}^{i=n} (y_i - E(y_i))^2 = \sum_{i=0}^{i=n} e_i^2 \quad (3.29)$$

Where, $\bar{y}$ is the mean of the observed data and e_i defines the residual.

When R^2 is close to 1, the model has a good predictive power. On the other hand, when R^2 is closer to 0, the model has a low predictive power. There is not a fixed R^2 value where a model should be rejected. Instead, it depends on the level of risk or the application for which the model is meant. In addition, R^2 can measure the strength of the relation for any number of predictors.

3.8 Research Flowchart

Figure 3.23, illustrates the flow of the research methodology. Industrial needs for the fast cooling of the continuous operating machines have been studied to set the scope of the research.

Existing knowledge and research methods were critically assessed through a comprehensive literature review. Detailed investigations on the effect of key technical parameters on the performance of the heat transfer were carried out in the combined experimental and numerical studies. The experimental setup is representing the fundamental study of separation flow and effect of nanofluids in the separation flow phenomena. The research is focused on the issues where the knowledge gaps remain in the research field, and will be continued until the research aims and objectives have been achieved.

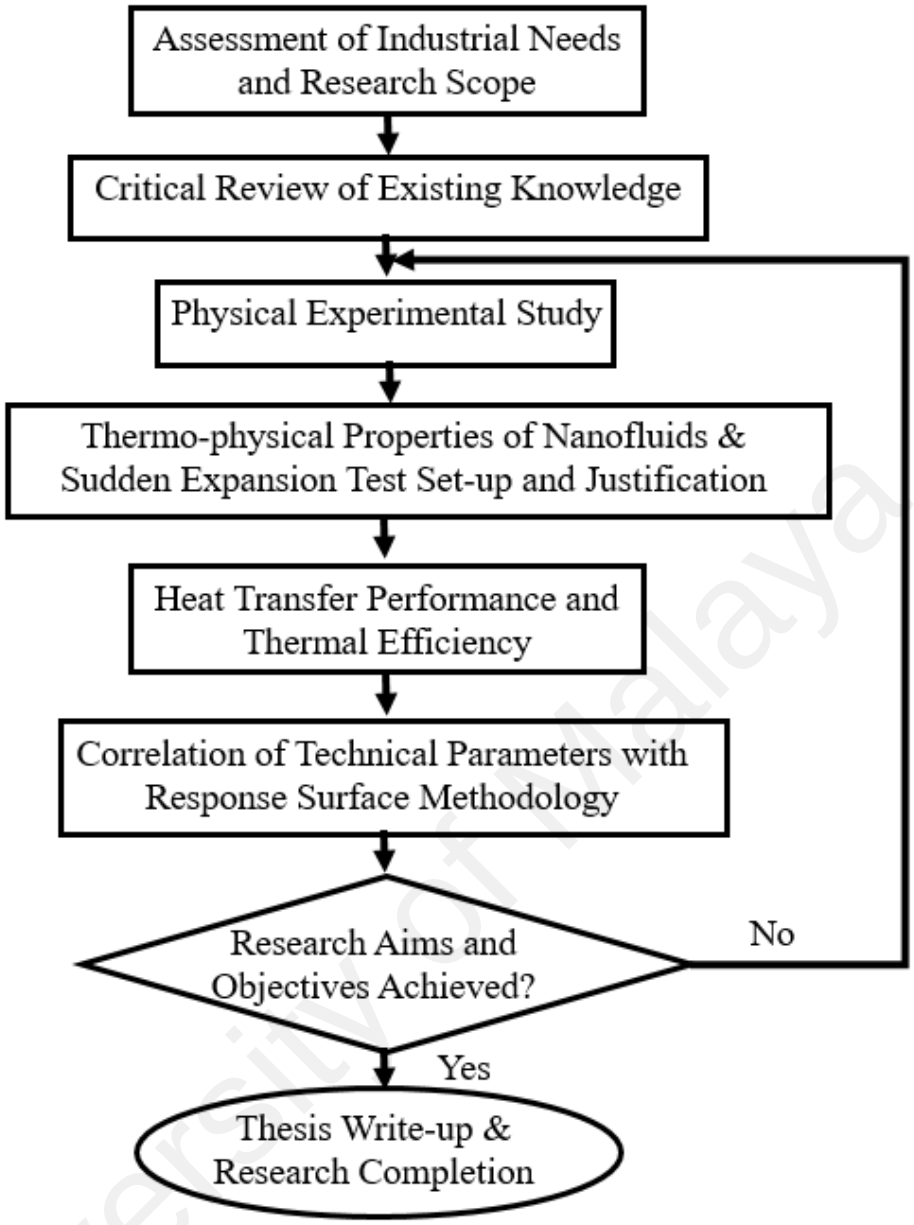

Figure 3. 23: Flowchart of the research methodology of the thesis

CHAPTER 4: RESULTS AND DISCUSSION

4.1 Thermo-physical Properties

Efficiency of heat transfer performance of fluids is improved by enhancing thermal conductivity and other heat transfer properties (viscosity, density, specific heat etc.). Nanostructures materials fluids typically have higher thermal conductivity than conventional fluids (e.g., water, ethylene glycol, and transformer oil) and microstructures materials fluids; thus, utilization of some nanostructures nanofluids has been proposed (Ghozatloo et al., 2013). Heat transfer performance of fluids is improved by adding some nanostructures, which should be stable in the fluid. Graphene has an extremely high thermal conductivity of approximately 5000 W/Mk (Balandin et al., 2008). Thus, thermal conductivity behaviour of the nanofluids would be interesting to study as a two-dimensional phenomenon (Baby & Ramaprabhu, 2010; Chandrasekar et al., 2012; Sadeghinezhad et al., 2014).

Thermal conductivity is the most notable essential thermos-physical properties which was measured by KD2 Pro analyser based on the transient hot wire technique. Figures 4.1 to 4.4 display the obtained values of thermal conductivity for the four aforementioned water-based nanofluids as well as distilled water. They clearly show that as temperature increases, the measured thermal conductivity increases, which is an expected phenomenon. Obviously, all the nanofluid samples were prepared at low weight concentration, however the amount of enhancements for various samples were fairly significant. From Figure 4.1 and Figure 4.2, there are 10.56% and 7.13% rise in the thermal conductivity of water-based ZnO and SiO_2 nanofluids respectively for the highest weight concentration of 0.2 wt% at 40˚C.

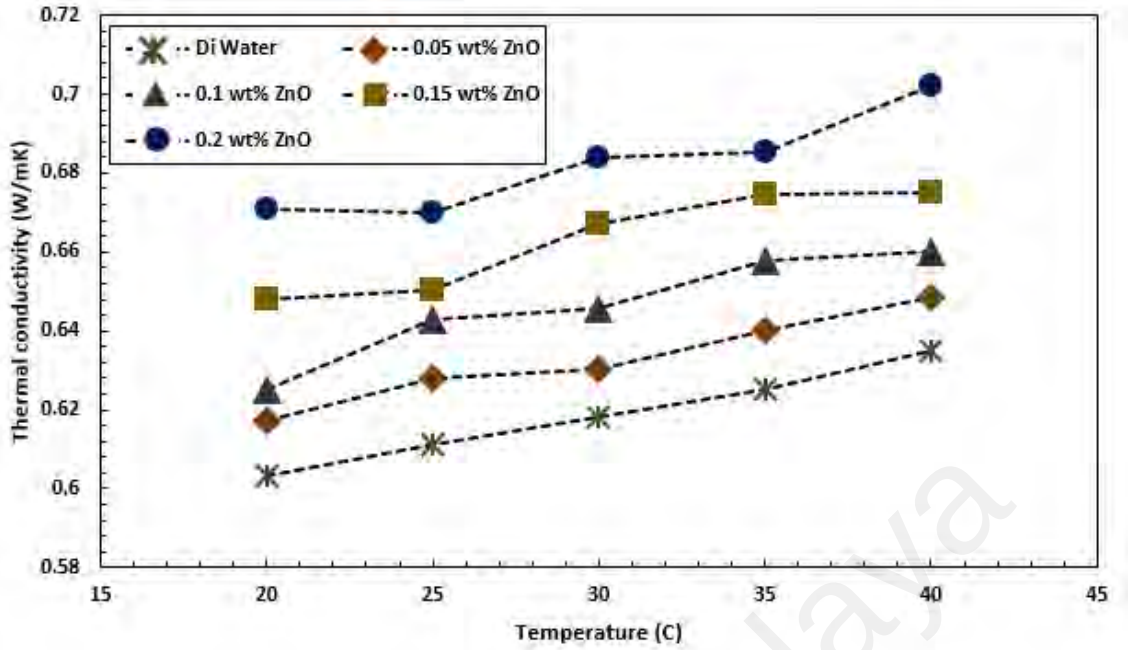

Figure 4. 1: Thermal conductivity plots of water based ZnO nanofluids at different temperatures and weight concentrations

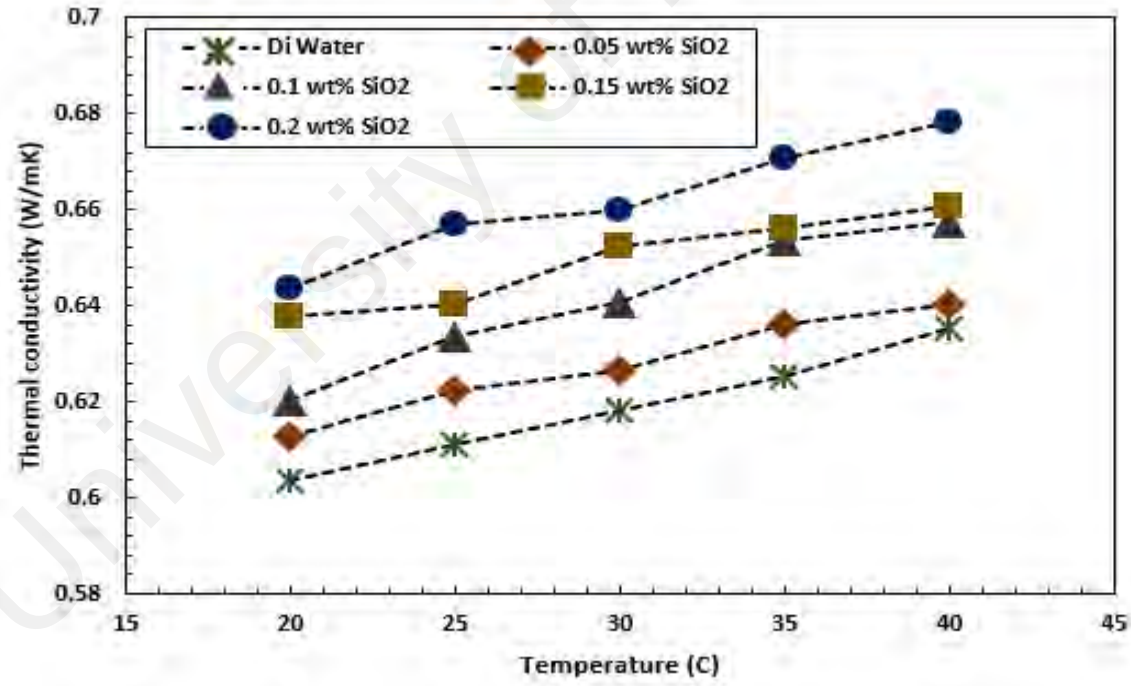

Figure 4. 2: Thermal conductivity plots of water based SiO_2 nanofluids at different temperatures and weight concentrations

Additionally, Figure 4.3 and Figure 4.4 display 14.36% and 13.51% increase in thermal conductivity for the highest weight concentration (0.1 wt%) of MWCNT-COOH and F-GNP nanofluids respectively at the same temperature.

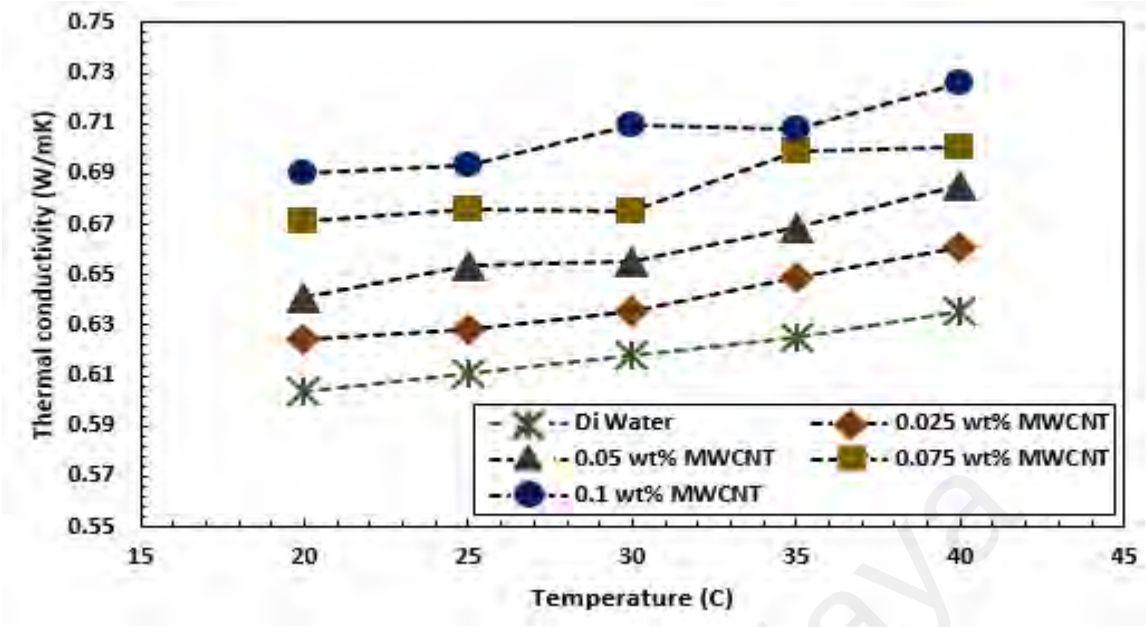

Figure 4. 3: Thermal conductivity plots of water based MWCNT-COOH nanofluids at different temperatures and weight concentrations

On the other hand, thermal conductivity of ZnO and SiO_2 nanofluids at 0.1 wt% increased 5.2% and 3.5% respectively compared to the base fluid. These results show that carbon-based nanoparticles have more positive effects on thermal conductivity of the suspension fluid compared to the metal-oxide particles based nanofluids. Regarding the mechanism of increasing thermal conductivity with the loading of graphene in base fluid, Keblinski et al. (2002) and Eastman et al. (2004a) reported four potential mechanisms to introduce the reasons for the enhancement, such as molecular-level layering of the liquid at the liquid/particle interface, Brownian motion, the effects of nanoparticle clustering, and the nature of heat transport in the nanoparticles.

According to the recent studies (S. Choi et al., 2001; Godson et al., 2010; Huxtable et al., 2003; Kang et al., 2006; Nan et al., 1997; Sarsam et al., 2016) the thermal conductivities of the nanofluids are affected by the thermal conductivities of the base fluids and nanoparticles, temperatures, concentrations, specific surface areas, shape/geometry of nanostructures etc. The present results show that the specific surface

areas of nanoparticles also affects the thermal conductivity as well as the colloidal stability.

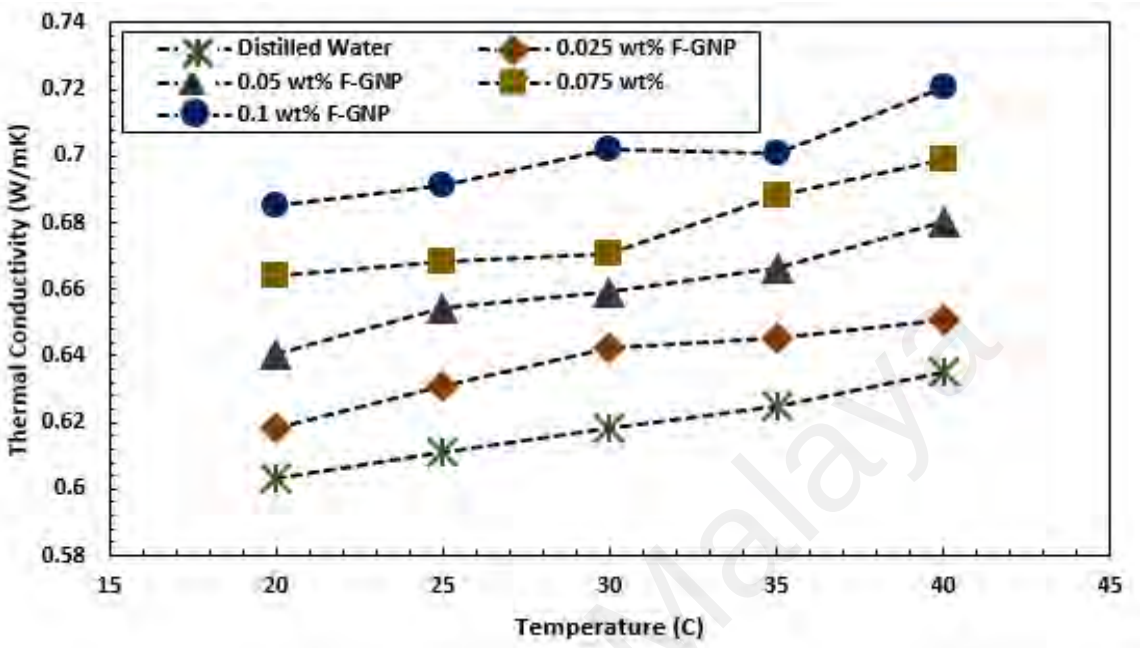

Figure 4. 4: Thermal conductivity plots of water-based F-GNP nanofluids at different temperatures and weight concentrations

A heat flux type differential calorimeter was (TA DSC Q20) used to measure the specific heat capacity of nanofluids. The specific heat capacity of the distilled water as well as water-based nanofluids are shown in Figure 4.5 at various temperatures and at 0.1% weight concentration. In comparison with distilled water, average drop of 3.9% and 7.9% in the specific heat capacities of carbon-based and metal-oxide nanofluids respectively are obtained. Specific heat capacities of the distilled water-based nanofluids are lower than those of water data due to the lower specific heat capacities of nanoparticles loaded in the base fluids (Table 3.11).

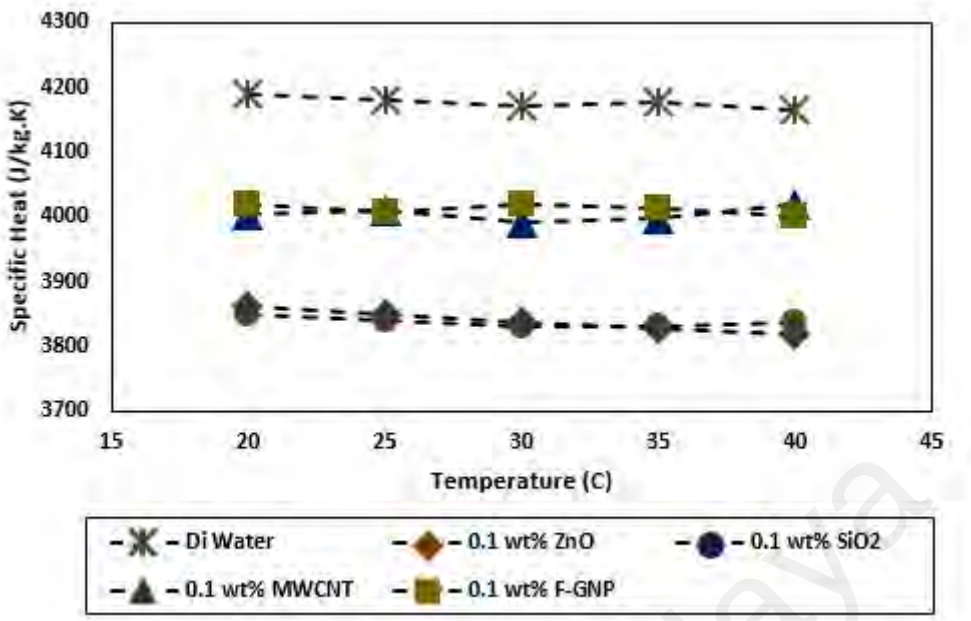

Figure 4. 5: Specific heat capacity plot for different nanofluids at 0.1 wt% and various temperatures

In order to determine the rheological behaviours of four aforementioned water-based nanofluids, the dynamic viscosities were measured at the temperature range of 20 to 40℃. The average values of dynamic viscosities of distilled water and nanofluids, as functions of temperature and weight concentration are presented in Figures 4.6 to 4.9. From which, it is seen that the measured viscosities increases with the nanoparticles weight concentration and the reduction of fluid temperature. The amount of fluctuation in viscosity at different share rate is insignificant.

From these figures, it can clearly be found that viscosity of nanofluids are higher than water and it increases with the increase of weight concentration. For example, the viscosities of ZnO and SiO_2 nanofluids were raised in the ranges of 2.24%-9.47% and 5.36% - 24.22% respectively with the changes in temperature and weight concentration.

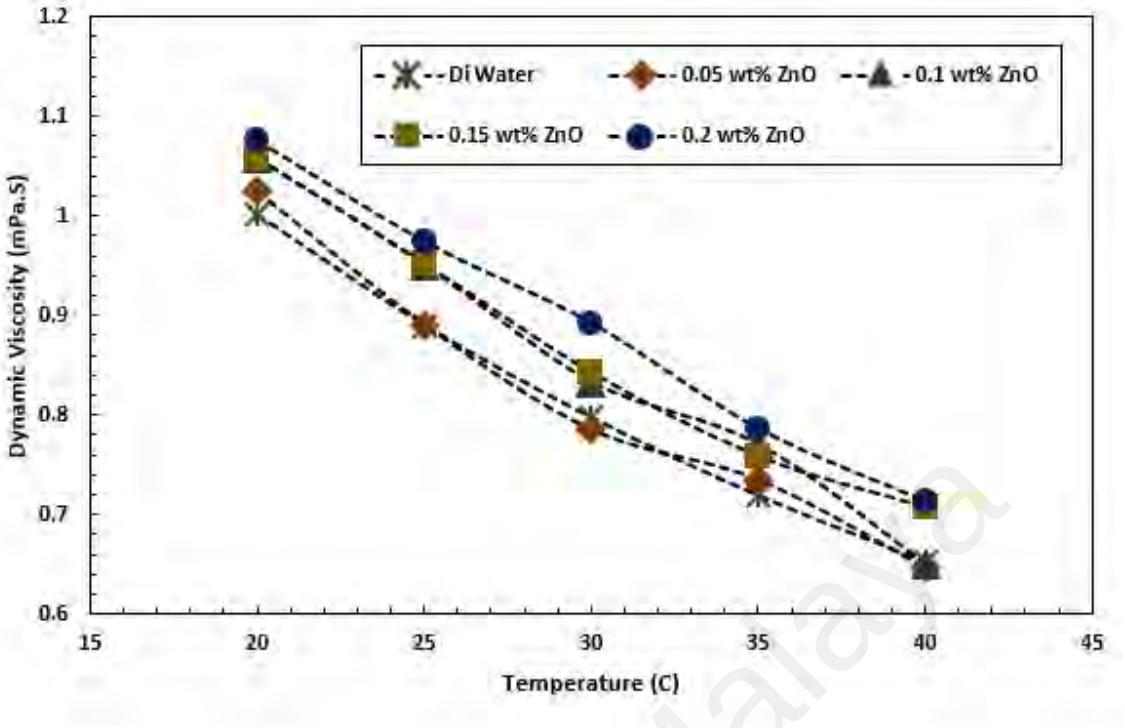

Figure 4. 6: Average dynamic viscosity of water-based ZnO nanofluids at different share rates versus temperature at different nanoparticles weight concentrations.

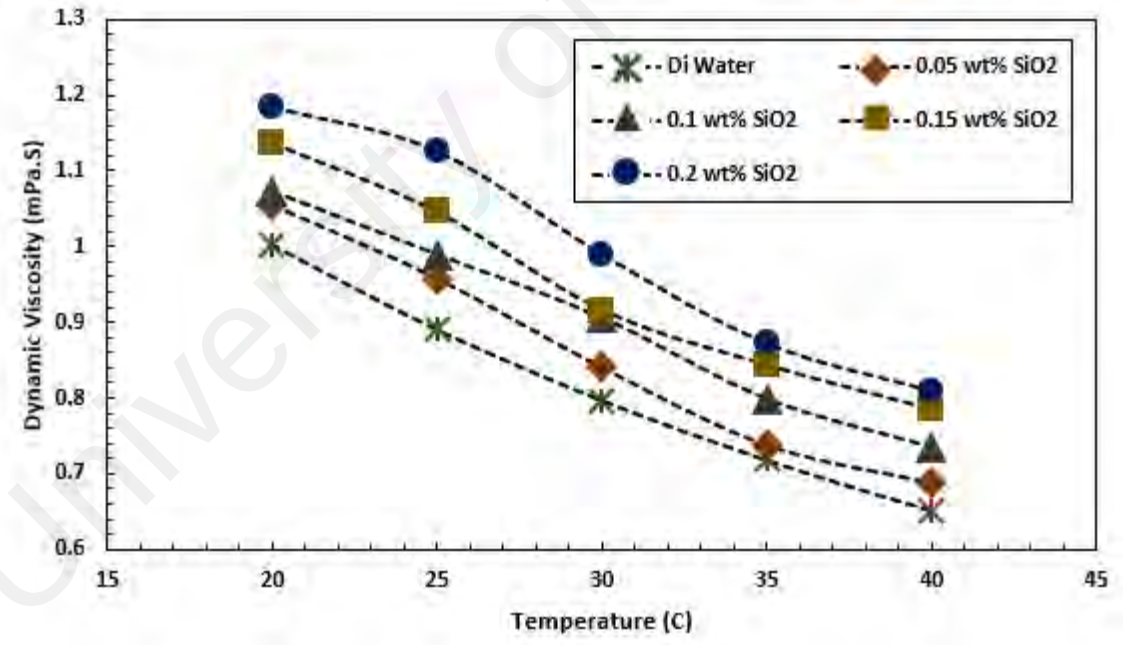

Figure 4. 7: Average dynamic viscosity of water-based SiO_2 nanofluids at different share rates versus temperature at different nanoparticles weight concentrations.

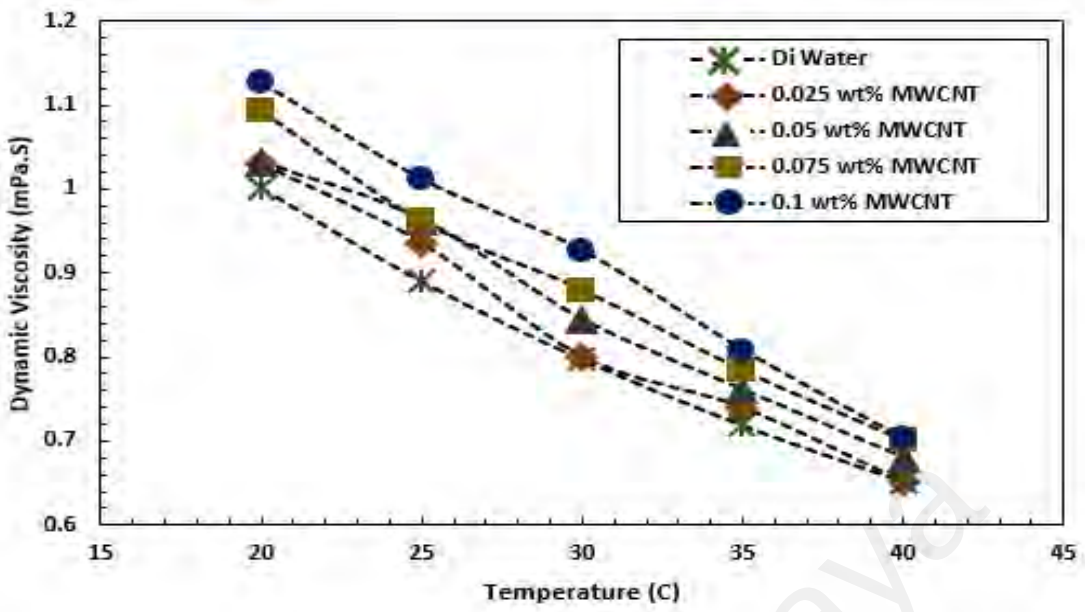

Figure 4. 8: Average dynamic viscosity of water-based MWCNT-COOH nanofluids at different share rates versus temperature at different nanoparticles weight concentrations.

In the following data analysis, based on the Figures 4.8 and 4.9, the values of thermos-physical properties of MWCNT-COOH and F-GNP nanofluids were increased in the ranges of 2.91%-12.48% and 2.74%-11.72%, respectively.

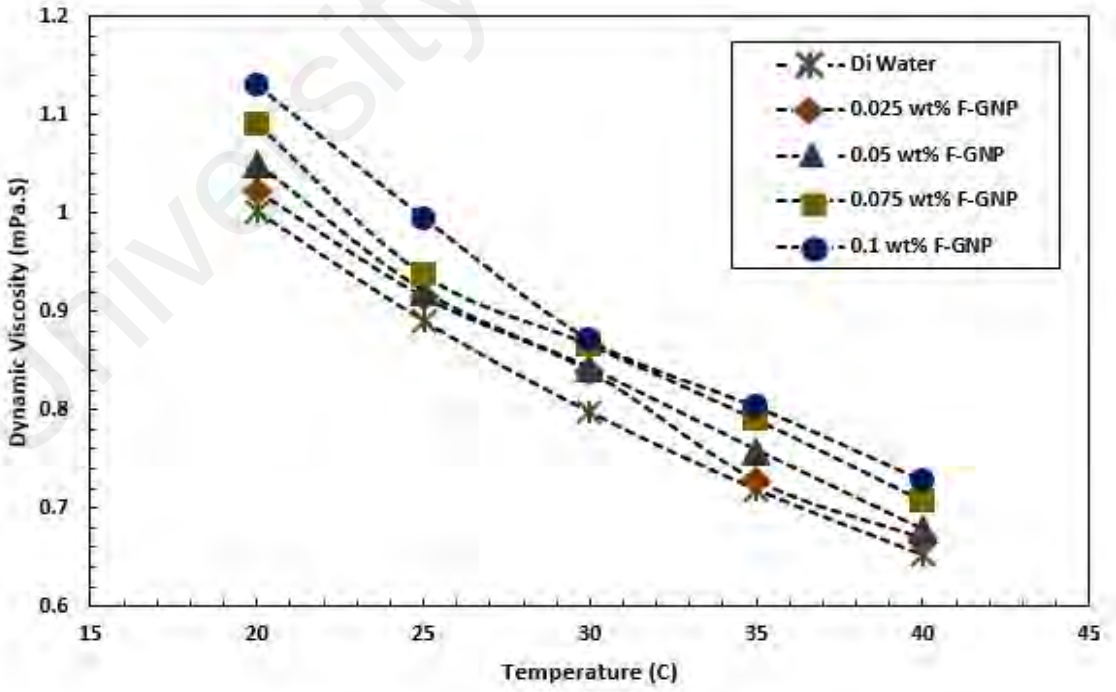

Figure 4. 9: Average dynamic viscosity of water-based F-GNP nanofluids at different share rates versus temperature at different nanoparticles weight concentrations.

The results indicate that the prepared nanofluids are suitable to use at elevated temperatures. Since, by increasing the temperature, thermal movement of molecules and Brownian motion intensifies, and intra-molecular interactions become weakened (Mehrali et al., 2014). In addition, rheological test on nanofluids revealed that the higher concentration increases the viscosity; however, other investigated parameters such as temperature and specific surface areas have an important influence on the viscosity behaviour of nanofluids. Viscosity is measured by the Rheometer, a rheometer consists of outer (chamber) cylinder, and inner (spindle) cylinder and the nanofluid is located between them. As the spindle rotates in the nanofluid, the structure of the nanoparticles molecule changes temporarily and slowly and aligns themselves in the direction of increasing shear.

The densities of distilled water and water-based nanofluids were measured as functions of weight concentration and temperature which are plotted in Figures 4.10-4.13.

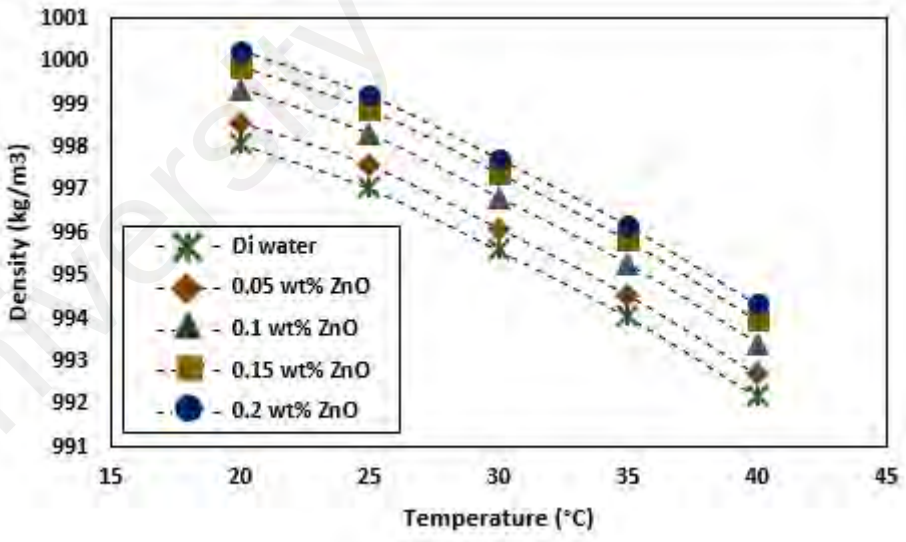

Figure 4. 10: The measured density of water-based ZnO nanofluids versus temperature at different weight concentrations

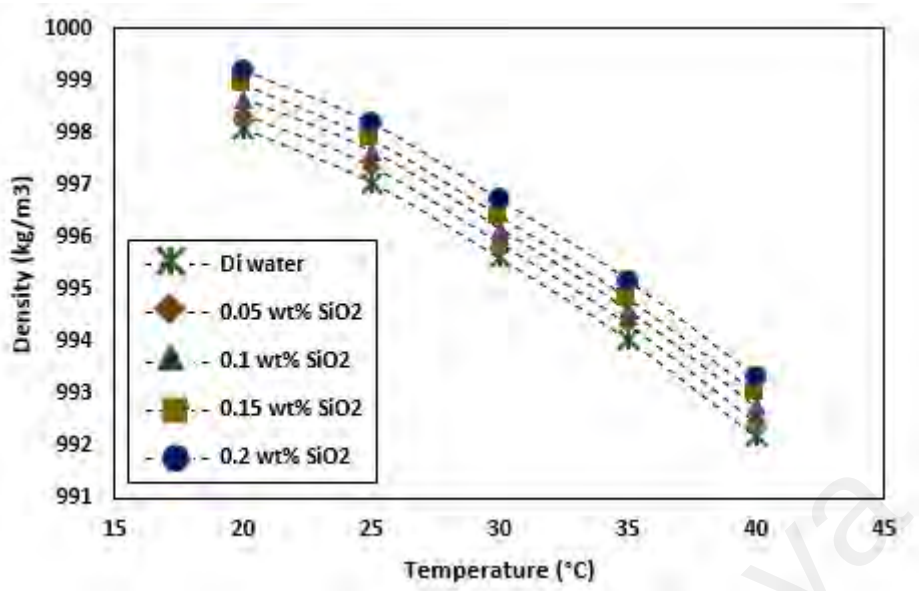

Figure 4. 11: The measured density of water-based SiO_2 nanofluids versus temperature at different weight concentrations

It can be inferred that the density of water-based nanofluids and distilled water decreases with the increase of the temperature, which is related to the thermal expansion of the liquid suspension. Furthermore, the density of the solid particles is usually higher than that of the liquids (Table 3.11) so as the weight concentration of the suspension increases, the density also enhances. The difference between density of the water-based nanofluids at the highest tested weight concentration for each of the ZnO, SiO_2, MWCNT-COOH and F-GNP nanofluids are approximately decreased by 0.59%, 0.58%, 0.604% and 0.59%, respectively, with the rise of the temperature from 20 to 40 °C.

Results show the behaviour of density of nanofluids. The data show that the temperature has reasonable impact on density of the nanofluids. Normally density of all the nanofluids are is higher than the base fluid (water) and with the increase of temperature the density of nanofluid goes on decreasing. Further, with the increase of the nanoparticle weight concentration the density of the suspension enhances.

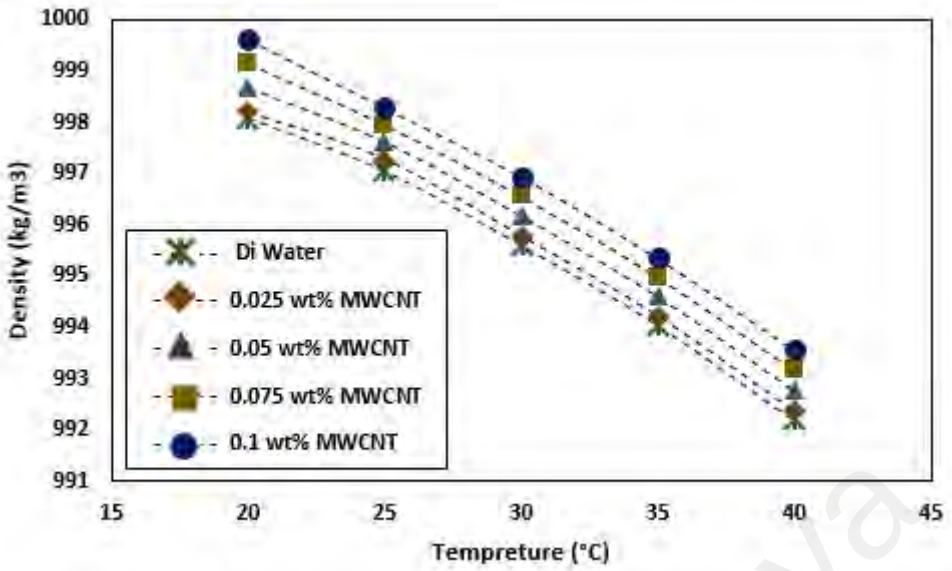

Figure 4. 12: The measured density of water-based MWCNT-COOH nanofluids versus temperature at different weight concentrations

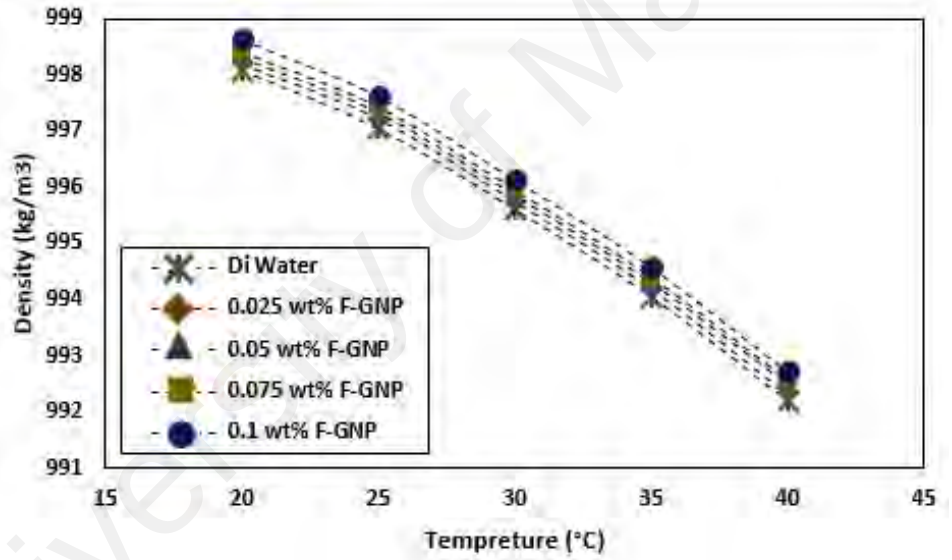

Figure 4. 13: The measured density of water-based F-GNP nanofluids versus temperature at different weight concentrations

4.2 Water-based Nanofluids Stability

The UV–Vis spectroscopy is a common method, which is utilized for the investigation of the stability of the suspended particles in nanofluids. The UV–vis spectrum for the distillated water-based HCFLG nanofluids with different weight concentrations was investigated and photometric analysis of the UV–vis spectrometer

was employed to trace the weight concentrations of samples versus time. The nanofluid solution was diluted with distilled water to allow sufficient transmission while each measurement was repeated three times to achieve better measurement accuracy.

To this end, a standard curve was drawn for each concentration. Figure 4.14 shows the colloidal stability for the four aforementioned water-based nanofluids (F-GNP, MWCNT-COOH, SiO2 and ZnO) versus time. It is seen that the concentration of the samples decreases slightly with time because of agglomeration and sedimentation. However, 4 panels of data in Figure 4.14 show that the relative reduction of weight concentration for all of the samples after 30 days were less than 2% and 14% for carbon-based nanofluids (F-GNP and MWCNT-COOH) and metal oxide nanofluids (SiO_2 and ZnO), respectively. The high colloidal stability of distillated water-based MWCNT-COOH and F-GNP nanofluids is attributed to the small particle size associated with very high specific surface areas.

It can be seen that the colloidal mixture shows a downward trend of relative concentration as the time progressed, indicating that the level of particle concentration and thus the stability subsided. Also, the relative concentration (absorbance intensity) including F-GNP and MWCNT-COOH show the low amount of sedimentation.

The sediment of all the samples remains almost constant after 20 days, representing almost 2% and 14% for carbon-based nanofluids (F-GNP and MWCNT-COOH) and metal oxide nanofluids (SiO_2 and ZnO), respectively. These amounts were obtained for the highest weight concentrations of each the nanofluids.

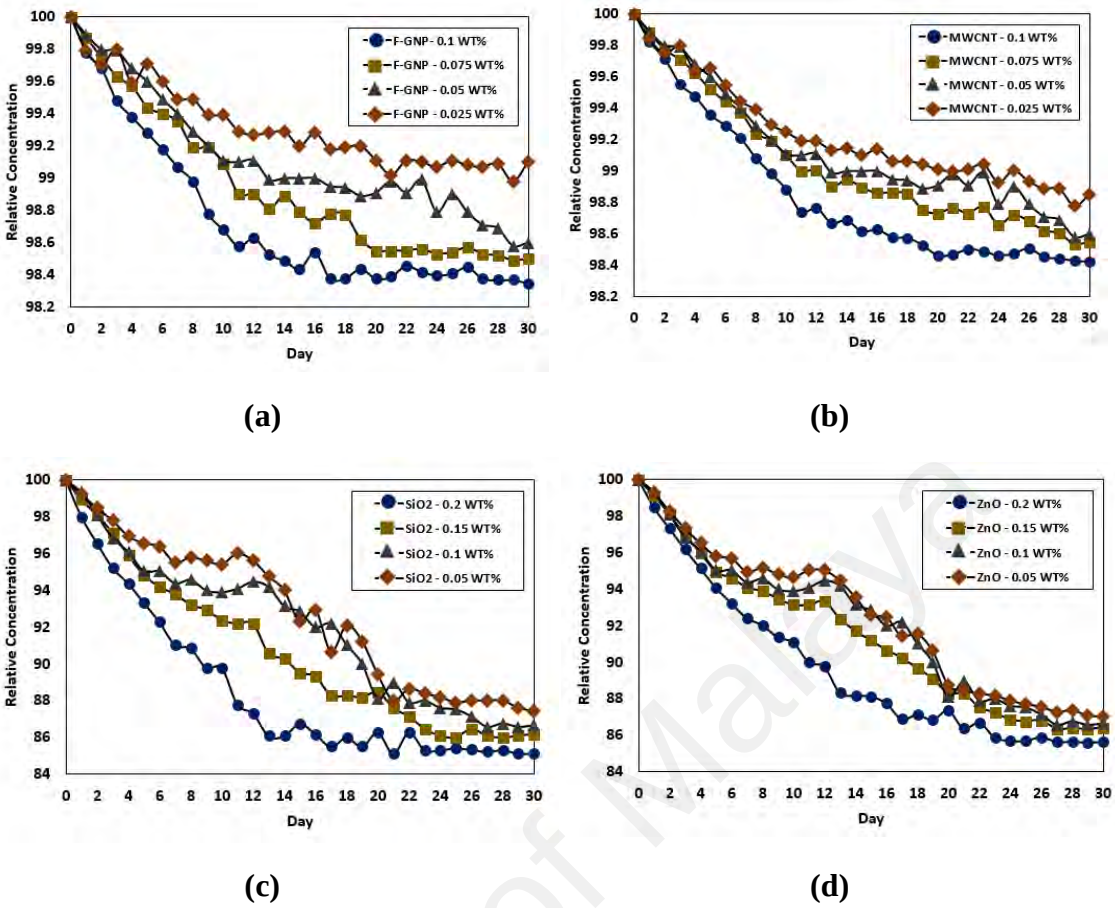

Figure 4. 14: The colloidal stability of water-based nanofluids as a function of time and weight concentration; (a) F-GNP nanofluids, (b) MWCNT-COOH nanofluid, (c) SiO_2 nanofluid, and (d) ZnO nanofluid.

4.3 Toward Improved Heat Transfer Performance through Sudden Expansion

The literature reviews of applications reveal that the majority of previous studies on the heat transfer over a backward-facing step used water-based suspension of metal or metal oxide nanofluids and the lack of highly-conductive nanofluids including the few-layered graphene and the single/multi wall carbon with high stability and specific surface area are obvious. They were also mostly focused on heat transfer in the laminar regime and just few numbers of works reported study on transition and turbulent flow regimes over a backward-facing step. Thus, discovering the heat transfer behaviour of water and highly-conductive nanofluids in the turbulent flow regimes is the second target of this study.

To this end, three phases of study have been performed to investigate the heat transfer behaviour of water-based nanofluids as well as water over a backward facing step. Accordingly, water-based F-GNP, MWCNT-COOH, SiO_2 and ZnO nanofluids for different low weight concentrations were prepared, and thermo-physical properties and colloidal stability were investigated (sections 4.1 and 4.2). Lastly, heat transfers parameters such as Nusselt number (Nu) and the convective heat transfer coefficient (h) over a backward-facing step in turbulent flow regimes were investigated for the four aforementioned nanofluids and compared with water as the base fluid. The results suggest that water-based F-GNP and water-based MWCNT-COOH nanfluids are the highly conductive nanofluids at very low weight concentrations.

4.3.1 Data Processing

Measurement of the thermo-physical properties containing density, viscosity, thermal conductivity and specific heat capacities at different volume fractions were done experimentally. An investigation of the heat transfer behavior of the nanofluids was performed by evaluating the heat transfer coefficient. The measurements were performed in the Reynolds number range of 4,000 to 16,000 for the distilled water, MWCNT-COOH, F-GNP, SiO_2 and ZnO nanofluids. Data were compared for a variety of nanofluid concentrations up to 0.2 wt. % and 0.1 wt. % for metal oxide nanofluids and carbon based nanofluids, respectively.

The convective heat transfer coefficients (h) could be determined by measuring the wall temperatures at different axial dimensional ratios and the temperature of bulk fluid along with the flow rate of the working fluids, and the inlet and outlet temperatures. The Reynolds number can be calculated from Equation 4.1.

$$Re = \frac{\rho\, U_{ave}\, D}{\mu} \tag{4.1}$$

Where, ρ and μ are density, viscosity of the working fluid and D is the downstream diameter. U_{ave}, is the average flow velocity which can be calculated from Equation 4.2.

$$U_{ave} = \frac{\dot{m}}{\rho\, A_c} \tag{4.2}$$

Where, ṁ and A_c are mass flow rate and surface area of the cross section.

The DC power supplies provided a total power (Q) to the heated section which equals to 600 W. Accordingly, the local heat transfer coefficient ($h_{(\frac{X}{H})}$) could be determined from Equation 4.5 at constant wall heat flux (q) of 12,128.56 W/m^2. The experiments were conducted at the Reynolds number range of 4,000–16,000.

$$Q = \dot{m}\, C_p\, (T_{out} - T_{in}) \tag{4.3}$$

$$q = \frac{Q}{A_w} \tag{4.4}$$

$$h_{(\frac{X}{H})} = \frac{q}{T_{s\,(\frac{X}{H})} - T_{b\,(\frac{X}{H})}} \tag{4.5}$$

Where, $T_{s\,(\frac{X}{H})}$ is the temperature of pipe surface at the distance of axial ratio ($\frac{X}{H}$) and the streamwise distance (X) is normalized by the step height H ($H = 0.5(D-d)$). Further, the temperature of the bulk fluid ($T_{b\,(\frac{X}{H})}$) at the distance of axial ratio is calculated by Equation (4.6) [32]:

$$T_{b\,(\frac{X}{H})} = T_{in} + \frac{Q\,(X/L)}{\dot{m}\, C_p} \tag{4.6}$$

Where L is a length of corresponding wall and C_p is specific heat capacity of working fluid.

The local Nusselt number ($Nu_{(\frac{X}{H})}$) could be evaluated from Equation 4.7

$$Nu_{\left(\frac{X}{H}\right)} = \frac{h_{\left(\frac{X}{H}\right)} D}{K} \tag{4.7}$$

Where, K is thermal conductivity of the working fluid.

In order to calculate the friction factor, "f", the pressure drop (ΔP) across the test section was measured by a Foxboro™ differential pressure transmitter and Equation (4.8) was used. That is,

$$f = \Delta P \frac{2D}{\rho U_{ave}^2 L} \tag{4.8}$$

Employing new working fluids as the coolant, it requires investigation of their thermal performance, as well as, their suitability as an appropriate alternative candidate for a range of Reynolds numbers and temperatures. According to researchers (Samira et al., 2015), use of nanofluids as the working fluids in heat exchangers provides increase in both heat transfer coefficient (positive effects) and pressure drop (negative effects). To assess the effectiveness of the four aforementioned water-based nanofluids, a performance index is evaluated which is represented by Equation 4.9.

$$PI = \frac{\left(h_{nf}/h_{bf}\right)}{\left(\Delta P_{nf}/\Delta P_{bf}\right)} \tag{4.9}$$

The subscripts, *nf* and *bf* refer to the nanofluid and base fluid, respectively. As mentioned above, the use of nanofluids along with the sudden expansion in the duct not only increases the Nusselt number, but also increases the friction factor. In order to assess the overall performance of the system, including the thermal performance, as well as, the hydraulic performance of the system, the performance evaluation criterion (PEC) is examined. The PEC shows the ratio of thermal performance of nanofluids in comparison to the Di-water to the hydraulic performance of nanofluids in comparison to Di-water. Mathematically, the PEC is given by Equation 4.10 (Manca et al., 2012).

$$PEC = \frac{Nu_{nf}/Nu_{bf}}{\left(f_{nf}/f_{bf}\right)^{\frac{1}{3}}} \tag{4.10}$$

Equation 4.11 provides an appropriate parameter for clarifying the range of temperatures and velocities that the synthesized coolant can be used (Samira et al., 2015). To study the energy saving in the turbulent flow region, the pumping power can be measured (Mansour et al., 2007). Thus the pumping power ratio is represented by Equation 4.11.

$$\frac{W_{nf}}{W_{bf}} = \left(\frac{\mu_{nf}}{\mu_{bf}}\right)^{0.25} \left(\frac{\rho_{bf}}{\rho_{nf}}\right)^{2} \tag{4.11}$$

Where, W_{nf} and W_{bf} are, the pumping powers for the nanofluid and the base fluid respectively.

The uncertainty analysis of the experimental data for the heat transfer and flow characteristics in the test-rig are of critical importance to ensure the range of validity and the applicability of the test results. Here uncertainty analysis according to the method described by Kline (1953) was performed and the resulting uncertainties in the Nusselt number, heat transfer coefficient and friction factor measurements are listed in Appendix A.

The analysis showed that the uncertainties in average Nusselt number, average heat transfer coefficient and friction factor and performance index are ±5%, ±6%, ±6% and ±6%, respectively.

4.3.2 Heat Transfer Performance Benchmark by Sudden Expansion

In this study, turbulent forced convection heat transfer to nanofluids in an axisymmetric abrupt expansion heat exchanger is investigated experimentally. The water-based nanofluids (Metal oxides and Carbon-based ones) with unique thermo-physical properties were prepared. In this investigation, the rate of heat transfer at fully developed

turbulent flow of nanofluids flowing through the sudden expansion with the expansion ratio (ER) of 2 was experimentally determined for various weight concentrations and Reynolds numbers of four different nanoparticles. To address this issue, water-based metal-oxide samples such as ZnO and SiO_2 with four weight concentrations of 0.05, 0.1, 0.15 and 0.2 wt% were utilized. The carbon based nanofluids were kept at maximum weight concentration of 0.1 wt%, where other three different weight concentrations such as, 0.025, 0.05 and 0.075 wt% were chosen for carbon-based nanofluids (MWCNT-COOH and F-GNP).

The local Nusselt number as a candidate for introducing heat transfer rate were measured in the Reynolds number range of 4000-16000. A constant heat flux of 600 W was provided after the expansion via two DC power supply units. The inlet fluid rate was in the range of 4 to 16 Lit/min. Also, the inlet flow temperature was always maintained at a constant temperature of 30 ± 1 ºC.

4.3.2.1 Water Run

Figure 4.16 shows the temperature of the heated wall (T_S), the temperature difference between the wall and the fluid bulk (T_S-T_b), local convective heat transfer coefficient (h) and Nusselt number (Nu) versus X/H (H is the step height) for distillated water at different Reynolds numbers (Re). In both plots of T_S versus X/H and T_S-T_b versus X/H, a U-shape variation of the T_S or T_S-T_b with X/H is seen. Heat transfer in back ward facing step was studied by a number of researches (Abu-Nada, 2008; Lancial et al., 2013; Mohammed et al., 2015) in the recent years. Here, the boundary layer flow separates at the sharp step edge and form a recirculation region, as shown schematically in Figure 4.15.

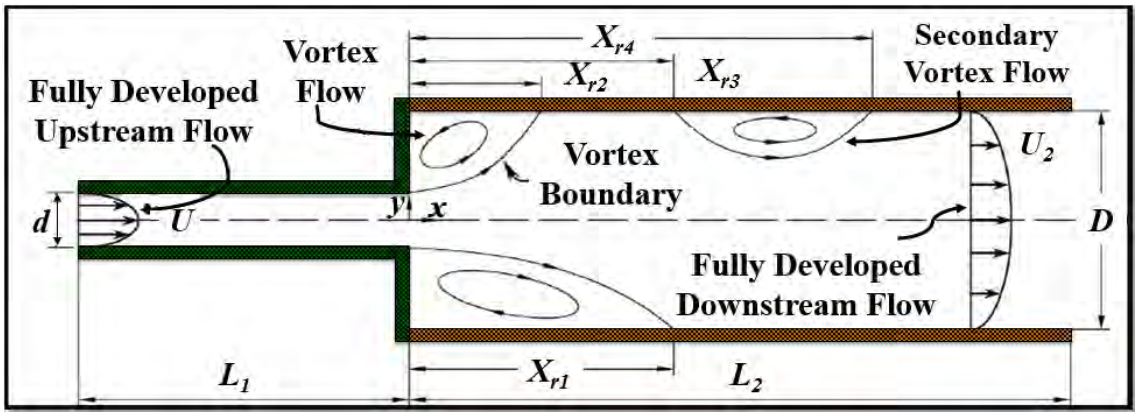

Figure 4. 15: Schematic view of different zones in upstream and downstream of backward facing step pipe.

The shear layer, downstream, impinges on the surface and reattaches to the lower wall at the so-called reattachment point (Eaton & Johnston, 1981). Downstream of the reattachment point, the boundary layer begins to redevelop and far downstream the flow approached fully developed flow in the larger diameter pipe. The separation and reattachment in this area cause major changes in the flow in the region. Close to the step, the velocity is insignificant, leading to the maximum wall temperature and consequently minimum Nusselt number. On the other hand, the velocity can reach the maximum amount in the recirculation zone, where the wall temperature is minimum and the Nusselt number is maximum. So, a U-shape variation of the T_S or T_S-T_b with X/H is reasonable and were reported by a majority of recent studies in this field (Abu-Nada, 2008; Lancial et al., 2013; Mohammed et al., 2015).

In general, within the separated region, the wall-to-bulk temperature difference decrease with increasing X/H until a minimum value is reached at the point of reattachment. Then, with further increase in X/H, the temperature difference becomes larger and finally achieves a constant value except Re = 4000, thereby indicating the attainment of the thermally developed state.

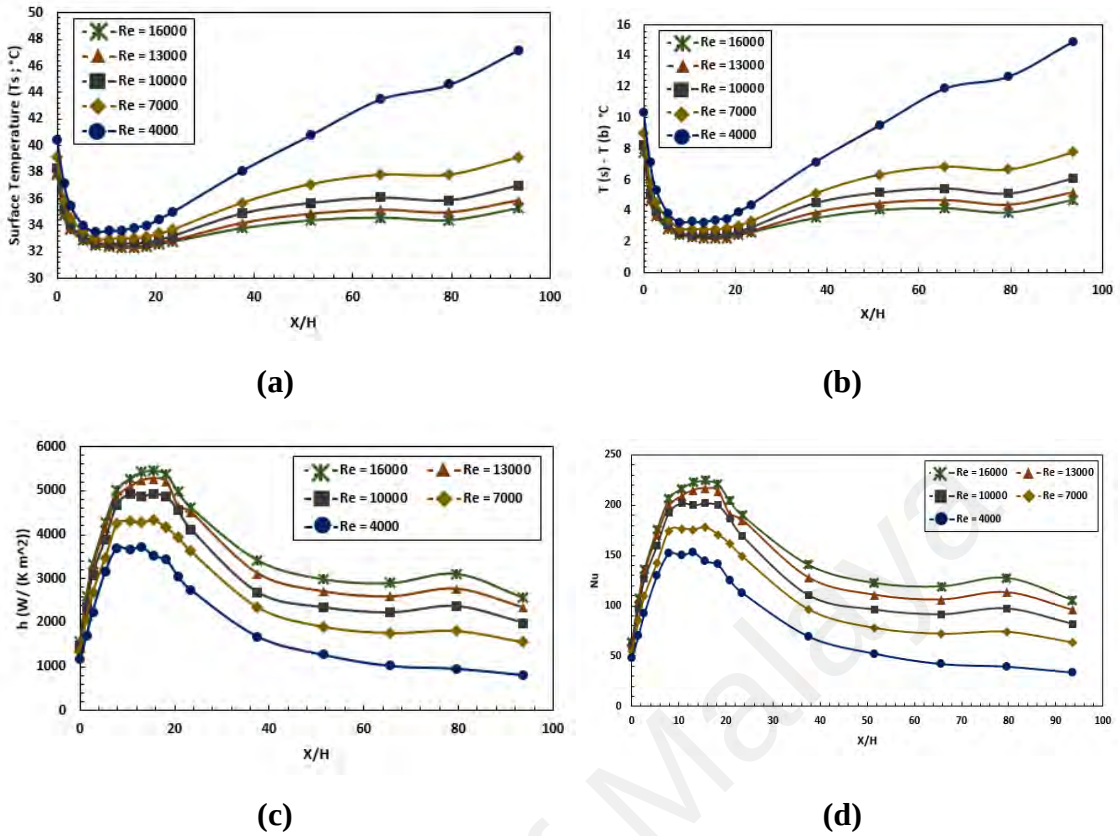

Figure 4. 16: The water run results; (a) Measured temperature of the heated wall (T_S), (b) the temperature difference between the wall and the fluid bulk (T_S-T_b), (c) local convective heat transfer coefficient (h) and (d) Nusselt number (Nu) versus X/H for distillated water at different Reynolds numbers (Re).

Furthermore, in Figure 4.16 there is a sharp downward trend of temperature with X/H up to around 7.87, after which the temperature of the heated wall (T_S) and the temperature difference between the wall and the fluid bulk (T_S-T_b) for the deionized water increase moderately with further increase of X/H.

Although the fully developed value of the wall-to-bulk temperature difference (T_S-T_b) were approximately 4° - 6° for Re ranges from 7000 to 16000, the local values at the point of reattachment were much more, ranging from 2° to 2.5° for the data conditions of the figure. In general, the smaller temperature differences at the point of reattachment corresponded to stronger separation.

The heat transfer coefficient was computed from the temperature given by the thermocouples in different positions. Equations (4.5) and (4.7) indicate that the local convective heat transfer coefficient ($h_{(X/H)}$) and local Nusselt number ($Nu_{(X/H)}$) have an

inverse relation with the temperature difference between the wall and the bulk fluid. Therefore, for X/H less than 7.87 for distillated water, the amount of local convective heat transfer coefficient (h) and local Nusselt number (Nu) increase. By contrast, the h and Nu show a downward trend for X/H higher than 7.87.

The measured variation of the local Nusselt number with the distance along downstream of the expansion over a range of Reynolds numbers is plotted for distilled water in Figure 4.17. Following convention, streamwise distance is normalized by the step height *H (H = 0.5(D-d)),* and The Nusselt number is normalized by the value for fully developed pipe flow given by the Dittus-Boelter formula (Equation 4.12).

$$Nu = 0.023Re^{0.8}Pr^{0.4} \tag{4.12}$$

Generally, the results display a similar character as shown in earlier studies with a peak level of heat transfer coefficient occurring at about ten step heights downstream, followed by a gradual reversion toward the value associated with fully developed pipe flow.

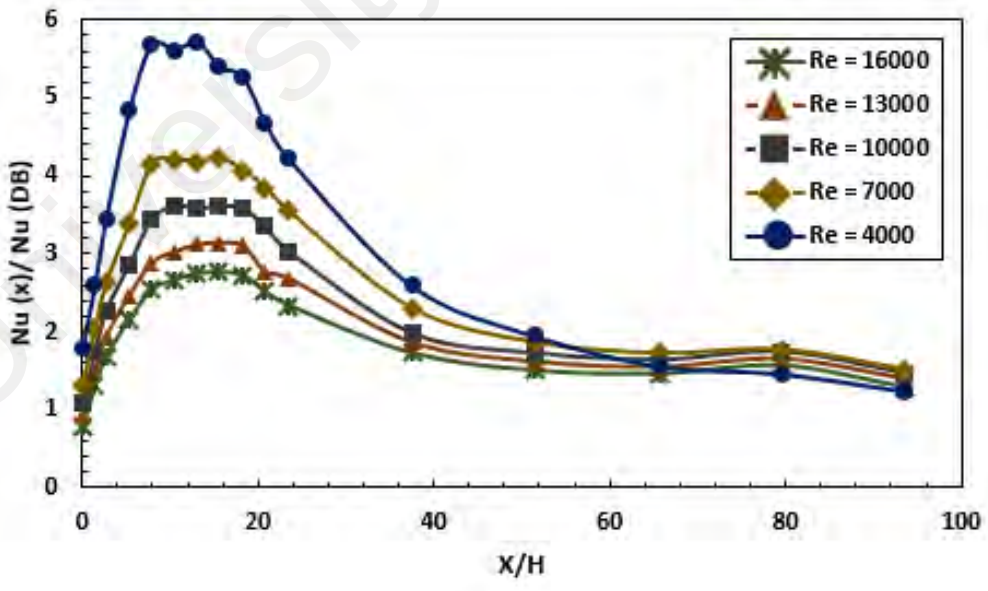

Figure 4. 17: Heat transfer at downstream of the abrupt expansion at various Re for distilled water

According to Figure 4.17, it can be observed that with the progressively increasing of the Reynolds number, the value of $Nu_{(X/H)}/Nu_{(DB)}$ drops down monotonically. This

behaviour is qualitatively in accord with the water tests data of Ede et al. (1956). The magnitude of the heat transfer coefficients in the separated region are remarkably high, several times the corresponding fully developed values.

From the data it is found that the Reynolds number affects the distance (*X/H*) locating the position of Nu_{max} (Fig. 4.17). However, although the uncertainties in the results are little, they are still large enough to make this suggestion speculative (Baughn et al., 1984).

A minimum value of Nu occurs at approximately one step height away from the downstream entry section, a feature that very strongly suggests the presence of a counter rotating eddy trapped in the corner beneath the larger and more active recirculating flow region. In this case, the Nusselt numbers are greater than the data from the fully developed pipe flow indicating that the level of the turbulent transport is high even though the recirculating velocities will be only a few percent of the bulk mean velocity. This feature agrees at least qualitatively with what is known about turbulent transport processes in recirculating flows.

The distillate water measurements show that the local heat transfer coefficient in separated, reattached, and redevelopment regions are several times as large as those for a fully developed flow. For instance, at the point of reattachment, the coefficients were 2.5 to 5.7 times greater than the corresponding fully developed values. Generally, the increase of the heat transfer coefficient owing to flow separation is accentuated as the Reynolds number decreases.

4.3.2.2 Heat Transfer for Nanofluids

Figures 4.18, 4.19, 4.20 and 4.21 represent the measured Nusselt number which is a candidate for introducing heat transfer rate of nanofluid samples with different weight concentrations at different Re numbers and axial dimension ratios (X/H). The striking

feature of these graphs is that the heat transfer coefficients in the separated, reattached, and re-development regions are several times as large as those for a fully developed flow.

For a given test condition, the figures very clearly show that the local Nusselt number ($Nu_{(X/H)}$) reached its peak at the X/H range of 10 to 12 before starting to decrease gradually. The location of the maximum Nu is believed to coincide with the point of flow reattachment. Also, these results display that the nanoparticles volume fraction does not affect considerably the recirculation zones size for turbulent flow. This interpretation is consistent with interpretations of experimental results for external flows. The separated region lies upstream of the point of reattachment and the redevelopment region lies downstream of this point. Further consideration of the Figures 4.18 – 4.21 reveal that in some cases, the curves separation peaks are sharp, while for some others are rounded. Thus, in former case, the point of reattachment appears to be quite well defined; for the latter, the reattachment is somewhat spread out, resulting from the effect of rigorous eddies.

It can be seen that the local Nusselt number has the various relationship with the measured temperature. The results clearly show as the weight concentration increases, the local Nusselt number for all the axial ratios rises, representing higher heat transfer rate than those of the base fluid. The increase in heat transfer performance owing to flow separation is strongly accentuated as the Reynolds numbers increases.

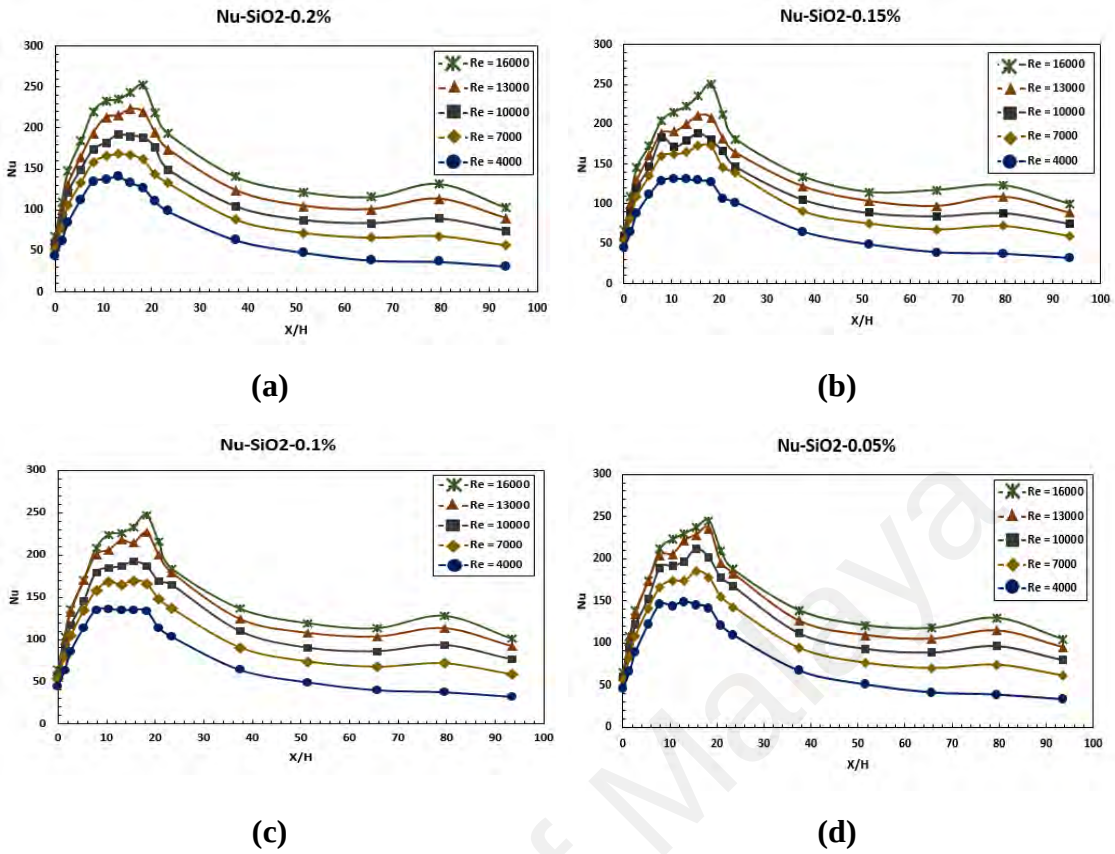

Figure 4. 18: Experimental Nusselt number of water based SiO_2 nanofluids at the downstream of sudden expansion at different weight concentrations as a function of Re and different positions along the downstream passage; (a) 0.2 wt%, (b) 0.15 wt%, (c) 0.1 wt% and (d) 0.05 wt%.

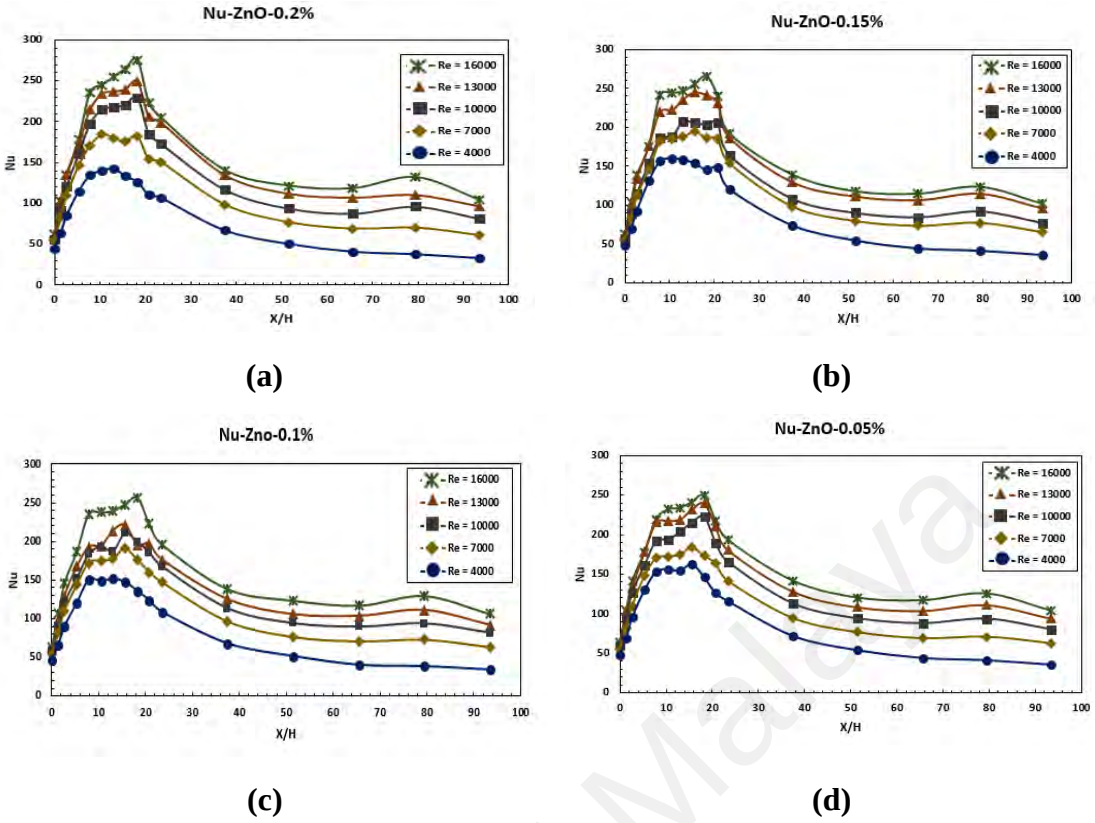

Figure 4. 19: Experimental Nusselt number of water based ZnO nanofluids at the downstream of sudden expansion at different weight concentrations as a function of Re and different positions along the downstream passage; (a) 0.2 wt%, (b) 0.15 wt%, (c) 0.1 wt% and (d) 0.05 wt%.

The comparison between these four types of nanofluids, show that the carbon-based nanofluids have a greater effect on enhancing heat transfer at the downstream of sudden expansion pipe flow. Figures 4.20a and 4.21a represent the highest weight concentration (0.1 wt%) of MWCNT-COOH and F-GNP nanofluids where the observed maximum Nusselt numbers are 262.03 and 300, respectively. The maximum Nu were occurring almost 10 to 12 step heights of the step in the downstream zone. According to Figures 4.18 and 4.19, for the same weight concertation, panels 4.18c and 4.19c display the maximum Nusselt numbers equal to 247.05 and 256.62 for SiO_2 and ZnO, respectively. Clearly these results show, the great enhancement in heat transfer performance for nanofluids in comparison with distilled water Nusselt number of 224.41 at the same axial position. At a point, the heat transfer performance improved 33.7 % and 16.7% by using F-GNP and MWCNT-COOH nanofluids at 0.1 wt% concentration instead of water.

Additionally, 14.35 % and 10.1 % enhancement were achieved by utilizing ZnO and SiO_2 nanofluids at the same weight concentration of 0.1 wt%.

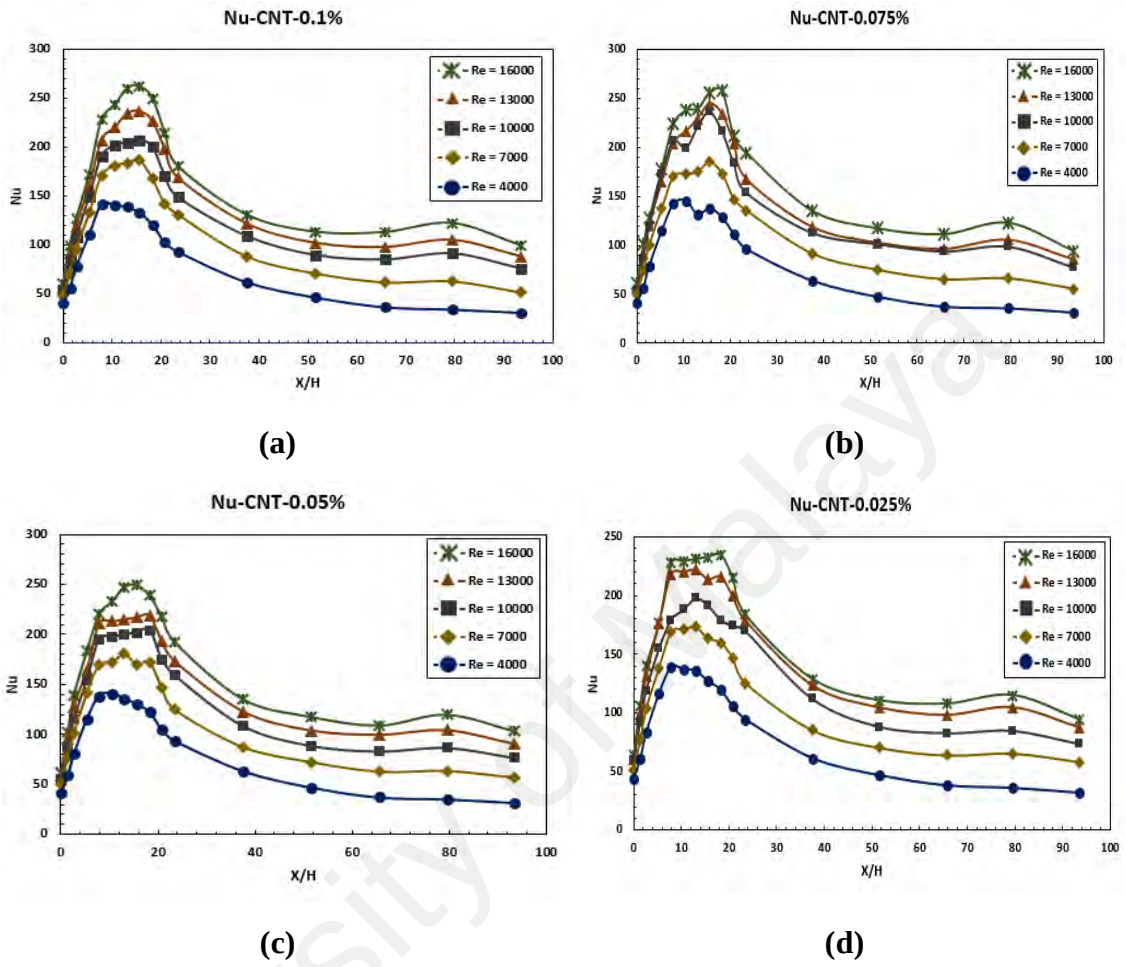

Figure 4. 20: Experimental Nusselt number of water based MWCNT-COOH nanofluids at the downstream of sudden expansion at different weight concentrations as a function of Re and different positions along the downstream passage; (a) 0.1 wt%, (b) 0.075 wt%, (c) 0.05 wt% and (d) 0.025 wt%.

For the metal-oxide nanofluids, the heat transfer performance improved up to 275.35 and 252.65 at the highest weight concentration of 0.2 wt%, which is virtually 22.7 % and 12.6 % increment on heat transfer performance by using ZnO and SiO_2 nanofluids, respectively.

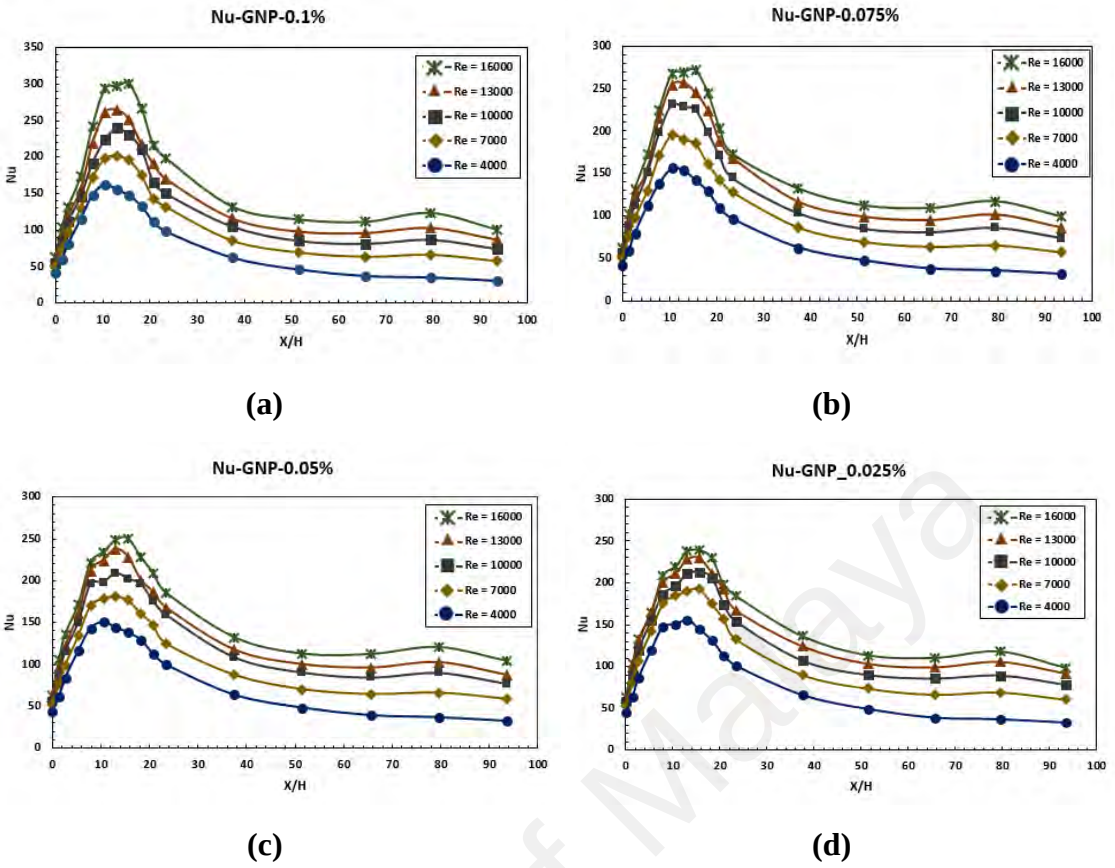

Figure 4. 21: Experimental Nusselt number of water based F-GNP nanofluids at the downstream of sudden expansion at different weight concentrations as a function of Re and different positions along the downstream passage; (a) 0.1 wt%, (b) 0.075 wt%, (c) 0.05 wt% and (d) 0.025 wt%.

The effect of weight concentration of nanoparticles in water-based nanofluids on the temperature gradient term ($T_{s\,(X/H)} - T_{b\,(X/H)}$) is not negligible. However, experimental results confirm that the effects of weight concentration of nanoparticles on the thermal conductivity and on the temperature gradient terms are more obvious. The reason for larger improvement of the Nusselt number of carbon-based nanofluids compared to that of the distilled water was introduced by Solangi et al. (2016) using a simple analogy that the connective heat transfer is proportional to k/δ_t, where δ_t is the thickness of the thermal boundary layer. Thus, to increase the convective heat transfer coefficient, k can be increased and/or δ_t can be decreased. Based on recent studies (Aravind & Ramaprabhu, 2013; Solangi et al., 2016), carbon nanomaterials such as carbon nanotubes and graphene have a tendency to reduce the thermal boundary layer thickness.

Alternatively, the measured thermal conductivity of nanofluids increases with the increase in the concentration. Therefore, both terms have positive effects on enhancing the heat transfer rate in the presence of nanofluids including carbon-based nanoparticles. This inference is similar to the observations in recent researches (Abu-Nada, 2008; Amiri et al., 2017; Elham Montazer et al., 2018).

Abu-Nada (2008) illustrated the peak value of Nusselt number occurs simultaneously with the point of reattachment. Like other studies by several observers (Abu-Nada, 2008; Amiri et al., 2017; Heshmati et al., 2014; Elham Montazer et al., 2018), an enhancement in the convective heat transfer coefficient is observed by loading more nanoparticles in the base fluid after the point of reattachment. Therefore, the high convective heat transfer coefficient inside the recirculation depends mainly on the thermos-physical properties of the nanoparticles. Correspondingly, both the thermo-physical properties of the nanofluids and its Reynolds number affect the value of the heat transfer coefficient outside the recirculation zone. In conclusion, Figures 4.18, 4.19, 4.20 and 4.21 display that the position of peak value of the local Nusselt number improves with the enhancement of weight concentration and Reynolds number.

In order to perform an appropriate comparison, the variation of average heat transfer coefficient with the Reynolds number for four aforementioned water-based nanofluids at different weight concentrations as well as water were evaluated, as shown in Figure 4.22. Approximately for most of the samples, the average heat transfer coefficient increases with the Reynolds number and weight concentrations. The highest average heat transfer coefficient was achieved for water-based F-GNP nanofluid with weight concentration of 0.1% and Re number of 16,000, representing the average heat transfer coefficient of 4950.61 W/m^2K. For instance, the maximum ratio of enhancement in the average heat transfer coefficient was almost 26% for water-based F-GNP nanofluid at 0.1 wt. % and Re number of 16,000 as compared with pure water, where the improvement is notable.

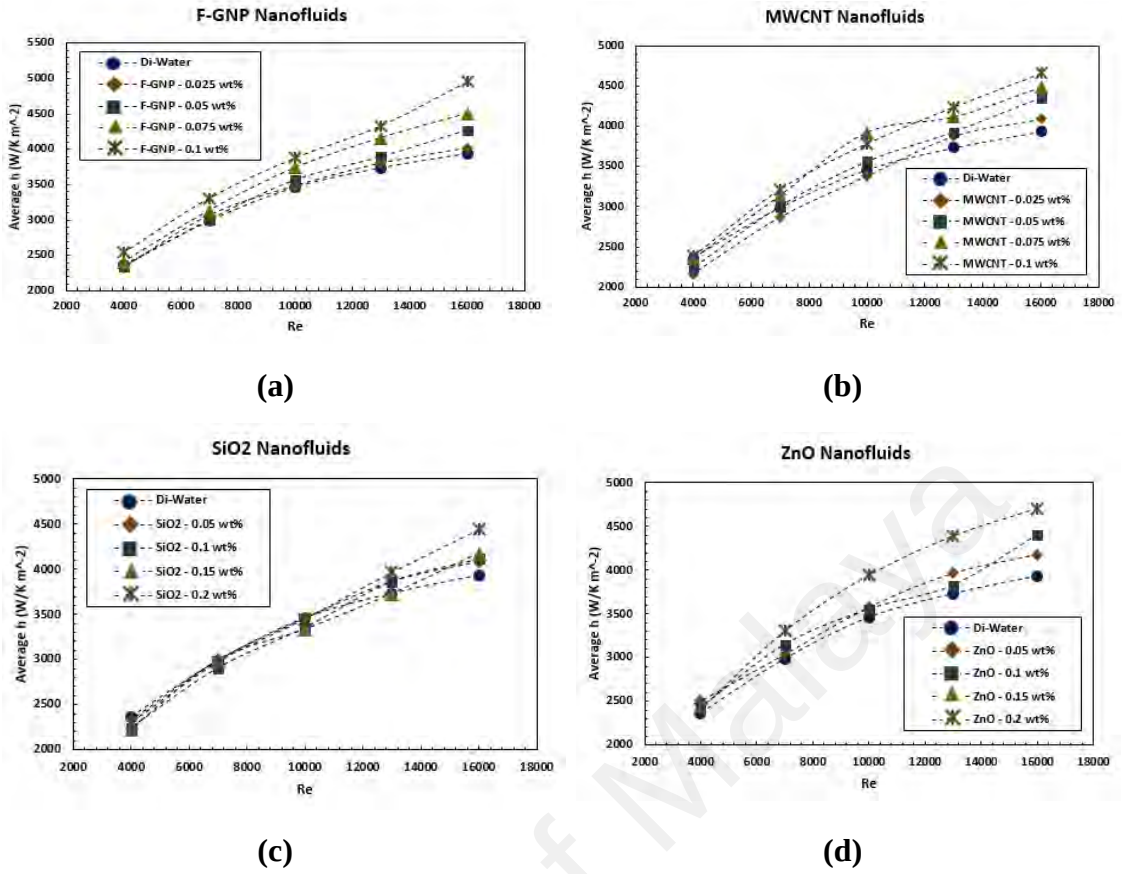

Figure 4. 22: Average heat transfer coefficient of distilled water and water based nanofluids flow through a sudden expansion; (a) F-GNP nanofluids, (b) MWCNT nanofluids, (c) SiO_2 nanofluids, and (d) ZnO nanofluids.

Figure 4.23 shows the variations of $(X/H)_{max}$ for the four aforementioned water-based nanofluids and distilled water for different Re numbers and weight concentrations. It is seen that the position of maximum value of Nusselt number increases (shifts up) with the Re number. It is observed that as the concentration increased, the temperature difference between the tube wall and the working fluid decreased due to higher thermal conductivity, implying higher heat transfer rate. For the same expansion ratio of 2, it is observed that the higher Re number leads to the higher local Nusselt number. The position as well as the value of $(X/H)_{max}$ increased as the Re number increased, representing that $(X/H)_{max}$ is dependent on Re and concentration of additives (thermal conductivity).

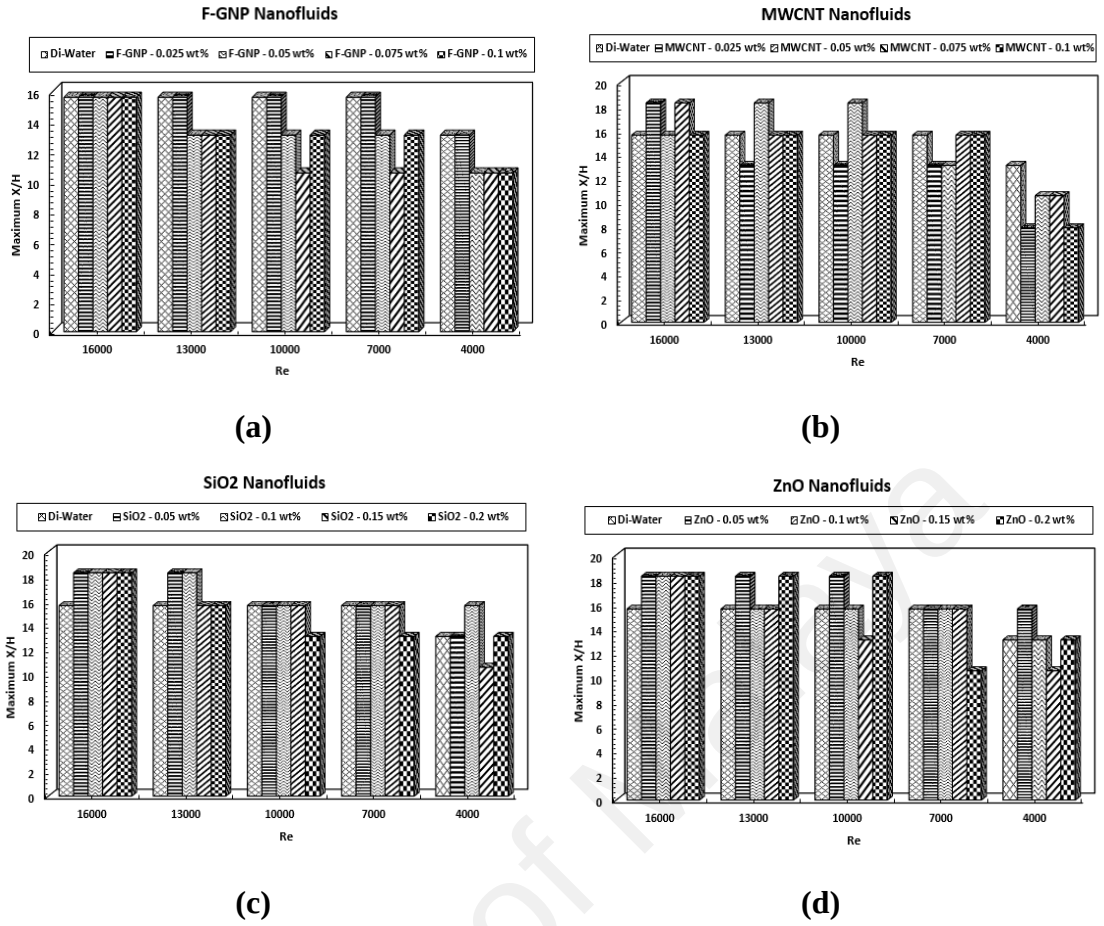

Figure 4. 23: The effect of Reynolds number and weight concentration on the position of maximum local Nusselt number for different water based nanofluids; (a) F-GNP nanofluids, (b) MWCNT-COOH nanofluids, (c) SiO_2 nanofluids, and (d) ZnO nanofluids.

Figure 4.24 represents the plots of the pressure drop of flow over the backward-facing step for different Re numbers and weight concentrations of the water based nanofluids as well as distilled water. It is seen that as the Re number and concentration of all the nanoparticle samples in the base fluid increase, then the pressure drop increases. It is noteworthy that the pressure drops for the prepared samples are quite close to that for the distilled water, which is attributed to the low concentrations. Figure 4.24 also shows that the pressure drop for carbon based samples at the concentration of 0.1 wt% and Re number of 16000 has the highest pressure drop for the current range of measurements. Also for the metal oxide samples, the highest pressure drop has been occurred at the concentration of 0.2 wt% and the same Reynolds number. Note that the pressure drop is proportional to the viscosity of the working fluids, which exhibit the highest and the

lowest amounts corresponding to the highest and the lowest viscosities in the similar conditions.

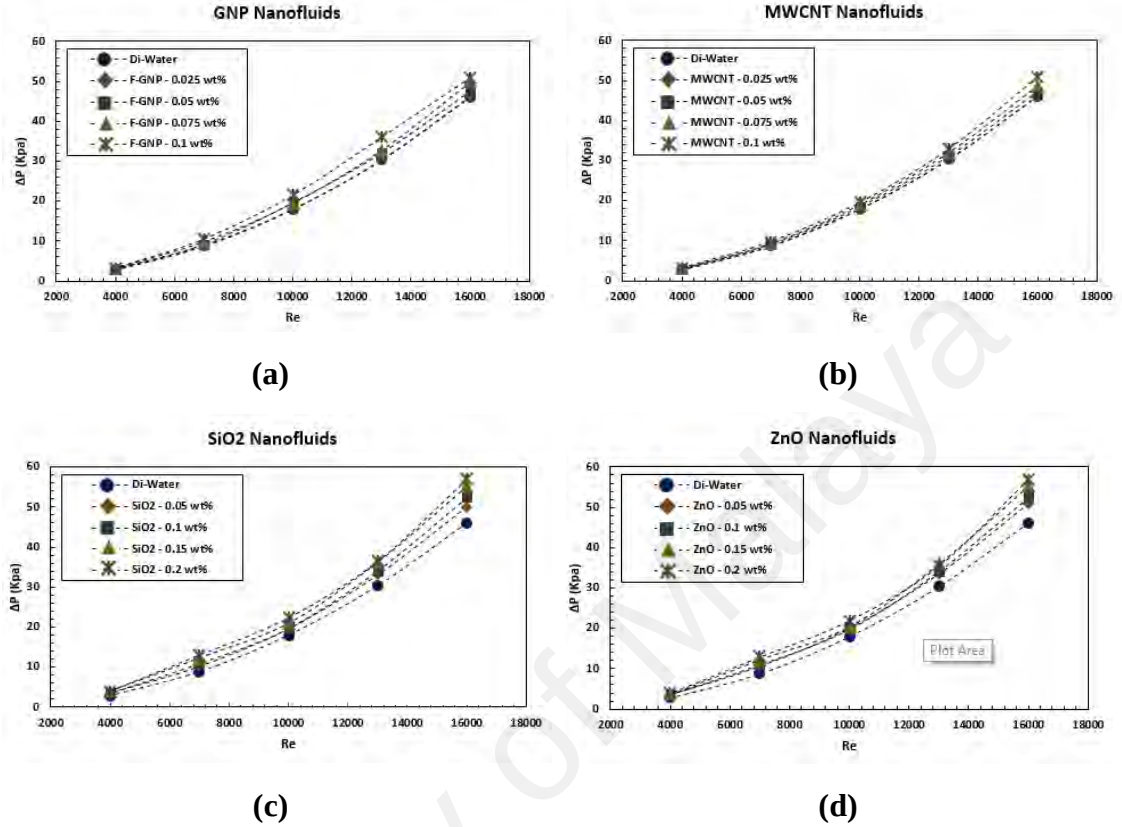

Figure 4. 24: The measured value of pressure drop at different Reynolds Number and weight concentrations for water based nanofluid as well as distilled water; (a) F-GNP nanofluids, (b) MWCNT-COOH nanofluids, (c) SiO_2 nanofluids, and (d) ZnO nanofluids.

The friction factor for the flow over the backward-facing step at different Re numbers as well as weight concentrations of four aforementioned nanofluids is shown in Figure 4.25. It is seen that the measured friction factor decreases with the increase of the Re number for different weight concentrations of the nanofluids. In addition, the friction factor increases as the concentration of nanoparticles increases, although percentage of enhancement is more obvious in low values of the Re numbers. As expected, the minimum value of friction factor occurs for the base fluid. It is also seen as the Re number increases, the dependence of friction factor on the weight concentration of nanofluids decreases. At low Reynolds numbers, the Brownian motion is the main mechanism that influences the momentum transfer between the nanoparticles and the base-fluid

molecules. Thus, as the Brownian motion increases, the concentration of nanoparticles in the nanofluids increases, which causes the increase of the friction factor with higher slope as compared with base fluid (Mohammed et al., 2011). In contrast, this mechanism loses its dominance for high Reynolds number flows, where turbulent agitations in flow play the key role. In summary, the turbulence of the working fluid can be considered as the most important parameters in increasing the friction factor at the high Reynolds numbers. Also, the small difference between the friction factors of the distilled water and the water-based F-GNP, MWCNT-COOH, SiO_2 and ZnO suspensions at different weight concentrations is attributed to the small difference between viscosities of base fluid and the prepared nanofluid samples.

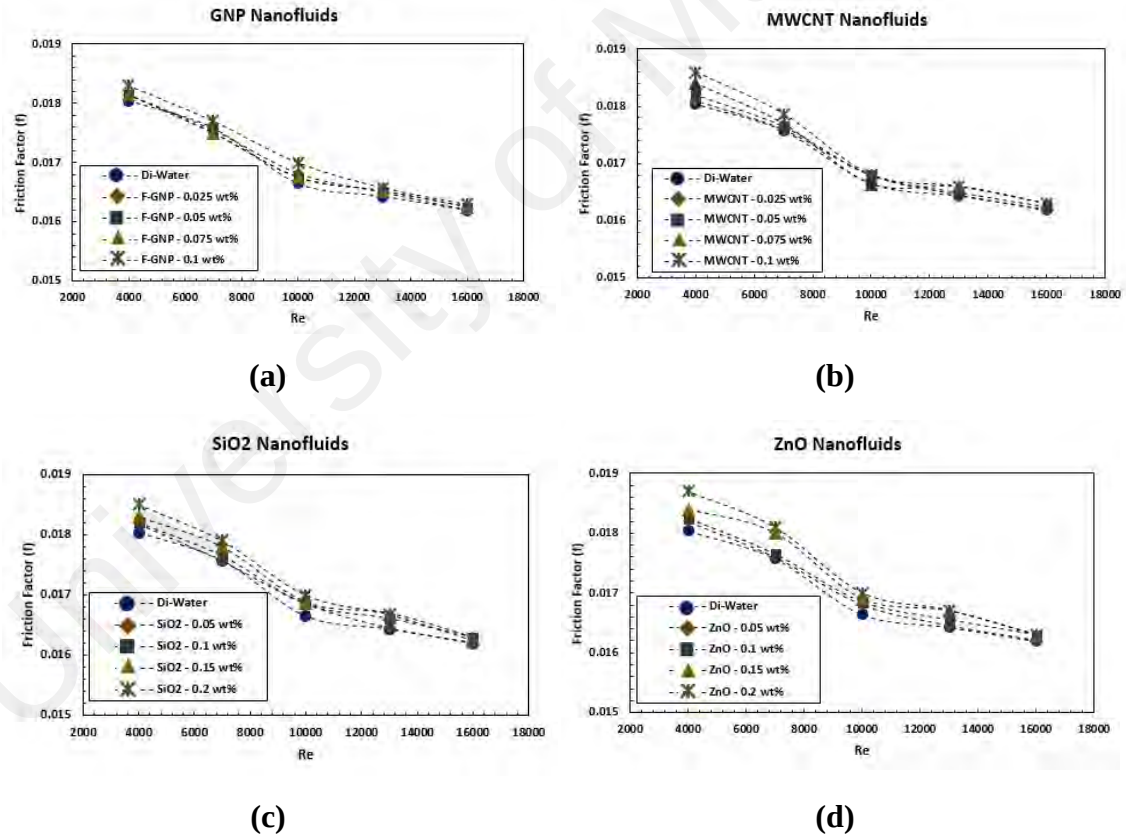

Figure 4. 25: Experimental friction factor for distilled water and various water-based nanofluids with different weight concentrations at different Re numbers; (a) F-GNP nanofluids, (b) MWCNT-COOH nanofluids, (c) SiO_2 nanofluids, and (d) ZnO nanofluids.

As stated earlier, using of nanofluid is a novel method for enhancing the heat transfer rate. Containing of nanoparticles in the fluid has improved the thermal

conductivity that enhances heat transfer and viscosity which offers more pressure drop and pumping power. As the weight concentration of the nanofluid increases, the required pumping power increases too. The pumping power for a fluid with density ρ and viscosity μ can be expressed as the product of the volumetric flow rate Q and the pressure drop ΔP ($W_{pumping} = Q*\Delta P$).

Figure 4.26 shows that at higher volumetric concentration of nanofluid and for a fixed weight concentration at higher Reynolds number, the pumping power requirement is maximum through the sudden expansion pipe. For 0.1% weight fraction of F-GNP and MWCNT water-based nanofluids approximately 10.57% extra pumping power is required than water at Reynolds number of 16000. Additionally, the 23.57% increase in pumping power has been reported for SiO_2 and ZnO at 0.2% weight concentration and at highest Reynolds number.

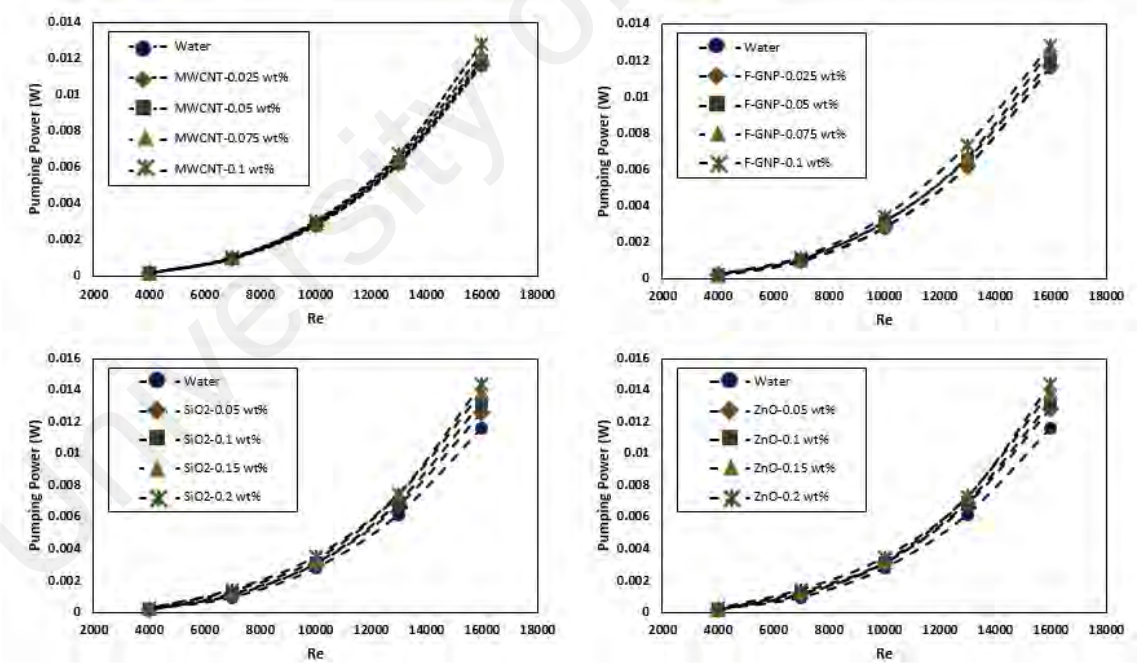

Figure 4. 26: Pumping power requirements for various weight fraction of the four aforementioned water-based nanofluids.

Nanofluids have the potential to increase thermal conductivities and heat transfer coefficients compared to their base fluids. However, the addition of nanoparticles to a fluid also increases the viscosity and therefore increases the power required to pump the

fluid through the system. When the benefit of the increased heat transfer is larger than the penalty of the increased pumping power, the nanofluid has the potential for commercial viability. Accordingly, comparisons of the increased pumping power requirements and heat transfer enhancements are shown in Figure 4.27. At a particular value of h, it is seen that the weight fractions of the aforementioned water-based nanofluids require less pumping power than water.

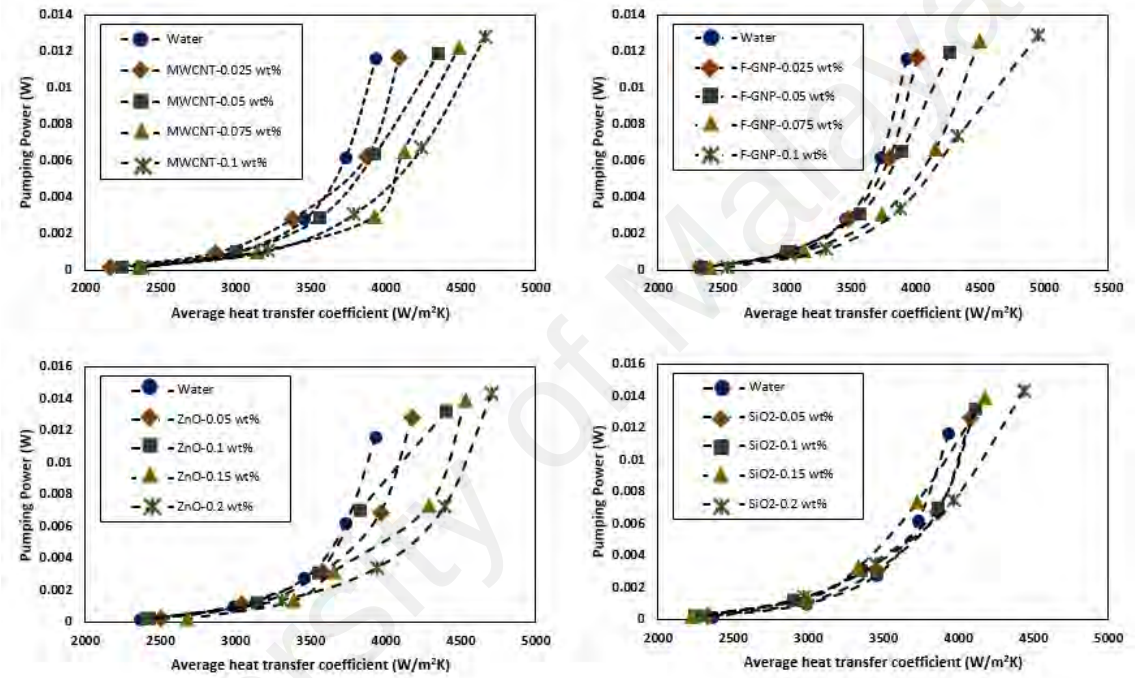

Figure 4. 27: Variation of pumping power and corresponding heat transfer coefficient for the four aforementioned water-based nanofluids.

4.4 Regression Analysis

4.4.1 Model Selection in Multiple Linear Regression

In regression, there are the concepts of over-fitting and under-fitting. There is over-fitting when unnecessary predictors are in the model. There is under-fitting when important effects are missed by omitting predictors. Choosing between different models to avoid over fitting and under fitting is called model selection. Studying different models with various numbers of predictors can be time-consuming. Statistical software usually has an algorithm capable of producing a summary of all possible regression models.

Although using software automates model selection, it is recommended that the potential models are based on theoretical grounds before analysing data. In addition, the model selection is an important concept of collinearity. That is when 2 or more predictors are highly correlated.

There are many methods of design of experiments used to analyse data, and each method will provide analysis of all parameters, interactions between parameters, and get a mathematical model of parameters.

RSM is a method combined with mathematical and statistical ways that are used to analyse experimental data and identify the optimum process parameters based on the response surface. The true relationship between the response surface and parameters is assumed to be unknown. Therefore, the first step is to determine an appropriate approximation of the response and process parameters. Next, an approximate region for the process parameters is determined by experimentation. Then a reduced set of experiments can be conducted to fit the approximate model to the response surface (Montgomery & Runger, 2010).

4.4.2 Multiple Linear Regression Model for the Local Nusselt Number

The mathematical model of the defects is determined based on the variables defined previously. Equation 4.13 shows the standard regression model.

$$y = b_i x_i + \varepsilon \tag{4.13}$$

$$E(y) = y - \varepsilon = \sum_{i=0}^{N} b_i x_i \tag{4.14}$$

where i = 1, 2, 3, .., N refer to the variables, y is response and E(y) is the predicted value of the response, b_i are experimentally determined coefficients, x_i are the variable values, and ε is the model error.

Minitab 18 was selected to implement RSM based on ease of use and familiarity. Building the RSM experiment matrix after setting up some variables, creating the matrix design, determining variables and levels, and choosing the design table are analytical procedures used in this research to determine a mathematical model. The experiments are given from Section 4.3. All the arrangement process depended on the RSM method. Equation 4.15 is a third-order (cubic) polynomial regression, and this equation was built depending on Equation 4.14 to represent the defects with independent parameters.

$$y = a_0 + \sum_{i=1}^{N} b_i x_i + \sum_{i=1}^{N} c_{ii} x_i^2 + \sum_{ij(i<j)} C_{ij} x_i x_j + \sum_{i=1}^{N} d_i x_i^3 + \sum_{ij(i<j)} e_{ij} x_i^2 x_j + \sum_{ij(i<j)} f_{ij} x_i x_j^2 + \sum_{ijk(i<j<k)} g_{ijk} x_i x_j x_k \quad (4.15)$$

Using Minitab and standard RSM through BBD, the data from experiments which were described in Section 4.3 was used to calculate the coefficients of Equation (4.15).

Once the experimental data was obtained, it was then arranged into a spreadsheet with each potential predictor detailed in a column format as shown in Figure 4.28. It may be noted that only the first 16 rows of the data set are shown in the Figure 4.28. There were a total of 1200 rows in the actual spreadsheet used for the final regression analysis.

↓	C1	C2	C3	C4	C5	C6	C7	C8	C9
	StdOrder	RunOrder	PtType	Blocks	Phi (Vol%)	Re	Pr	X/H	Nu (x)
39	62	39	2	1	0.0108222	10000	5.25433	20.7874	174.635
40	88	40	0	1	0.0108222	10000	5.25433	23.4646	153.797
41	51	41	2	1	0.0108222	10000	5.25433	37.4803	107.150
42	80	42	2	1	0.0108222	10000	5.25433	51.4961	89.872
43	20	43	2	1	0.0108222	10000	5.25433	65.6693	85.656
44	73	44	2	1	0.0108222	10000	5.25433	79.5276	89.347
45	31	45	2	1	0.0108222	10000	5.25433	93.5433	78.251
46	21	46	2	1	0.0108222	7000	5.25433	1.4173	81.193
47	71	47	2	1	0.0108222	7000	5.25433	2.6772	106.621
48	4	48	2	1	0.0108222	7000	5.25433	5.3543	142.382
49	23	49	2	1	0.0108222	7000	5.25433	7.8740	175.181
50	83	50	2	1	0.0108222	7000	5.25433	10.5512	184.324
51	44	51	0	1	0.0108222	7000	5.25433	13.0709	190.470
52	7	52	2	1	0.0108222	7000	5.25433	15.5906	193.097
53	50	53	2	1	0.0108222	7000	5.25433	18.2677	174.685
54	61	54	2	1	0.0108222	7000	5.25433	20.7874	156.775

Figure 4. 28: Sample of raw data for regression analysis

Experimental values of Nusselt number were calculated by converting the experimental data of heat transfer coefficient (h) to the local Nusselt number via the thermal conductivity correlations of the four nanofluids which are presented in Sections 4.1 - 4.3. The Reynolds number and the Prandtl number were determined from each measured velocity and the thermophysical properties were subsequently evaluated at the bulk temperature. After carefully analysing the data of all the four nanofluids presented in Figures 4.18 – 4.21. The experimental results agree quite well with the influence of axial distance variation which has great effect on the local Nusselt number but there is no notable available dealing with the prediction of the local Nusselt number ($Nu_{(\frac{x}{H})}$) at a in distance in terms of the axial ratio at the downstream of the flow.

Finally, Response Surface Methodology through Box-Behnken design (BBD) of experiments was applied to build a regression model. Four variables were used in this research: nanoparticle concentration, Reynolds number, Prandtl number and the axial ratio. The resulting model for the local Nusselt number based on the selected variables is given in Equation (4.16) where E(y) represents the local Nusselt number in the various axial ratio.

So, a correlation which is proposed for the first time, expresses the local Nusselt number versus axial ratio, Reynolds number, Prandtl number and volume fraction acceptable for the base fluid and the nanofluids ($Nu_{(\frac{x}{H})} = f(\frac{X}{H}, Re, Pr, \emptyset)$). This new correlation, which contains an additional term for the axial ratio, is given by equation (4.16).

$$\mathrm{E(y)} = Nu_{\left(\frac{X}{H}\right)} = \begin{cases} 61.77 - 78.98\emptyset + 0.0063Re \\ \quad -13.79Pr + 26.44\dfrac{X}{H} \\ \quad -1.47\left(\dfrac{X}{H}\right)^2 + 0.025\left(\dfrac{X}{H}\right)^3 \end{cases} ; 0 \le \frac{X}{H} \le \left(\frac{X}{H}\right)_{peak}$$

$$\begin{cases} 348.68 - 40.63\emptyset + 0.0069Re \\ \quad -8.41\,\mathrm{Pr} - 13.43\dfrac{X}{H} \\ \quad +0.204\left(\dfrac{X}{H}\right)^2 - 0.001\left(\dfrac{X}{H}\right)^3 \end{cases} ; \frac{X}{H} > \left(\frac{X}{H}\right)_{peak} \tag{4.16}$$

In regression analysis, the multiple coefficient of determination (R^2) is used to measure the strength of the relation which is calculated by Equation 3.27 (refer to Section 3.7.2). R^2 can take any value between 0 and 1. When R^2 is close to 1, the model has a good predictive power (Magee, 1990). The regression model (Equation 4.16) which proposed for the local Nusselt number has R^2 equals to 0.89.

To investigate whether the mathematical models can satisfactorily describe the suggested responses, the obtained models were analysed statistically by ANOVA. The concept of ANOVA is to compare the variations due to experiments with the ones due to random errors that are inevitable in the measurements (Bezerra et al., 2008). The models capability in fitting was evaluated by coefficient of determination R^2 and adjusted R^2, whereas the prediction capability was indicated by R^2 prediction coefficient and adequate precision. The significance of regression was measured by F-test, the lack of fit and P-value, shows that the Equation 4.16's model is adequate, though some weak adequacy were observed for other responses. The final subset of variables was selected based on P-value with 95% confidence level, except for the axial ratio response for which the confidence level of 85% was used (Table 4.1).

Table 4. 1: Cubic model prepared by RSM for local Nu and related statistical criteria

Response	Proposed Cubic Model	R^2	Adj R^2	Pre R^2	AP	SD	CV	PRESS
E(y)	Eq. 4.16	0.89	0.88	0.86	15.23	2.34	6.59	161.04

The response (E(y)) are defined in text; R^2: determination coefficient, Adj R^2: Adjusted R^2, Pre R^2: Prediction R^2, AP: adequate precision, SD: standard deviation, CV: coefficient of variation, PRESS: predicted residual error sum of squares.

The high values of R^2 and adjusted R^2 show that the experimental results and the obtained models have considerable compatibility. The close values of R^2 and adjusted R^2, indicate the lack of R^2 inflation effect due to introduction of insignificant variables. The prediction capability of the models was evaluated through the prediction of R^2 and adequate precision (AP) of the extracted data. In concept, prediction R^2 is calculated by excluding an observed value and making a regression model based on the remaining data. This R^2 value reflects how the built regression is successful in predicting the excluded data and is calculated from the predicted residual sum of squares (PRESS) (Myers et al., 2016). The AP is a measure of predicted response range to its average standard error. For a model to be an appropriate predictor, this indicator should be 4 or more (Mason et al., 2003). The value of 0.86 for prediction R^2 and 15.23 for AP show the strong prediction capability of the models. The coefficient of variation (CV) is an appropriate measure to consider variation relative to the mean. Since CV is a dimensionless number, it is better to use it instead of standard deviation to compare the model's variations. The lower the CV values are the closer the predicted values to the actual ones.

In Figures 4.29 – 4.32, the experimental data discussed above are plotted against the corresponding values of the local Nusselt number based on the present equation (Eq. 4.16). These results demonstrate how the correlated equation improves upon the previous equations by considering the influence of axial ratio on flow through sudden expansion passage. Note that the dashed lines represent good agreement between the experimental data and the predictions for each case.

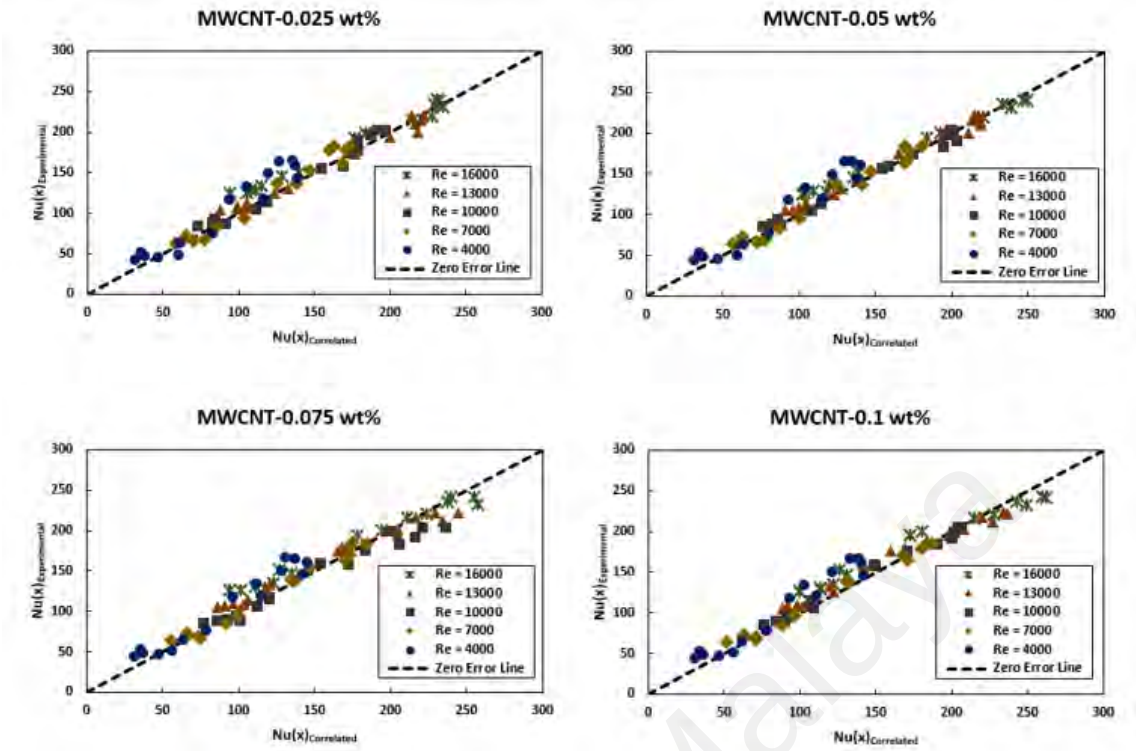

Figure 4. 29: Comparison of experimental data with the predictions of the local Nusselt Number of water based MWCNT-COOH nanofluids based on the new $Nu_{(\frac{x}{H})}$ correlation equation (Eq. 4.16).

From figure 4.29 the maximum deviation for water based MWCNT-COOH is 9.20% and the average deviation is 4.61%.

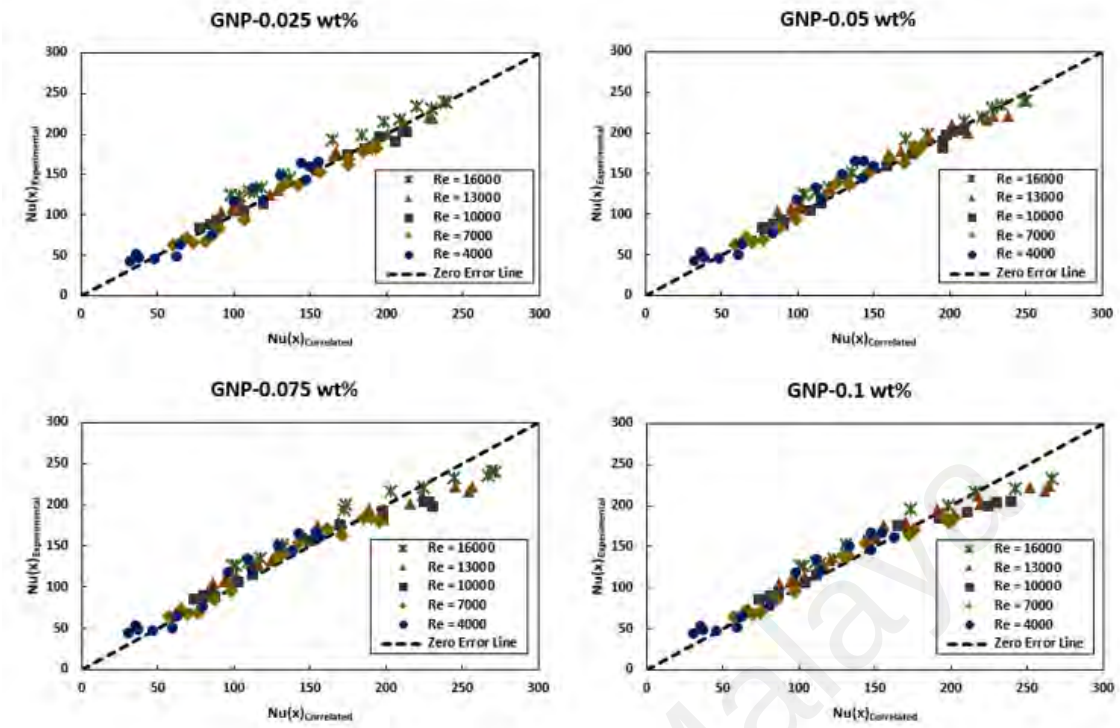

Figure 4. 30: Comparison of experimental data with the predictions of the local Nusselt Number of water based F-GNP nanofluids based on the new $Nu_{(\frac{x}{H})}$ correlation equation (Eq. 4.16).

From figure 4.30 the maximum deviation for water based F-GNP is 9.22% and the average deviation is 5.2%.

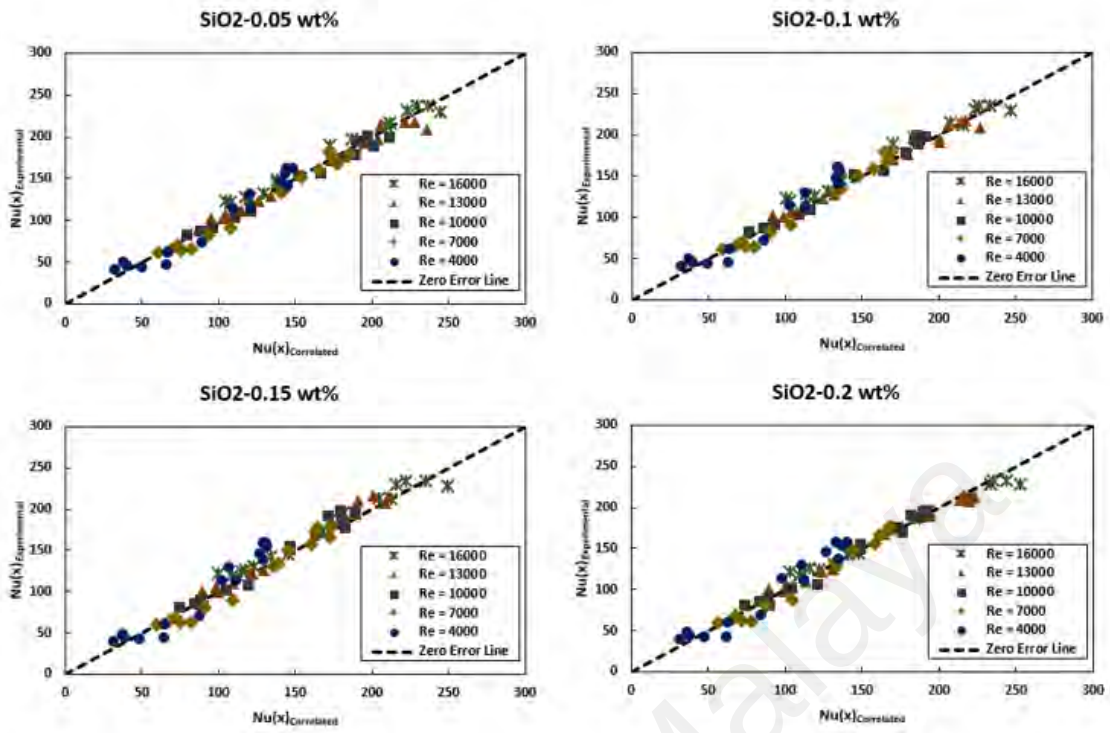

Figure 4. 31: Comparison of experimental data with the predictions of the local Nusselt Number of water based SiO_2 nanofluids based on the new $Nu_{(\frac{x}{H})}$ correlation equation (Eq. 4.16).

From figure 4.31 the maximum deviation for water based SiO_2 is 7.23% and the average deviation is 2.93%.

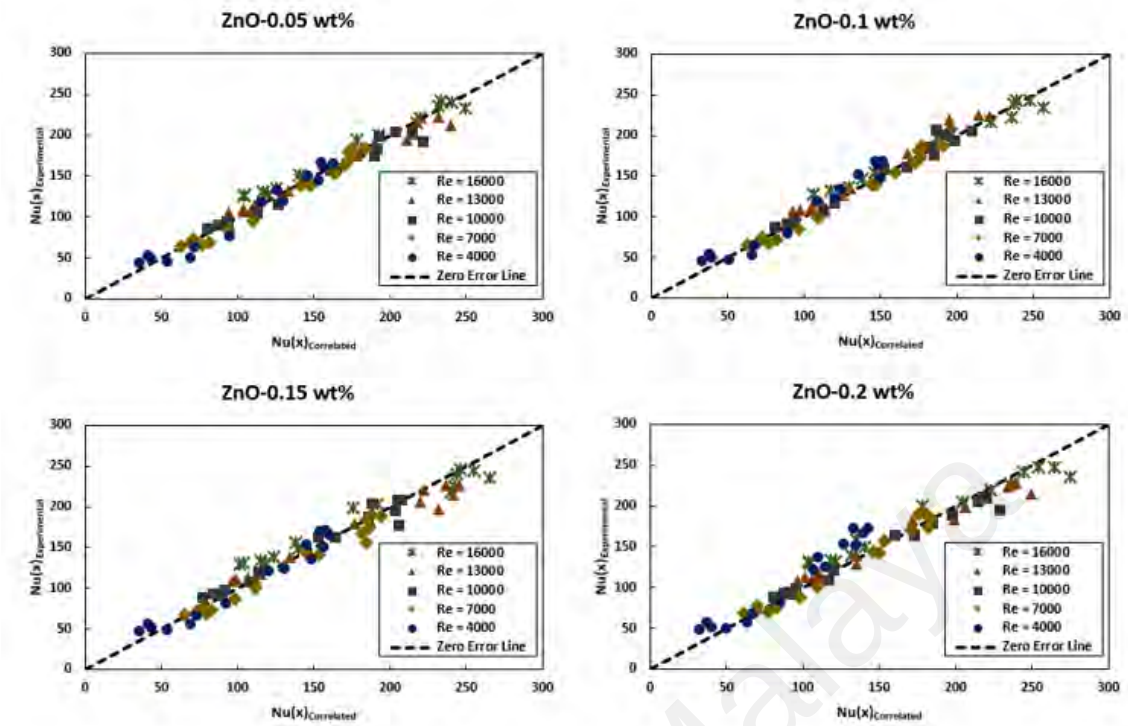

Figure 4. 32: Comparison of experimental data with the predictions of the local Nusselt Number of water based ZnO nanofluids based on the new $Nu_{(\frac{x}{H})}$ correlation equation (Eq. 4.16).

From figure 4.32 the maximum deviation for water based ZnO is 7.71% and the average deviation is 3.27%.

4.4.3 Multiple Non-Linear Regression Models for the Average Nusselt Number and the Friction Factor

Average Nusselt number along with the heated walls after expansion are deduced from Equation (4.17) as:

$$\overline{Nu} = \frac{1}{L}\int_0^L Nu\, dl \tag{4.17}$$

Where, L represents the total length of the corresponding wall.

While simple and multiple linear regression functions are adequate for modelling a wide variety of relationships between response variable and predictor variables, many situations require nonlinear functions.

In some situation it may be possible to transform a nonlinear regression function E(y) using appropriate transformations of the response variable, the predictor variables, the parameters, or any combination of these, such that the transformed function is linear in the unknown parameters.

When a multiple linear regression shows poor overall level of significance, researchers are encouraged to use non-linear regression by taking the natural logarithm of all variables and then running the multiple linear regression on the logged variables which is called "Linearizable Method".

Another type of non-linear regression situation occurs in the average Nusselt number in the form of heat transfer analysis. This important class of multiple non-linear regression of the average Nusselt number equation can be solved using Minitab. The average Nusselt number equations based on Reynolds number, Prandtl number and volume concentration are typically exponential equations of the form shown in Equation 4.18.

$$E\ (y) = \beta_0\, X_1^{\beta_1}\, X_2^{\beta_2}\ \cdots\ X_n^{\beta_n} \tag{4.18}$$

Where E(y) is the predicted value of the response, β_0 is experimentally determined coefficients, x_1, x_2, … x_n are the variable values, and β_1, β_2, … β_n are coefficients less than 1 according to Section 2.6.2. By taking the natural logarithm of both sides of Equation 4.18 transforms the non-linear equation into a linear equation (Eq. 4.19):

$$\ln(E(y)) = \ln\beta_0 + \beta_1 \ln x_1 + \cdots + \beta_2 \ln x_2 \tag{4.19}$$

Note that Equation 4.19 is in the same form as Equation 4.14, with the dependent variable on the left and a constant ($\ln\beta_0$) plus coefficients times dependent variables on the right. Thus, to perform multiple non-linear regressions on the average Nusselt number and friction factor data, take the natural log of the data and perform the multiple linear regressions on the logged data, then transform the resulting equations into the form of Equation 4.18 by taking the natural exponential of both sides. All that remains is to raise

both sides of logged regression equations to the power of e, giving the final nonlinear average Nusselt number and friction factor Equations 4.20 and 4.21:

$$\overline{Nu} = 1.16\, Re^{0.55}\, Pr^{-0.312}\, (1+\phi)^{-0.25} \tag{4.20}$$

$$f = 0.044 Re^{-0.09} Pr^{-0.08} (1+\emptyset)^{0.21} \tag{4.21}$$

Two correlations (Equations 4.20 and 4.21) of average Nusselt number and friction factor for turbulent nanofluids separation flow are proposed with $R^2 = 0.98$ and $R^2 = 0.96$ (refer to Equation 3.27), respectively. They express average Nusselt number and friction factor versus Reynolds number, volume fraction and Prantl number as shown by equations 4.20 and 4.21. Table 4.2 shows the final subsets of variables, which were selected, based on P-value with 97% confidence level.

Table 4. 2: Non-linear models prepared by RSM for average Nu and friction factor as well as related statistical criteria

Response	Proposed Model	R^2	Adj R^2	Pre R^2	AP	SD	CV	PRESS
Average Nu	Eq. 4.20	0.98	0.96	0.92	22.35	2.05	7.45	141.04
Friction Factor	Eq. 4.21	0.96	0.95	0.90	16.86	2.61	8.24	202.69

The response (E(y)) are defined in text; R^2: determination coefficient, Adj R^2: Adjusted R^2, Pre R^2: Prediction R^2, AP: adequate precision, SD: standard deviation, CV: coefficient of variation, PRESS: predicted residual error sum of squares.

The effects of Reynolds number and nanoparticles volume fraction on the average Nusselt number and friction factor at the downstream of abrupt expansion are represented in Figures 4.33 and 4.34, where the average Nusselt number and friction factor enhance moderately with the nanoparticles volume concentration and Reynolds number. Types of nanoparticles affect the heat transfer where there is a small linear increment is noticed for all the cases. The inclination angle of this linear increment depends on the nanoparticle types and the correlations (Equations 4.20 and 4.21) are plotted in Figures 4.33 and 4.34 for each of the nanoparticle types. These correlations have fitted the data from all the sources, rather than from just one or two, of the sources.

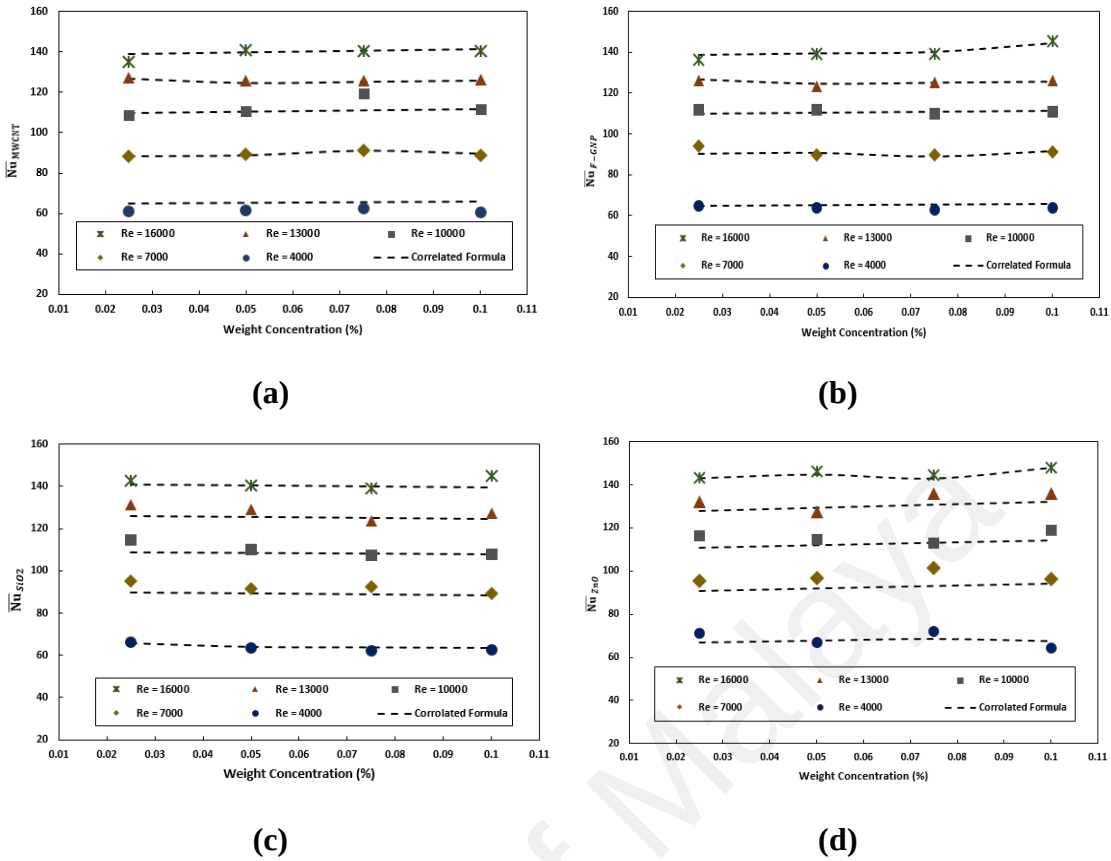

Figure 4. 33: Effect of nanoparticles weight fraction and Reynolds number on average Nusselt number for four nanofluids at the downstream of sudden expansion. The dashed lines represent data from the new $\overline{Nu}$ correlation of equation 4.20; (a) MWCNT-COOH nanofluids, (b) F-GNP nanofluids, (c) SiO_2 nanofluids and (d) ZnO nanofluids.

From figure 4.33 the maximum deviation for the average Nusselt number is 6.54% and the average deviation is 2.16%.

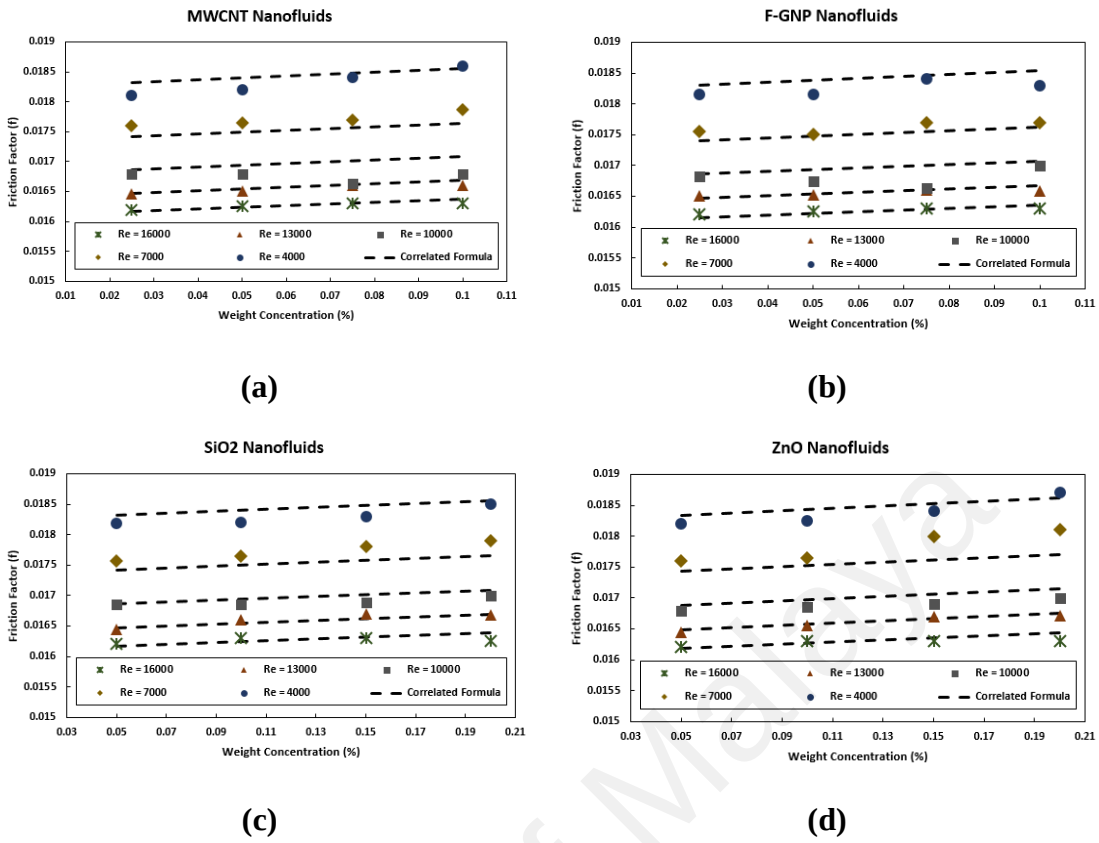

Figure 4. 34: Effect of nanoparticles weight fraction and Reynolds number on the friction factor for four nanofluids at the downstream of sudden expansion. The dashed lines represent data from the new f correlation of equation 4.21; (a) MWCNT-COOH nanofluids, (b) F-GNP nanofluids, (c) SiO_2 nanofluids and (d) ZnO nanofluids.

From figure 4.34 the maximum deviation for the friction factor is 2.23% and the average deviation is 0.64%.

4.5 Economic Performance

The economic performance of working fluids for different heat transfer equipment is measured via performance index (ε), which identified as the ratio of the heat transfer rate to the pressure drop ratios. Recent studies (e.g., (Samira et al., 2015)) suggested that while the addition of solid nanoparticles improves the heat transfer rate, the pressure drop in the flow loops also increases, which is undesirable. Therefore, performance index (PI) is presented to consider both parameters. The variations of the average performance index (PI) and performance evaluation criterion (PEC) for four aforementioned water-based nanofluids are illustrated for different Re numbers and weight concentrations in Figures

4.35 and 4.36. It is seen that the average PI as well as PEC of all the samples containing nanoparticles is higher than 1, representing the effectiveness of the prepared coolant samples for use over the backward-facing step flows. It is also seen that the average performance index enhances with the increase of weight concentration of nanofluids, which infers that the enhancement in heat transfer is more effective compared to the increase in pressure drop.

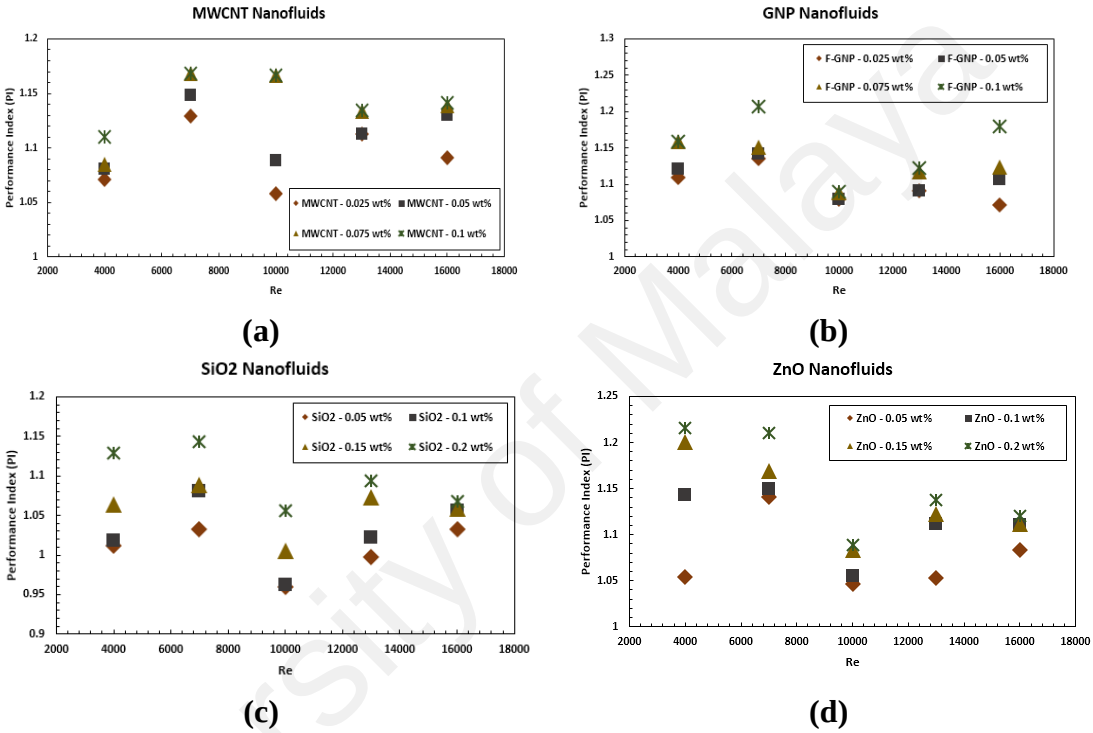

Figure 4. 35: Performance index (PI) of water-based nanofluids for the backward-facing step at different weight concentrations; (a) MWCNT-COOH nanofluids, (b) F-GNP nanofluids, (c) SiO_2 nanofluids and (d) ZnO nanofluids.

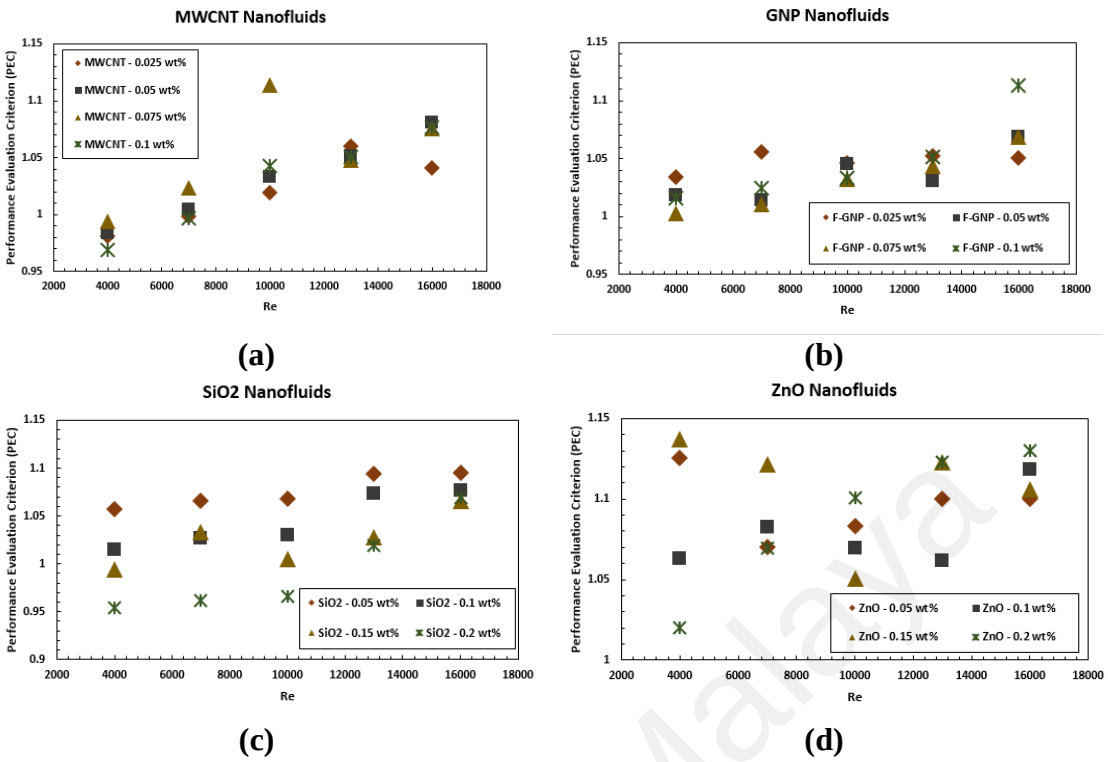

Figure 4. 36: Performance evaluation criterion (PEC) of water-based nanofluids for the backward-facing step at different weight concentrations; (a) MWCNT-COOH nanofluids, (b) F-GNP nanofluids, (c) SiO_2 nanofluids and (d) ZnO nanofluids.

Pumping power ratio can be considered as an economic performance indicator in a loop system for evaluating the operability of fluid and performance of the power plant. Figure 4.37 compares the pumping power of the water-based nanofluids at different weight concentrations with that of the base-fluid. This figure shows that there is a slight increase in the pumping power with the nanoparticles loading but the percentage of pumping power increase is negligible. The small growth in the pumping power can be due to the low weight fraction of nanoparticles in the base fluid.

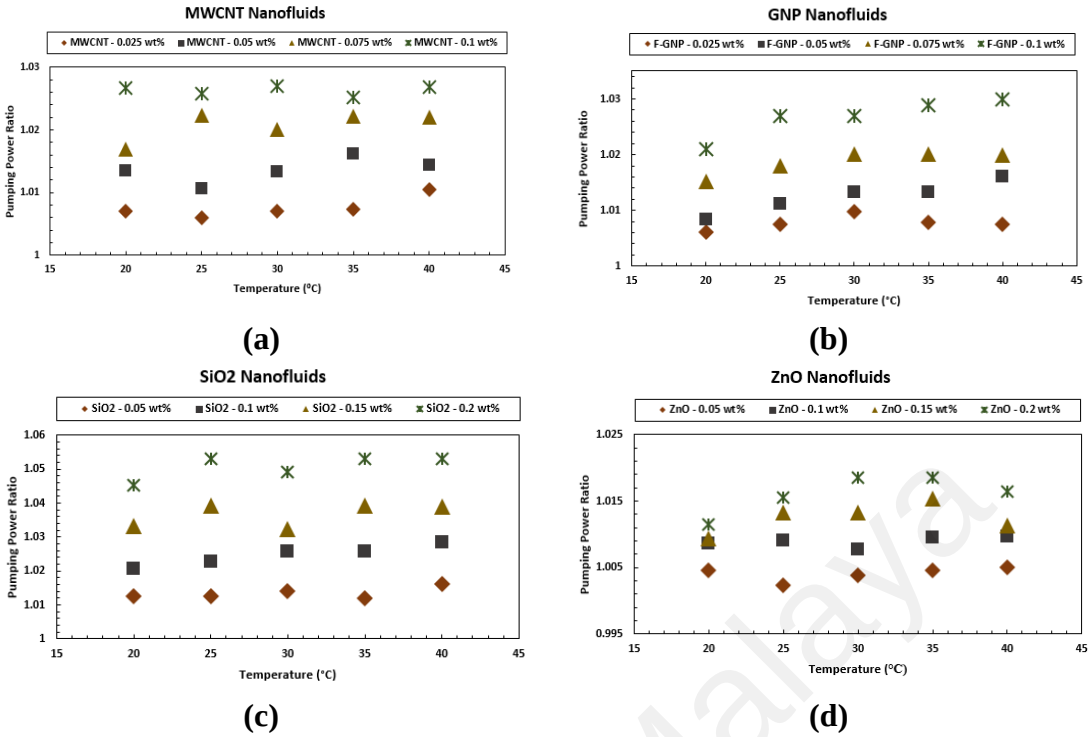

Figure 4. 37: Pumping power ratio of water-based nanofluids for the backward-facing step in the different weight concentrations and temperature; (a) MWCNT-COOH nanofluids, (b) F-GNP nanofluids, (c) SiO_2 nanofluids and (d) ZnO nanofluids.

On the other hand, different characteristics of the new coolant such as weak increase in the pressure drop for varied concentrations and inlet temperatures, low friction factor, lack of corrosive agent, appropriate performance index ($\varepsilon > 1$), and slight increase in the required pumping power are all highly favourable for introducing new fluid for wide industrial applications.

The experimental setup is representing the fundamental study of separation flow and the effect of nanofluids in the separation flow phenomena. The results of the experimental observation reveals enhancement of heat removal in the separation and reattachment regions of the step flow. In reality many equipment need fast cooling preferred over friction loss in that flow system such as blow molding, injection molding and other continuous operating machines where cooling is the main concern.

In the present research, single stage step flow shown good efficiency, when nanofluids where applied. There was more cooling effects, noted when nanofluids were used instead of base fluid alone. Thus, multi stage separation flow could be preferred for

those specific cooling where cumulative effect will meet the requirement of efficient and continuous cooling of the devices.

As a summary of study, the results suggested that the thermo-physical properties of water-based nanofluids were enhanced, that makes the nanofluid well suited for heat transfer applications. The heat transfer results showed that the water-based F-GNP nanofluids at very low concentrations exhibited noticeably higher heat transfer rate compared to the distillate water. The overall heat transfer rate showed a 33.7% enhancement by loading just 0.1 wt% of F-GNP into the distillate water. In addition, experimental data for the Nu number and the local heat transfer coefficient of the four aforementioned water-based nanofluids for turbulent flow regimes were presented. The data showed that with the increase of weight concentration of the four different nanoparticles in the nanofluids and/or Re number increase over backward-facing step, the position of maximum heat transfer point shifts to the longer distances, leading to larger recirculation zone. The presented results showed that the water-based F-GNP nanofluid is a great candidate for a new generation of heat transfer fluids.

CHAPTER 5: CONCLUSIONS AND FUTURE WORKS

5.1 Conclusions

In this thesis, turbulent forced convection heat transfer to nanofluids in an axisymmetric abrupt expansion heat exchanger is investigated experimentally. A number of studies on the effect of nanofluids on heat transfer augmentation have been conducted in addition to the investigation of rearrangement of flow passage configurations.

In heat transfer investigation, this study has focused on functionalized multiwalled carbon nanotubes (MWCNT-COOH), polycarboxylate functionalized graphene nanoplatelets (F-GNP), SiO_2 and ZnO water based nanofluids. In this investigation the convective heat transfer coefficient and friction factor at fully developed turbulent flow of nanofluids flowing through the sudden expansion with the expansion ratio (ER) of 2 was experimentally determined at constant wall heat flux of 12,128.56 W/m^2. The experiments were conducted at the Reynolds number range of 4,000–16,000. To validate the reliability and repeatability of the experimental data, several tests were conducted for distilled water and compared with the data from standard equations and themselves.

Stability study showed more than 85% of all the four aforementioned nanofluids water dispersed even after 1 month. In the materials effect study the F-GNP showed the highest heat transfer performance while in size effect study the lowest diameter showed the maximum increment in heat transfer performance. In this research all the prepared nanofluids have provided significant enhancement in heat transfer characteristics. The measured thermal conductivity, viscosity, specific heat capacity and density of all the samples showed reasonable performance requirement for a good heat exchanging liquid. The following conclusions could be drawn from the observations.

1. In step configuration, the local heat transfer coefficient in separated, reattached, and redevelopment regions for water flow are several times larger than those for the fully developed flow. For instance, at the point of reattachment, the coefficients were 2.5 to 5.7 times greater than the corresponding fully developed values.
2. The thermo-physical properties of carbon-based nanoparticles have enhanced thermal conductivity compared to the metal-oxide particle based nanofluids. Thermal conductivity enhancement further increased with the temperature, which is attributable to the increased Brownian motion of the colloidal particles at higher temperatures. In comparison with distilled water, average drop of 3.9% and 7.9% in the specific heat capacity of carbon-based and metal-oxide based nanofluids respectively are obtained. From the Rheometer results, it can be seen that the viscosities of nanofluids are higher than those of base fluids, and it increases with the increase of weight concentration. The viscosities of ZnO and SiO_2 nanofluids were raised in the ranges of 2.24%-9.47% and 5.36% - 24.22% respectively with the changes in temperature and weight concentrations. Densities of all the specified nanofluids are higher than the base fluid (water) and with the increase of temperature, the densities of nanofluids lead on decreasing. Further, if nanoparticle weight concentration increases, density is enhanced.

   Exploration of the heat transfer behaviour of water and highly conductive nanofluids in the turbulent flow separation regimes is the second target of this study. The comparison between the four aforementioned nanofluids, show that the carbon-based nanofluids have a greater effect on enhancing heat transfer at the downstream of sudden expansion pipe flow. An enhancement in the convective heat transfer coefficient is observed after the point of reattachment with the increase of nanoparticles in the base fluid. Therefore, the high convective heat

transfer coefficient inside the recirculation zone depends mainly on the thermos-physical properties of the nanoparticles. In addition, both of the thermo-physical properties of the nanofluids and Reynolds number affect the value of the heat transfer coefficient outside the recirculation zone.

The heat transfer performance improved 33.7 % and 16.7% by using F-GNP and MWCNT-COOH nanofluids at 0.1wt% concentration instead of water. Additionally, 14.35 % and 10.1 % enhancement were achieved by utilizing ZnO and SiO_2 nanofluids at the same weight concentration of 0.1wt%. The position as well as the value of $(X/H)_{max}$ enhance with the increase of Re number.

3. In this investigation, the development of more generally applicable correlations based on the research concepts were considered. The Response Surface Methodology through Box-Behnken design (BBD) of experiments was applied to build the regression models. In conclusion, three excellent correlations for the average Nusselt number, the friction factor and the Local Nusselt number are proposed where the first two correlations predict the average Nusselt number and the friction factor relating Reynolds number, Prandtl number and volume fraction with reasonably good accuracy ($\overline{Nu} = f(Re, Pr, \emptyset);\ f = f(Re, Pr, \emptyset)$). There is no available work dealing with the prediction of the local Nusselt number at the distance of the axial ratio of flow through sudden expansion. So, the third one which is proposed for the first time, expresses the local Nusselt number versus axial ratio, Reynolds number, Prandtl number and volume fraction acceptable for the base fluid and the nanofluids ($Nu_{(\frac{x}{H})} = f(\frac{x}{H}, Re, Pr, \emptyset)$). This correlation has fitted the data from all sources, rather than from just one or two, of the sources.

5.2 Recommendations for Future Works

The results presented here have demonstrated the effectiveness of the separation flow in heat transfer prediction of nanofluids during forced convention. To keep investigation in the same line and to enhance investigation the separation problem in such geometry, this research could be further developed in a number of ways:

1. Investigate heat transfer to turbulent flow over a double sudden expansion passage and study the mutual effect of two separation zones after each flow separation on the heat transfer process.
2. Investigation of the bottom wall eddy and their effect on heat transfer performance.
3. Experimental on convective heat transfer performance can be extended by incorporating the above and different materials. Investigation on heat transfer augmentation can be further conducted at much higher Re as well as at different test section configurations (i.e. different cross section profile)
4. Investigate the heat transfer by combined forced and natural convection (mixed convection) in inclined sudden expansion tubes which is significant in many industrial applications such as solar energy collectors, supercritical boilers and nuclear reactors. The contribution of natural convection may enhance the rate of heat transfer to a fluid in laminar flow through a horizontal tube by a factor of three or four. The irregular motion of nanoparticles may increase the secondary flow strength so as to increase the heat transfer by natural convection (Mirmasoumi & Behzadmehr, 2008a, 2008b).

REFERENCES

Abbott, D., & Kline, S. (1962). Experimental investigation of subsonic turbulent flow over single and double backward facing steps. *Journal of Fluids Engineering, 84*(3), 317-325.

Abu-Nada, E. (2008). Application of nanofluids for heat transfer enhancement of separated flows encountered in a backward facing step. *International Journal of Heat and Fluid Flow, 29*(1), 242-249.

Abu-Nada, E. (2009). Effects of variable viscosity and thermal conductivity of Al2O3–water nanofluid on heat transfer enhancement in natural convection. *International Journal of Heat and Fluid Flow, 30*(4), 679-690.

Akbarinia, A., & Behzadmehr, A. (2007). Numerical study of laminar mixed convection of a nanofluid in horizontal curved tubes. *Applied Thermal Engineering, 27*(8-9), 1327-1337.

Alawi, O. A., Sidik, N. A. C., & Tey, W. Y. (2015). A numerical study of heat transfer to turbulent separation nanofluid flow in an annular passage. *J. Teknologi, 77*.

Allahyari, S., Behzadmehr, A., & Sarvari, S. H. (2011). Conjugate heat transfer of laminar mixed convection of a nanofluid through a horizontal tube with circumferentially non-uniform heating. *International Journal of Thermal Sciences, 50*(10), 1963-1972.

Alleborn, N., Nandakumar, K., Raszillier, H., & Durst, F. (1997). Further contributions on the two-dimensional flow in a sudden expansion. *Journal of Fluid Mechanics, 330*, 169-188.

Aloui, F., & Madani, S. (2008). Experimental investigation of a wet foam flow through a horizontal sudden expansion. *Experimental Thermal and Fluid Science, 32*(4), 905-926.

Amiri, A., Shanbedi, M., Rafieerad, A., Rashidi, M. M., Zaharinie, T., Zubir, M. N. M., . . . Chew, B. (2017). Functionalization and exfoliation of graphite into mono layer graphene for improved heat dissipation. *Journal of the Taiwan Institute of Chemical Engineers, 71*, 480-493.

Aravind, S. J., & Ramaprabhu, S. (2013). Graphene–multiwalled carbon nanotube-based nanofluids for improved heat dissipation. *RSC Advances, 3*(13), 4199-4206.

Armaly, B. F., Durst, F., Pereira, J., & Schönung, B. (1983). Experimental and theoretical investigation of backward-facing step flow. *Journal of Fluid Mechanics, 127*, 473-496.

Assael, M., Chen, C.-F., Metaxa, I., & Wakeham, W. (2004). Thermal conductivity of suspensions of carbon nanotubes in water. *International Journal of Thermophysics, 25*(4), 971-985.

Baby, T. T., & Ramaprabhu, S. (2010). Investigation of thermal and electrical conductivity of graphene based nanofluids. *Journal of Applied Physics, 108*(12), 124308.

Balakhrisna, T., Ghosh, S., Das, G., & Das, P. (2010). Oil–water flows through sudden contraction and expansion in a horizontal pipe–Phase distribution and pressure drop. *International Journal of Multiphase Flow, 36*(1), 13-24.

Balandin, A. A., Ghosh, S., Bao, W., Calizo, I., Teweldebrhan, D., Miao, F., & Lau, C. N. (2008). Superior thermal conductivity of single-layer graphene. *Nano letters, 8*(3), 902-907.

Barbés, B., Páramo, R., Blanco, E., Pastoriza-Gallego, M. J., Pineiro, M. M., Legido, J. L., & Casanova, C. (2013). Thermal conductivity and specific heat capacity measurements of Al 2 O 3 nanofluids. *Journal of Thermal Analysis and Calorimetry, 111*(2), 1615-1625.

Batchelor, G. (1977). The effect of Brownian motion on the bulk stress in a suspension of spherical particles. *Journal of Fluid Mechanics, 83*(01), 97-117.

Baughn, J., Hoffman, M., Takahashi, R. K., & Launder, B. (1984). Local heat transfer downstream of an abrupt expansion in a circular channel with constant wall heat flux. *Journal of heat transfer, 106*(4), 789-796.

Beck, M. P., Yuan, Y., Warrier, P., & Teja, A. S. (2010). The thermal conductivity of aqueous nanofluids containing ceria nanoparticles: AIP.

Bezerra, M. A., Santelli, R. E., Oliveira, E. P., Villar, L. S., & Escaleira, L. A. (2008). Response surface methodology (RSM) as a tool for optimization in analytical chemistry. *Talanta, 76*(5), 965-977.

Bhattacharya, P., Saha, S., Yadav, A., Phelan, P., & Prasher, R. (2004). Brownian dynamics simulation to determine the effective thermal conductivity of nanofluids. *Journal of Applied Physics, 95*(11), 6492-6494.

Bianco, V., Manca, O., & Nardini, S. (2014). Performance analysis of turbulent convection heat transfer of Al2O3 water-nanofluid in circular tubes at constant wall temperature. *Energy, 77*, 403-413.

Boelter, L., Young, G., & Iversen, H. (1948). An Investigation of Aircraft Heaters XXVII: Distribution of Heat-transfer Rate in the Entrance Section of a Circular Tube.

Box, G. E., & Draper, N. R. (1987). *Empirical model-building and response surfaces* (Vol. 424): Wiley New York.

Brinkman, H. (1952). The viscosity of concentrated suspensions and solutions. *The Journal of Chemical Physics, 20*(4), 571-571.

Bühler, L., Horanyi, S., & Arbogast, E. (2007). Experimental investigation of liquid-metal flows through a sudden expansion at fusion-relevant Hartmann numbers. *Fusion Engineering and Design, 82*(15), 2239-2245.

Buongiorno, J. (2006). Convective transport in nanofluids. *Journal of Heat Transfer, 128*(3), 240-250.

Chakrabarti, S., Ray, S., & Sarkar, A. (2003). Low Reynolds Number flow Through Sudden Expansion from a Diffuser Viewpoint. *Journal of Energy Heat and Mass Transfer, 25*, 45-66.

Chandrasekar, M., Suresh, S., & Bose, A. C. (2010). Experimental investigations and theoretical determination of thermal conductivity and viscosity of Al 2 O 3/water nanofluid. *Experimental Thermal and Fluid Science, 34*(2), 210-216.

Chandrasekar, M., Suresh, S., & Senthilkumar, T. (2012). Mechanisms proposed through experimental investigations on thermophysical properties and forced convective heat transfer characteristics of various nanofluids–A review. *Renewable and Sustainable Energy Reviews, 16*(6), 3917-3938.

Chang, H., Jwo, C., Fan, P., & Pai, S. (2007). Process optimization and material properties for nanofluid manufacturing. *The International Journal of Advanced Manufacturing Technology, 34*(3), 300-306.

Chein, R., & Huang, G. (2005). Analysis of microchannel heat sink performance using nanofluids. *Applied Thermal Engineering, 25*(17-18), 3104-3114.

Chen, G., Yu, W., Singh, D., Cookson, D., & Routbort, J. (2008). Application of SAXS to the study of particle-size-dependent thermal conductivity in silica nanofluids. *Journal of Nanoparticle Research, 10*(7), 1109-1114.

Chen, H., Yang, W., He, Y., Ding, Y., Zhang, L., Tan, C., . . . Bavykin, D. V. (2008). Heat transfer and flow behaviour of aqueous suspensions of titanate nanotubes (nanofluids). *Powder Technology, 183*(1), 63-72.

Cheng, L. (2009). Nanofluid heat transfer technologies. *Recent Patents on Engineering, 3*(1), 1-7.

Cherdron, W., Durst, F., & Whitelaw, J. H. (1978). Asymmetric flows and instabilities in symmetric ducts with sudden expansions. *Journal of Fluid Mechanics, 84*(01), 13-31.

Chiesa, M., & Simonsen, A. (2007). *The Importance of Suspension Stability for the Hot-wire Measurements of Thermal Conductivity of Colloidal Suspensions.* Paper presented at the 16th Australasian Fluid Mechanics Conference (AFMC).

Choi, S., Zhang, Z., Yu, W., Lockwood, F., & Grulke, E. (2001). Anomalous thermal conductivity enhancement in nanotube suspensions. *Applied physics letters, 79*(14), 2252-2254.

Choi, S. U., & Eastman, J. A. (1995). Enhancing thermal conductivity of fluids with nanoparticles: Argonne National Lab., IL (United States).

Chol, S. (1995). Enhancing thermal conductivity of fluids with nanoparticles. *ASME-Publications-Fed, 231*, 99-106.

Chon, C., & Kihm, K. (2005). Thermal conductivity enhancement of nanofluids by Brownian motion. *Journal of Heat Transfer, 127*(8), 810-810.

Chon, C. H., Kihm, K. D., Lee, S. P., & Choi, S. U. (2005). Empirical correlation finding the role of temperature and particle size for nanofluid (Al 2 O 3) thermal conductivity enhancement. *Applied Physics Letters, 87*(15), 153107.

Corcione, M. (2011a). Empirical correlating equations for predicting the effective thermal conductivity and dynamic viscosity of nanofluids. *Energy Conversion and Management, 52*(1), 789-793.

Corcione, M. (2011b). Rayleigh-Bénard convection heat transfer in nanoparticle suspensions. *International Journal of Heat and Fluid Flow, 32*(1), 65-77.

Das, S. K., Putra, N., Thiesen, P., & Roetzel, W. (2003). Temperature dependence of thermal conductivity enhancement for nanofluids. *Journal of heat transfer, 125*(4), 567-574.

Derjaguin, B., & Landau, L. (1941). Theory of the 44: 369-395. stability of strongly charged lyophobic sols and of 61. Parsegian, VA, RP Rand and NL Fuller, 1991. the adhesion of strongly charged particles in Directosmoticstressmeasurementsofhydrationand solutions of electrolytes. *Acta Physicochim. URSS, electrostatic double-layer forces between bilayers of, 14*, 633.

Ding, Y., Alias, H., Wen, D., & Williams, R. A. (2006). Heat transfer of aqueous suspensions of carbon nanotubes (CNT nanofluids). *International Journal of Heat and Mass Transfer, 49*(1), 240-250.

Dittus, F., & Boelter, L. (1930). University of California publications on engineering. *University of California publications in Engineering, 2*, 371.

DOUGALL, R. (1970). Local heat transfer downstream of abrupt circular channel expansion.

Drikakis, D. (1997). Bifurcation phenomena in incompressible sudden expansion flows. *Physics of Fluids (1994-present), 9*(1), 76-87.

Durst, F., Melling, A., & Whitelaw, J. (1974). Low Reynolds number flow over a plane symmetric sudden expansion. *Journal of Fluid Mechanics, 64*(01), 111-128.

Durst, F., Pereira, J., & Tropea, C. (1993). The plane symmetric sudden-expansion flow at low Reynolds numbers. *Journal of Fluid Mechanics, 248*, 567-581.

Eastman, J. A., Choi, S., Li, S., Yu, W., & Thompson, L. (2001). Anomalously increased effective thermal conductivities of ethylene glycol-based nanofluids containing copper nanoparticles. *Applied physics letters, 78*(6), 718-720.

Eastman, J. A., Phillpot, S., Choi, S., & Keblinski, P. (2004a). Thermal transport in nanofluids. *Annu. Rev. Mater. Res., 34*, 219-246.

Eastman, J. A., Phillpot, S., Choi, S., & Keblinski, P. (2004b). Thermal transport in nanofluids 1. *Annu. Rev. Mater. Res., 34*, 219-246.

Eaton, J., & Johnston, J. (1981). A review of research on subsonic turbulent flow reattachment. *AIAA journal, 19*(9), 1093-1100.

Ede, A., Hislop, C., & Morris, R. (1956). Effect on the local heat-transfer coefficient in a pipe of an abrupt disturbance of the fluid flow: abrupt convergence and divergence of diameter ratio 2/1. *Proceedings of the Institution of Mechanical Engineers, 170*(1), 1113-1130.

El-Brolossy, T., & Saber, O. (2013). Non-intrusive method for thermal properties measurement of nanofluids. *Experimental Thermal and Fluid Science, 44*, 498-503.

El Bécaye Maïga, S., Tam Nguyen, C., Galanis, N., Roy, G., Maré, T., & Coqueux, M. (2006). Heat transfer enhancement in turbulent tube flow using Al2O3 nanoparticle suspension. *International Journal of Numerical Methods for Heat & Fluid Flow, 16*(3), 275-292.

Fang, X., Fan, L.-W., Ding, Q., Wang, X., Yao, X.-L., Hou, J.-F., . . . Cen, K.-F. (2013). Increased thermal conductivity of eicosane-based composite phase change materials in the presence of graphene nanoplatelets. *Energy & Fuels, 27*(7), 4041-4047.

Fearn, R., Mullin, T., & Cliffe, K. (1990). Nonlinear flow phenomena in a symmetric sudden expansion. *Journal of Fluid Mechanics, 211*, 595-608.

Fendler, J. H. (2001). Colloid chemical approach to nanotechnology. *Korean Journal of Chemical Engineering, 18*(1), 1-13.

Foumeny, E., Ingham, D., & Walker, A. (1996). Bifurcations of incompressible flow through plane symmetric channel expansions. *Computers & Fluids, 25*(3), 335-351.

Gherasim, I., Roy, G., Nguyen, C. T., & Vo-Ngoc, D. (2009). Experimental investigation of nanofluids in confined laminar radial flows. *International Journal of Thermal Sciences, 48*(8), 1486-1493.

Gherasim, I., Roy, G., Nguyen, C. T., & Vo-Ngoc, D. (2011). Heat transfer enhancement and pumping power in confined radial flows using nanoparticle suspensions (nanofluids). *International Journal of Thermal Sciences, 50*(3), 369-377.

Ghozatloo, A., Shariaty-Niasar, M., & Rashidi, A. M. (2013). Preparation of nanofluids from functionalized graphene by new alkaline method and study on the thermal conductivity and stability. *International Communications in Heat and Mass Transfer, 42*, 89-94.

Giunta, A. A., Balabanov, V., Haim, D., Grossman, B., Mason, W. H., Watson, L. T., & Haftka, R. T. (1996). Wing design for a high-speed civil transport using a design of experiments methodology.

Gnielinski, V. (1975). New equations for heat and mass transfer in the turbulent flow in pipes and channels. *NASA STI/Recon Technical Report A, 75*, 8-16.

Gnielinski, V. (1976). New equations for heat and mass-transfer in turbulent pipe and channel flow. *International chemical engineering, 16*(2), 359-368.

Godson, L., Raja, B., Lal, D. M., & Wongwises, S. (2010). Experimental investigation on the thermal conductivity and viscosity of silver-deionized water nanofluid. *Experimental Heat Transfer, 23*(4), 317-332.

Graham, A. L. (1981). On the viscosity of suspensions of solid spheres. *Applied Scientific Research, 37*(3-4), 275-286.

Hadadian, M., Goharshadi, E. K., & Youssefi, A. (2014). Electrical conductivity, thermal conductivity, and rheological properties of graphene oxide-based nanofluids. *Journal of Nanoparticle Research, 16*(12), 2788.

Haftka, R. T., Scott, E. P., & Cruz, J. R. (1998). Optimization and experiments: a survey. *Applied Mechanics Reviews, 51*, 435-448.

Haghighi, E., Nikkam, N., Saleemi, M., Behi, M., Mirmohammadi, S. A., Poth, H., . . . Palm, B. (2013). Shelf stability of nanofluids and its effect on thermal conductivity and viscosity. *Measurement Science and Technology, 24*(10), 105301.

Halelfadl, S., Estellé, P., Aladag, B., Doner, N., & Maré, T. (2013). Viscosity of carbon nanotubes water-based nanofluids: Influence of concentration and temperature. *International Journal of Thermal Sciences, 71*, 111-117.

Hamilton, R., & Crosser, O. (1962). Thermal conductivity of heterogeneous two-component systems. *Industrial & Engineering chemistry fundamentals, 1*(3), 187-191.

Hammad, K. J., Ötügen, M. V., & Arik, E. B. (1999). A PIV study of the laminar axisymmetric sudden expansion flow. *Experiments in fluids, 26*(3), 266-272.

Harris, P. J. F. (2009). *Carbon nanotube science: synthesis, properties and applications*: Cambridge University Press.

Hasselman, D., & Johnson, L. F. (1987). Effective thermal conductivity of composites with interfacial thermal barrier resistance. *Journal of Composite Materials, 21*(6), 508-515.

Hawa, T., & Rusak, Z. (2001). The dynamics of a laminar flow in a symmetric channel with a sudden expansion. *Journal of Fluid Mechanics, 436*, 283-320.

Heris, S. Z., Etemad, S. G., & Esfahany, M. N. (2006). Experimental investigation of oxide nanofluids laminar flow convective heat transfer. *International Communications in Heat and Mass Transfer, 33*(4), 529-535.

Heshmati, A., Mohammed, H., & Darus, A. (2014). Mixed convection heat transfer of nanofluids over backward facing step having a slotted baffle. *Applied Mathematics and Computation, 240*, 368-386.

Hong, K., Hong, T.-K., & Yang, H.-S. (2006). Thermal conductivity of Fe nanofluids depending on the cluster size of nanoparticles. *Applied Physics Letters, 88*(3), 031901.

Huxtable, S. T., Cahill, D. G., Shenogin, S., Xue, L., Ozisik, R., Barone, P., . . . Shim, M. (2003). Interfacial heat flow in carbon nanotube suspensions. *Nature materials, 2*(11), 731.

Hwang, Y.-j., Lee, J., Lee, C., Jung, Y., Cheong, S., Lee, C., . . . Jang, S. (2007). Stability and thermal conductivity characteristics of nanofluids. *Thermochimica Acta, 455*(1-2), 70-74.

Hwang, Y., Ahn, Y., Shin, H., Lee, C., Kim, G., Park, H., & Lee, J. (2006). Investigation on characteristics of thermal conductivity enhancement of nanofluids. *Current Applied Physics, 6*(6), 1068-1071.

Hwang, Y., Lee, J.-K., Lee, J.-K., Jeong, Y.-M., Cheong, S.-i., Ahn, Y.-C., & Kim, S. H. (2008). Production and dispersion stability of nanoparticles in nanofluids. *Powder Technology, 186*(2), 145-153.

Iijima, S. (1991). Helical microtubules of graphitic carbon. *Nature, 354*(6348), 56.

Iijima, S., & Ichihashi, T. (1993). Single-shell carbon nanotubes of 1-nm diameter. *Nature, 363*(6430), 603-605.

Jang, S. P., & Choi, S. U. (2004). Role of Brownian motion in the enhanced thermal conductivity of nanofluids. *Applied Physics Letters, 84*(21), 4316-4318.

Jang, S. P., & Choi, S. U. (2007). Effects of various parameters on nanofluid thermal conductivity. *Journal of Heat Transfer, 129*(5), 617-623.

Kadja, M., & Bergeles, G. (2002). Numerical investigation of bifurcation phenomena occurring in flows through planar sudden expansions. *Acta mechanica, 153*(1-2), 47-61.

Kakaç, S., & Pramuanjaroenkij, A. (2009). Review of convective heat transfer enhancement with nanofluids. *International Journal of Heat and Mass Transfer, 52*(13), 3187-3196.

Kallay, N., & Žalac, S. (2002). Stability of nanodispersions: a model for kinetics of aggregation of nanoparticles. *Journal of colloid and interface science, 253*(1), 70-76.

Kang, H. U., Kim, S. H., & Oh, J. M. (2006). Estimation of thermal conductivity of nanofluid using experimental effective particle volume. *Experimental Heat Transfer, 19*(3), 181-191.

Karthikeyan, N., Philip, J., & Raj, B. (2008). Effect of clustering on the thermal conductivity of nanofluids. *Materials Chemistry and Physics, 109*(1), 50-55.

Kaushik, V., Ghosh, S., Das, G., & Das, P. K. (2012). CFD simulation of core annular flow through sudden contraction and expansion. *Journal of Petroleum Science and Engineering, 86*, 153-164.

Keblinski, P., Phillpot, S., Choi, S., & Eastman, J. (2002). Mechanisms of heat flow in suspensions of nano-sized particles (nanofluids). *International Journal of Heat and Mass Transfer, 45*(4), 855-863.

Khanafer, K., Vafai, K., & Lightstone, M. (2003). Buoyancy-driven heat transfer enhancement in a two-dimensional enclosure utilizing nanofluids. *International Journal of Heat and Mass Transfer, 46*(19), 3639-3653.

Khezzar, L., De Zilwa, S., & Whitelaw, J. (1999). Combustion of premixed fuel and air downstream of a plane sudden-expansion. *Experiments in fluids, 27*(4), 296-309.

Khoshvaght-Aliabadi, M. (2014). Influence of different design parameters and Al 2 O 3-water nanofluid flow on heat transfer and flow characteristics of sinusoidal-corrugated channels. *Energy Conversion and Management, 88*, 96-105.

Khuri, A. I., & Cornell, J. A. (1996). *Response surfaces: designs and analyses* (Vol. 152): CRC press.

Kimouche, A., Mataoui, A., Oztop, H. F., & Abu-Hamdeh, N. (2017). Analysis of heat transfer of different nanofluids flow through an abrupt expansion pipe. *Applied Thermal Engineering, 112*, 965-974.

Kline, S. J. (1953). Describing uncertainty in single-sample experiments. *Mechanical engineering, 75*, 3-8.

Koo, J., & Kleinstreuer, C. (2004). A new thermal conductivity model for nanofluids. *Journal of Nanoparticle Research, 6*(6), 577-588.

Kreith, F., Bohn, M. S., & Ulrich, R. D. (1997). *Principles of heat transfer* (Vol. 5): PWS publishing company Boston.

Krishnamurthy, S., Bhattacharya, P., Phelan, P., & Prasher, R. (2006). Enhanced mass transport in nanofluids. *Nano letters, 6*(3), 419-423.

Kulkarni, D. P., Das, D. K., & Patil, S. L. (2007). Effect of temperature on rheological properties of copper oxide nanoparticles dispersed in propylene glycol and water mixture. *Journal of nanoscience and nanotechnology, 7*(7), 2318-2322.

Kumar, D. H., Patel, H. E., Kumar, V. R., Sundararajan, T., Pradeep, T., & Das, S. K. (2004). Model for heat conduction in nanofluids. *Physical Review Letters, 93*(14), 144301.

Lamas, B., Abreu, B., Fonseca, A., Martins, N., & Oliveira, M. (2014). Critical analysis of the thermal conductivity models for CNT based nanofluids. *International Journal of Thermal Sciences, 78*, 65-76.

Lancial, N., Beaubert, F., Harmand, S., & Rolland, G. (2013). Effects of a turbulent wall jet on heat transfer over a non-confined backward-facing step. *International Journal of Heat and Fluid Flow, 44*, 336-347.

Lautenschlager, U., Eschenauer, H. A., & Mistree, F. (1997). Multiobjective flywheel design: a doe-based concept exploration task. *Advances in Design Automation (Dutta, D., ed.)*, 14-17.

Lee, D., Kim, J.-W., & Kim, B. G. (2006). A new parameter to control heat transport in nanofluids: surface charge state of the particle in suspension. *The Journal of Physical Chemistry B, 110*(9), 4323-4328.

Lee, D. H., Lee, J. S., Park, H. J., & Kim, M. K. (2011). Experimental and numerical study of heat transfer downstream of an axisymmetric abrupt expansion and in a cavity of a circular tube. *Journal of Mechanical Science and Technology, 25*(2), 395-401.

Lee, K. J., Yoon, S. H., & Jang, J. (2007). Carbon nanofibers: a novel nanofiller for nanofluid applications. *Small, 3*(7), 1209-1213.

Lee, S., Choi, S.-S., Li, S., and, & Eastman, J. (1999). Measuring thermal conductivity of fluids containing oxide nanoparticles. *Journal of Heat Transfer, 121*(2), 280-289.

Lee, T., & Mateescu, D. (1998). Experimental and numerical investigation of 2-D backward-facing step flow. *Journal of Fluids and Structures, 12*(6), 703-716.

Li, C. H., & Peterson, G. (2006). Experimental investigation of temperature and volume fraction variations on the effective thermal conductivity of nanoparticle suspensions (nanofluids). *Journal of Applied Physics, 99*(8), 084314.

Li, F.-C., Yang, J.-C., Zhou, W.-W., He, Y.-R., Huang, Y.-M., & Jiang, B.-C. (2013). Experimental study on the characteristics of thermal conductivity and shear viscosity of viscoelastic-fluid-based nanofluids containing multiwalled carbon nanotubes. *Thermochimica Acta, 556*, 47-53.

Li, S., & Eastman, J. (1999). Measuring thermal conductivity of fluids containing oxide nanoparticles. *J. Heat Transf, 121*(2), 280-289.

Lima, R., Andrade, C., & Zaparoli, E. (2008). Numerical study of three recirculation zones in the unilateral sudden expansion flow. *International Communications in Heat and Mass Transfer, 35*(9), 1053-1060.

Lundgren, T. S. (1972). Slow flow through stationary random beds and suspensions of spheres. *Journal of Fluid Mechanics, 51*(2), 273-299.

Macagno, E. O., & Hung, T.-K. (1967). Computational and experimental study of a captive annular eddy. *Journal of Fluid Mechanics, 28*(01), 43-64.

Magee, L. (1990). R 2 measures based on Wald and likelihood ratio joint significance tests. *The American Statistician, 44*(3), 250-253.

Maïga, S. E. B., Nguyen, C. T., Galanis, N., & Roy, G. (2004). Heat transfer behaviours of nanofluids in a uniformly heated tube. *Superlattices and Microstructures, 35*(3), 543-557.

Maiga, S. E. B., Palm, S. J., Nguyen, C. T., Roy, G., & Galanis, N. (2005). Heat transfer enhancement by using nanofluids in forced convection flows. *International Journal of Heat and Fluid Flow, 26*(4), 530-546.

Manca, O., Nardini, S., & Ricci, D. (2012). A numerical study of nanofluid forced convection in ribbed channels. *Applied Thermal Engineering, 37*, 280-292.

Mandal, D., Bandyopadhyay, S., & Chakrabarti, S. (2011). A numerical study on the flow through a plane symmetric sudden expansion with a fence viewed as a diffuser. *International Journal of Engineering, Science and Technology, 3*(8), 210-233.

Manica, R., & De Bortoli, A. (2004). Simulation of sudden expansion flows for power-law fluids. *Journal of Non-Newtonian Fluid Mechanics, 121*(1), 35-40.

Mansour, R. B., Galanis, N., & Nguyen, C. T. (2007). Effect of uncertainties in physical properties on forced convection heat transfer with nanofluids. *Applied Thermal Engineering, 27*(1), 240-249.

Mason, R. L., Gunst, R. F., & Hess, J. L. (2003). *Statistical design and analysis of experiments: with applications to engineering and science* (Vol. 474): John Wiley & Sons.

Masuda, H., Ebata, A., & Teramae, K. (1993). Alteration of thermal conductivity and viscosity of liquid by dispersing ultra-fine particles. Dispersion of Al2O3, SiO2 and TiO2 ultra-fine particles.

Mavris, D. (2006). Introduction to Design of Experiments and Response Surface Methods. *AE6373: Advanced Design Methods I Lecture Notes*.

Maxwell, J. C. (1881). *A treatise on electricity and magnetism* (Vol. 1): Clarendon press.

Mehrali, M., Sadeghinezhad, E., Latibari, S. T., Kazi, S. N., Mehrali, M., Zubir, M. N. B. M., & Metselaar, H. S. C. (2014). Investigation of thermal conductivity and rheological properties of nanofluids containing graphene nanoplatelets. *Nanoscale research letters, 9*(1), 15.

Meng, Z., Wu, D., Wang, L., Zhu, H., & Li, Q. (2012). Carbon nanotube glycol nanofluids: photo-thermal properties, thermal conductivities and rheological behavior. *Particuology, 10*(5), 614-618.

Mintsa, H. A., Roy, G., Nguyen, C. T., & Doucet, D. (2009). New temperature dependent thermal conductivity data for water-based nanofluids. *International Journal of Thermal Sciences, 48*(2), 363-371.

Mirmasoumi, S., & Behzadmehr, A. (2008a). Effect of nanoparticles mean diameter on mixed convection heat transfer of a nanofluid in a horizontal tube. *International Journal of Heat and Fluid Flow, 29*(2), 557-566.

Mirmasoumi, S., & Behzadmehr, A. (2008b). Numerical study of laminar mixed convection of a nanofluid in a horizontal tube using two-phase mixture model. *Applied Thermal Engineering, 28*(7), 717-727.

Mishra, S., & Jayaraman, K. (2002). Asymmetric flows in planar symmetric channels with large expansion ratio. *International journal for numerical methods in fluids, 38*(10), 945-962.

Mistrangelo, C., & Bühler, L. (2007). Numerical investigation of liquid metal flows in rectangular sudden expansions. *Fusion Engineering and Design, 82*(15), 2176-2182.

Mitróová, Z., Tomašovičová, N., Lancz, G., Kováč, J., Vávra, I., & Kopčanský, P. (2010). Preparation and characterization of carbon nanotubes functionalized by magnetite nanoparticles. *Olomouc, Czech Republic, EU, 10*, 12-14.

Mizushima, J., & Shiotani, Y. (2000). Structural instability of the bifurcation diagram for two-dimensional flow in a channel with a sudden expansion. *Journal of Fluid Mechanics, 420*, 131-145.

Moffat, R. J. (1988). Describing the uncertainties in experimental results. *Experimental Thermal and Fluid Science, 1*(1), 3-17.

Mohammed, H., Al-Aswadi, A., Shuaib, N., & Saidur, R. (2011). Convective heat transfer and fluid flow study over a step using nanofluids: a review. *Renewable and Sustainable Energy Reviews, 15*(6), 2921-2939.

Mohammed, H., Alawi, O. A., & Wahid, M. (2015). Mixed convective nanofluid flow in a channel having backward-facing step with a baffle. *Powder Technology, 275*, 329-343.

Montazer, E., Mirzaei, M., Salami, E., Ward, T., Romli, F., & Kazi, S. (2016). *Optimization of a synthetic jet actuator for flow control around an airfoil.* Paper presented at the IOP Conference Series: Materials Science and Engineering.

Montazer, E., Salami, E., Yarmand, H., Kazi, S., & Badarudin, A. The RSM approach to develop a new correlation for density of metal-oxide aqueous nanofluids.

Montazer, E., Yarmand, H., Salami, E., Muhamad, M. R., Kazi, S., & Badarudin, A. (2018). A brief review study of flow phenomena over a backward-facing step and its optimization. *Renewable and Sustainable Energy Reviews, 82*, 994-1005.

Montgomery, D. C. (1991). Design and analysis of experiments.

Montgomery, D. C. (1997). Analysis and design of experiments: New York, NY: Wiley.

Montgomery, D. C., & Myers, R. H. (1995). Response surface methodology: process and product optimization using designed experiments. *Raymond H. Meyers and Douglas C. Montgomery. A Wiley-Interscience Publications*.

Montgomery, D. C., & Runger, G. C. (2010). *Applied statistics and probability for engineers*: John Wiley & Sons.

Murshed, S., Leong, K., & Yang, C. (2005). Enhanced thermal conductivity of TiO2—water based nanofluids. *International Journal of Thermal Sciences, 44*(4), 367-373.

Murshed, S., Leong, K., & Yang, C. (2008a). Investigations of thermal conductivity and viscosity of nanofluids. *International Journal of Thermal Sciences, 47*(5), 560-568.

Murshed, S., Leong, K., & Yang, C. (2008b). Thermophysical and electrokinetic properties of nanofluids–a critical review. *Applied Thermal Engineering, 28*(17-18), 2109-2125.

Myers, R. H. (1971). Response Surface Methodology, Allyn and Bacon. *Boston, MA*.

Myers, R. H., Montgomery, D. C., & Anderson-Cook, C. M. (2016). *Response surface methodology: process and product optimization using designed experiments*: John Wiley & Sons.

Namburu, P., Kulkarni, D., Dandekar, A., & Das, D. (2007). Experimental investigation of viscosity and specific heat of silicon dioxide nanofluids. *Micro & Nano Letters, 2*(3), 67-71.

Namburu, P. K., Das, D. K., Tanguturi, K. M., & Vajjha, R. S. (2009). Numerical study of turbulent flow and heat transfer characteristics of nanofluids considering variable properties. *International Journal of Thermal Sciences, 48*(2), 290-302.

Namburu, P. K., Kulkarni, D. P., Misra, D., & Das, D. K. (2007). Viscosity of copper oxide nanoparticles dispersed in ethylene glycol and water mixture. *Experimental Thermal and Fluid Science, 32*(2), 397-402.

Nan, C.-W., Birringer, R., Clarke, D. R., & Gleiter, H. (1997). Effective thermal conductivity of particulate composites with interfacial thermal resistance. *Journal of Applied Physics, 81*(10), 6692-6699.

Nassar, B., de Souza Mendes, P. R., & Naccache, M. F. (2011). Flow of elasto-viscoplastic liquids through an axisymmetric expansion–contraction. *Journal of Non-Newtonian Fluid Mechanics, 166*(7), 386-394.

Neofytou, P. (2006). Transition to asymmetry of generalised Newtonian fluid flows through a symmetric sudden expansion. *Journal of Non-Newtonian Fluid Mechanics, 133*(2), 132-140.

Nguyen, C., Desgranges, F., Roy, G., Galanis, N., Maré, T., Boucher, S., & Mintsa, H. A. (2007). Temperature and particle-size dependent viscosity data for water-based nanofluids–hysteresis phenomenon. *International Journal of Heat and Fluid Flow, 28*(6), 1492-1506.

Nguyen, C. T., Roy, G., Gauthier, C., & Galanis, N. (2007). Heat transfer enhancement using Al 2 O 3–water nanofluid for an electronic liquid cooling system. *Applied Thermal Engineering, 27*(8), 1501-1506.

Nikkhah, V., Sarafraz, M., Hormozi, F., & Peyghambarzadeh, S. (2015). Particulate fouling of CuO–water nanofluid at isothermal diffusive condition inside the conventional heat exchanger-experimental and modeling. *Experimental Thermal and Fluid Science, 60*, 83-95.

Nikkhah, Z., Karimipour, A., Safaei, M. R., Forghani-Tehrani, P., Goodarzi, M., Dahari, M., & Wongwises, S. (2015). Forced convective heat transfer of water/functionalized multi-walled carbon nanotube nanofluids in a microchannel with oscillating heat flux and slip boundary condition. *International Communications in Heat and Mass Transfer, 68*, 69-77.

Oliveira, P., & Pinho, F. (1997). Pressure drop coefficient of laminar Newtonian flow in axisymmetric sudden expansions. *International Journal of Heat and Fluid Flow, 18*(5), 518-529.

Overbeek, J. T. G. (1952). Electrochemistry of the double layer. *Irreversible Systems. Colloid Science, 1*, 115-193.

Pak, B. C., & Cho, Y. I. (1998). Hydrodynamic and heat transfer study of dispersed fluids with submicron metallic oxide particles. *Experimental Heat Transfer an International Journal, 11*(2), 151-170.

Palm, S. J., Roy, G., & Nguyen, C. T. (2006). Heat transfer enhancement with the use of nanofluids in radial flow cooling systems considering temperature-dependent properties. *Applied Thermal Engineering, 26*(17-18), 2209-2218.

Papari, M. M., Yousefi, F., Moghadasi, J., Karimi, H., & Campo, A. (2011). Modeling thermal conductivity augmentation of nanofluids using diffusion neural networks. *International Journal of Thermal Sciences, 50*(1), 44-52.

Park, S.-K., & Ota, T. (2010). An experimental approach to turbulent heat transfer using a symmetric expanded plane channel. *Journal of Mechanical Science and Technology, 24*(4), 857-863.

Pastoriza-Gallego, M., Casanova, C., Legido, J. a., & Piñeiro, M. (2011). CuO in water nanofluid: influence of particle size and polydispersity on volumetric behaviour and viscosity. *Fluid Phase Equilibria, 300*(1), 188-196.

Patel, H. E., Das, S. K., Sundararajan, T., Sreekumaran Nair, A., George, B., & Pradeep, T. (2003). Thermal conductivities of naked and monolayer protected metal nanoparticle based nanofluids: Manifestation of anomalous enhancement and chemical effects. *Applied Physics Letters, 83*(14), 2931-2933.

Petukhov, B. (1970). Heat transfer and friction in turbulent pipe flow with variable physical properties. *Advances in heat transfer, 6*, 503-564.

Peyghambarzadeh, S., Hashemabadi, S., Chabi, A., & Salimi, M. (2014). Performance of water based CuO and Al 2 O 3 nanofluids in a Cu–Be alloy heat sink with rectangular microchannels. *Energy Conversion and Management, 86*, 28-38.

Philip, J., & Shima, P. (2012). Thermal properties of nanofluids. *Advances in colloid and interface science, 183*, 30-45.

Phuoc, T. X., Massoudi, M., & Chen, R.-H. (2011). Viscosity and thermal conductivity of nanofluids containing multi-walled carbon nanotubes stabilized by chitosan. *International Journal of Thermal Sciences, 50*(1), 12-18.

Ponmani, S., William, J. K. M., Samuel, R., Nagarajan, R., & Sangwai, J. S. (2014). Formation and characterization of thermal and electrical properties of CuO and ZnO nanofluids in xanthan gum. *Colloids and Surfaces A: Physicochemical and Engineering Aspects, 443*, 37-43.

Ponmozhi, J., Gonçalves, F., Ferreira, A., Fonseca, I., Kanagaraj, S., Martins, N., & Oliveira, M. S. (2010). *Thermodynamic and transport properties of CNT-water based nanofluids.* Paper presented at the Journal of nano Research.

Poole, R., & Ridley, B. (2007). Development-length requirements for fully developed laminar pipe flow of inelastic non-Newtonian liquids. *Journal of Fluids Engineering, 129*(10), 1281-1287.

Popiel, C., & Wojtkowiak, J. (1998). Simple formulas for thermophysical properties of liquid water for heat transfer calculations (from 0 C to 150 C). *Heat Transfer Engineering, 19*(3), 87-101.

Prasher, R., Bhattacharya, P., & Phelan, P. E. (2005). Thermal conductivity of nanoscale colloidal solutions (nanofluids). *Physical Review Letters, 94*(2), 025901.

Prasher, R., Phelan, P. E., & Bhattacharya, P. (2006). Effect of aggregation kinetics on the thermal conductivity of nanoscale colloidal solutions (nanofluid). *Nano letters, 6*(7), 1529-1534.

Putra, N., Roetzel, W., & Das, S. K. (2003). Natural convection of nano-fluids. *Heat and mass transfer, 39*(8-9), 775-784.

Rao, Y. (2010). Nanofluids: stability, phase diagram, rheology and applications. *Particuology, 8*(6), 549-555.

Rashidi, M., Hosseini, A., Pop, I., Kumar, S., & Freidoonimehr, N. (2014). Comparative numerical study of single and two-phase models of nanofluid heat transfer in wavy channel. *Applied Mathematics and Mechanics, 35*(7), 831-848.

Ren, Y., Xie, H., & Cai, A. (2005). Effective thermal conductivity of nanofluids containing spherical nanoparticles. *Journal of Physics D: Applied Physics, 38*(21), 3958.

Roy, G., Nguyen, C. T., & Lajoie, P.-R. (2004). Numerical investigation of laminar flow and heat transfer in a radial flow cooling system with the use of nanofluids. *Superlattices and Microstructures, 35*(3-6), 497-511.

Sadeghinezhad, E., Mehrali, M., Tahan Latibari, S., Mehrali, M., Kazi, S., Oon, C. S., & Metselaar, H. S. C. (2014). Experimental investigation of convective heat transfer using graphene nanoplatelet based nanofluids under turbulent flow conditions. *Industrial & Engineering Chemistry Research, 53*(31), 12455-12465.

Samira, P., Saeed, Z. H., Motahare, S., & Mostafa, K. (2015). Pressure drop and thermal performance of CuO/ethylene glycol (60%)-water (40%) nanofluid in car radiator. *Korean journal of chemical engineering, 32*(4), 609-616.

Sarkar, S., Ganguly, S., & Biswas, G. (2012). Mixed convective heat transfer of nanofluids past a circular cylinder in cross flow in unsteady regime. *International Journal of Heat and Mass Transfer, 55*(17-18), 4783-4799.

Sarkar, S., Ganguly, S., Dalal, A., Saha, P., & Chakraborty, S. (2013). Mixed convective flow stability of nanofluids past a square cylinder by dynamic mode decomposition. *International Journal of Heat and Fluid Flow, 44*, 624-634.

Sarsam, W. S., Amiri, A., Zubir, M. N. M., Yarmand, H., Kazi, S., & Badarudin, A. (2016). Stability and thermophysical properties of water-based nanofluids containing triethanolamine-treated graphene nanoplatelets with different specific surface areas. *Colloids and Surfaces A: Physicochemical and Engineering Aspects, 500*, 17-31.

Schoofs, A., Van Asperen, F., Maas, P., & Lehr, A. (1987). I. computation of bell profiles using structural optimization. *Music Perception: An Interdisciplinary Journal, 4*(3), 245-254.

Shapira, M., Degani, D., & Weihs, D. (1990). Stability and existence of multiple solutions for viscous flow in suddenly enlarged channels. *Computers & Fluids, 18*(3), 239-258.

Simpson, T. W., Peplinski, J., Koch, P. N., & Allen, J. K. (1997). On the use of statistics in design and the implications for deterministic computer experiments. *Design Theory and Methodology-DTM'97*, 14-17.

So, R. M., & Ahmed, S. A. (1989). Characteristics of dump combustor flows. *International Journal of Heat and Fluid Flow, 10*(1), 66-74.

Solangi, K., Amiri, A., Luhur, M., Ghavimi, S. A. A., Kazi, S., Badarudin, A., & Zubir, M. N. M. (2016). Experimental investigation of heat transfer performance and frictional loss of functionalized GNP-based water coolant in a closed conduit flow. *RSC Advances, 6*(6), 4552-4563.

Sousa, P., Coelho, P., Oliveira, M., & Alves, M. (2011). Laminar flow in three-dimensional square–square expansions. *Journal of Non-Newtonian Fluid Mechanics, 166*(17), 1033-1048.

Sudeep, P., Taha-Tijerina, J., Ajayan, P., Narayanan, T., & Anantharaman, M. (2014). Nanofluids based on fluorinated graphene oxide for efficient thermal management. *RSC Advances, 4*(47), 24887-24892.

Tantra, R., Schulze, P., & Quincey, P. (2010). Effect of nanoparticle concentration on zeta-potential measurement results and reproducibility. *Particuology, 8*(3), 279-285.

Taylor, J. (1997). *Introduction to error analysis, the study of uncertainties in physical measurements*.

Ternik, P. (2009). Planar sudden symmetric expansion flows and bifurcation phenomena of purely viscous shear-thinning fluids. *Journal of Non-Newtonian Fluid Mechanics, 157*(1), 15-25.

Ternik, P. (2010). New contributions on laminar flow of inelastic non-Newtonian fluid in the two-dimensional symmetric expansion: Creeping and slowly moving flow conditions. *Journal of Non-Newtonian Fluid Mechanics, 165*(19), 1400-1411.

Ternik, P., Marn, J., & Žunič, Z. (2006). Non-Newtonian fluid flow through a planar symmetric expansion: Shear-thickening fluids. *Journal of Non-Newtonian Fluid Mechanics, 135*(2), 136-148.

Timofeeva, E. V., Gavrilov, A. N., McCloskey, J. M., Tolmachev, Y. V., Sprunt, S., Lopatina, L. M., & Selinger, J. V. (2007). Thermal conductivity and particle agglomeration in alumina nanofluids: experiment and theory. *Physical Review E, 76*(6), 061203.

Timofeeva, E. V., Routbort, J. L., & Singh, D. (2009). Particle shape effects on thermophysical properties of alumina nanofluids. *Journal of Applied Physics, 106*(1), 014304.

Toropov, V., Filatov, A., & Polynkin, A. (1993). Multiparameter structural optimization using FEM and multipoint explicit approximations. *Structural and Multidisciplinary Optimization, 6*(1), 7-14.

Toropov, V., va, F., Markine, V., & d, H. (1996). *Refinements in the multi-point approximation method to reduce the effects of noisy structural responses.* Paper presented at the 6th Symposium on Multidisciplinary Analysis and Optimization.

Tu, J., Dinh, N., & Theofanous, T. (2004). *An experimental study of nanofluid boiling heat transfer.* Paper presented at the Proceedings of 6th international symposium on heat transfer, Beijing, China.

Turgut, A., Tavman, I., Chirtoc, M., Schuchmann, H., Sauter, C., & Tavman, S. (2009). Thermal conductivity and viscosity measurements of water-based TiO2 nanofluids. *International Journal of Thermophysics, 30*(4), 1213-1226.

Unal, R., Lepsch, R., Engelund, W., & Stanley, D. (1996). *Approximation model building and multidisciplinary design optimization using response surface methods.* Paper presented at the 6th Symposium on Multidisciplinary Analysis and Optimization.

Vajjha, R., Das, D., & Mahagaonkar, B. (2009). Density measurement of different nanofluids and their comparison with theory. *Petroleum Science and Technology, 27*(6), 612-624.

Vajjha, R. S., Das, D. K., & Kulkarni, D. P. (2010). Development of new correlations for convective heat transfer and friction factor in turbulent regime for nanofluids. *International Journal of Heat and Mass Transfer, 53*(21), 4607-4618.

Van Campen, D., Nagtegaal, R., Schoofs, A., Eschenauer, H., Koski, J., & Osyczka, A. (1990). Approximation methods in structural optimization using experimental designs for for multiple responses. *Multicriteria Design Optimization-Procedures and Applications*, 205-228.

van Keulen, F., Liu, B., & Haftka, R. (2000). *Noise and discontinuity issues in response surfaces based on functions and derivatives.* Paper presented at the 41st Structures, Structural Dynamics, and Materials Conference and Exhibit.

Venter, G., Haftka, R., & Starnes, J., James. (1996). *Construction of response surfaces for design optimization applications.* Paper presented at the 6th Symposium on Multidisciplinary Analysis and Optimization.

Wang, B.-X., Zhou, L.-P., & Peng, X.-F. (2003). A fractal model for predicting the effective thermal conductivity of liquid with suspension of nanoparticles. *International Journal of Heat and Mass Transfer, 46*(14), 2665-2672.

Wang, X.-j., Li, X., & Yang, S. (2009). Influence of pH and SDBS on the stability and thermal conductivity of nanofluids. *Energy & Fuels, 23*(5), 2684-2689.

Wang, X.-Q., & Mujumdar, A. S. (2008). A review on nanofluids-part II: experiments and applications. *Brazilian Journal of Chemical Engineering, 25*(4), 631-648.

Wasan, D., Nikolov, A., & Moudgil, B. (2005). Colloidal dispersions: Structure, stability and geometric confinement. *Powder Technology, 153*(3), 135-141.

Wasp, E. J., Kenny, J. P., & Gandhi, R. L. (1977). Solid--liquid flow: slurry pipeline transportation.[Pumps, valves, mechanical equipment, economics]. *Ser. Bulk Mater. Handl.;(United States), 1*(4).

Wen, D., & Ding, Y. (2005). Experimental investigation into the pool boiling heat transfer of aqueous based γ-alumina nanofluids. *Journal of Nanoparticle Research, 7*(2), 265-274.

Wensel, J., Wright, B., Thomas, D., Douglas, W., Mannhalter, B., Cross, W., . . . Roy, W. (2008). Enhanced thermal conductivity by aggregation in heat transfer nanofluids containing metal oxide nanoparticles and carbon nanotubes. *Applied Physics Letters, 92*(2), 023110.

Witharana, S. (2011). *Thermal transport in nanofluids: boiling heat transfer.* University of Leeds.

Witharana, S., Palabiyik, I., Musina, Z., & Ding, Y. (2013). Stability of glycol nanofluids—the theory and experiment. *Powder Technology, 239*, 72-77.

Wong, K.-F. V., & Kurma, T. (2008). Transport properties of alumina nanofluids. *Nanotechnology, 19*(34), 345702.

Xuan, Y., & Li, Q. (2000). Heat transfer enhancement of nanofluids. *International Journal of Heat and Fluid Flow, 21*(1), 58-64.

Xuan, Y., & Li, Q. (2003). Investigation on convective heat transfer and flow features of nanofluids. *Journal of heat transfer, 125*(1), 151-155.

Xuan, Y., Li, Q., & Hu, W. (2003). Aggregation structure and thermal conductivity of nanofluids. *AIChE Journal, 49*(4), 1038-1043.

Xuan, Y., & Roetzel, W. (2000). Conceptions for heat transfer correlation of nanofluids. *International Journal of Heat and Mass Transfer, 43*(19), 3701-3707.

Yarmand, H., Ahmadi, G., Gharehkhani, S., Kazi, S. N., Safaei, M. R., Alehashem, M. S., & Mahat, A. B. (2014). Entropy generation during turbulent flow of zirconia-water and other nanofluids in a square cross section tube with a constant heat flux. *Entropy, 16*(11), 6116-6132.

Yarmand, H., Gharehkhani, S., Ahmadi, G., Shirazi, S. F. S., Baradaran, S., Montazer, E., . . . Dahari, M. (2015). Graphene nanoplatelets–silver hybrid nanofluids for enhanced heat transfer. *Energy Conversion and Management, 100*, 419-428.

Yarmand, H., Gharehkhani, S., Shirazi, S. F. S., Amiri, A., Alehashem, M. S., Dahari, M., & Kazi, S. (2016). Experimental investigation of thermo-physical properties, convective heat transfer and pressure drop of functionalized graphene nanoplatelets aqueous nanofluid in a square heated pipe. *Energy Conversion and Management, 114*, 38-49.

You, S., Kim, J., & Kim, K. (2003). Effect of nanoparticles on critical heat flux of water in pool boiling heat transfer. *Applied Physics Letters, 83*(16), 3374-3376.

Yu, W., & Choi, S. (2004). The role of interfacial layers in the enhanced thermal conductivity of nanofluids: a renovated Hamilton–Crosser model. *Journal of Nanoparticle Research, 6*(4), 355-361.

Yuki, N. O., Hiroyuki, Y., & Terukazu, O. (2004). *Turbulent heat transfer in a symmetric sudden expansion channel.* Paper presented at the Proceedings of the Thermal Engineering Conference.

Zdanski, P., & Vaz, M. (2009). Non-isothermal polymer melt flow in sudden expansions. *Journal of Non-Newtonian Fluid Mechanics, 161*(1), 42-47.

Zhang, X.-R., Deng, B.-L., & Yamaguchi, H. (2010). Bifurcation phenomenon for forced convection of supercritical CO 2 sudden expansion flow and heat transfer in symmetric regime. *International Journal of Heat and Mass Transfer, 53*(21), 4467-4473.

Zhou, S.-Q., & Ni, R. (2008). Measurement of the specific heat capacity of water-based Al 2 O 3 nanofluid. *Applied Physics Letters, 92*(9), 093123.

Zohir, A., Aziz, A. A., & Habib, M. (2011). Heat transfer characteristics in a sudden expansion pipe equipped with swirl generators. *International Journal of Heat and Fluid Flow, 32*(1), 352-361.

Zohir, A., & Gomaa, A. (2013). Heat transfer enhancement through sudden expansion pipe airflow using swirl generator with different angles. *Experimental Thermal and Fluid Science, 45*, 146-154.

LIST OF PUBLICATIONS AND AWARDS

1. Montazer, E., Salami, E., Yarmand, H., Chowdhury, Z.Z., Dahari, M., Kazi, S.N. and Badarudin, A., 2018. Development of a new density correlation for carbon-based nanofluids using response surface methodology. *Journal of Thermal Analysis and Calorimetry*, pp.1-9.

2. Montazer, E., Yarmand, H., Salami, E., Muhamad, M.R., Kazi, S.N. and Badarudin, A., 2018. A brief review study of flow phenomena over a backward-facing step and its optimization. *Renewable and Sustainable Energy Reviews*, *82*, pp.994-1005.

Collaborative Articles

1. Gharehkhani, S., Shirazi, S.F.S., Yarmand, H., Montazer, E., Kazi, S.N., Ibrahim, R., Ashjaei, M., Zulkifli, N.W.B.M. and Rahmati, S., 2018. The effect of nanocrystalline cellulose on flow properties of fiber crop aqueous suspension. *Carbohydrate polymers*, *184*, pp.376-382.

2. Yarmand, H., Gharehkhani, S., Ahmadi, G., Shirazi, S. F. S., Baradaran, S., Montazer, E., ... & Dahari, M. (2015). Graphene nanoplatelets–silver hybrid nanofluids for enhanced heat transfer. *Energy Conversion and Management*, *100*, 419-428.

3. Amiri, A., Shanbedi, M., Yarmand, H., Arzani, H. K., Gharehkhani, S., Montazer, E., ... & Kazi, S. N. (2015). Laminar convective heat transfer of hexylamine-treated MWCNTs-based turbine oil nanofluid. *Energy Conversion and Management*, *105*, 355-367.

4. Yarmand, H., Gharehkhani, S., Shirazi, S. F. S., Amiri, A., Montazer, E., Arzani, H. K., ... & Kazi, S. N. (2016). Nanofluid based on activated hybrid of biomass carbon/graphene oxide: synthesis, thermo-physical and electrical properties. *International Communications in Heat and Mass Transfer*, *72*, 10-15.

Conference Articles

1. Montazer, E., Salami, E., Yarmand, H., Kazi, S. N., & Badarudin, A. (2017, June). The RSM approach to develop a new correlation for density of metal-oxide aqueous nanofluids. In *Materials Science and Engineering Conference Series* (Vol. 210, No. 1, p. 012071).

2. Montazer, E., Mirzaei, M., Salami, E., Ward, T. A., Romli, F. I., & Kazi, S. N. (2016, October). Optimization of a synthetic jet actuator for flow control around an airfoil. In *IOP Conference Series: Materials Science and Engineering* (Vol. 152, No. 1, p. 012023). IOP Publishing.

3. Eskandari, M.A., Mazraeshahi, H.K., Ramesh, D., Montazer, E., Salami, E. and Romli, F.I., 2017, December. An algorithm on simultaneous optimization of performance and mass parameters of open-cycle liquid-propellant engine of

launch vehicles. In *IOP Conference Series: Materials Science and Engineering* (Vol. 270, No. 1, p. 012015). IOP Publishing.

4. Salami, E., Montazer, E., Ward, T. A., & Ganesan, P. B. (2017, June). Nano-mechanical properties and structural of a 3D-printed biodegradable biomimetic micro air vehicle wing. In *Materials Science and Engineering Conference Series* (Vol. 210, No. 1, p. 012073).

5. Ahmed, S. M., Kazi, S. N., Khan, G., Dahari, M., Zubir, M. N. M., Ahmad, P., & Montazer, E. (2017, June). Experimental investigation on momentum and drag reduction of Malaysian crop suspensions in closed conduit flow. In *Materials Science and Engineering Conference Series* (Vol. 210, No. 1, p. 012065).

Under Revision Article

1. "Heat Transfer to Turbulent Nanofluids Separation Flow-Studies in Evaluation of its Novel Correlations" by Elham Montazer, Hooman Yarmand, Erfan Salami, Kazi Md. Salim Newaz, Mohd Ridha Muhamad and Ahmad Badarudin Bin Mohamad Badry under revision on International Communications in Heat and Mass (ISI index - Q1).

Award

The present study got the Bronze medal and the award certificate on Pecipta 2017, The International Conference and Exposition on Inventions by Institutions of Higher Learning, Kuala Terengganu, Malaysia.